



**Università  
degli Studi  
di Ferrara**

DOCTORAL COURSE IN  
"MOLECULAR MEDICINE"

CYCLE XXXVI

COORDINATOR **Prof. Di Virgilio Francesco**

# **Regenerative Medicine: Multiple Approaches for Innovative Therapies Development**

Scientific/Disciplinary Sector (SDS) MED/46

**PhD Candidate**

Dott.ssa **Zanotti Federica**

**Supervisor**

**Prof. Zavan Barbara**

Year 2020/2023

*A Barbara,*

*grazie di aver creduto in me fin dal principio, oltre ogni cosa, anche i momenti di sfida con la vita per i quali avrei mollato. Non hai mai smesso di spronarmi e donarmi opportunità di crescita, in grado di farmi lottare per un futuro professionale e umano, che rappresenteranno le basi su cui costruire il mio domani.*

## Table of contents:

Aims .....	5
<b>Chapter 1: Mesenchymal Stem Cell and deriving Extracellular Vesicles to induce a Regenerative Process in Endothelial Cells.....</b>	<b>7</b>
<b>Abstract:.....</b>	<b>7</b>
<b>Introduction .....</b>	<b>8</b>
<b>Results: .....</b>	<b>13</b>
<b>1) ASCs Morphology and Viability Analysis.....</b>	<b>13</b>
<b>2) DFO-sEVs Production and HUVEC Treatment .....</b>	<b>13</b>
<b>3) RNA Sequencing of HUVECs After Treatment with DFO-sEVs and Mitochondria Membrane Potential analysis .....</b>	<b>16</b>
<b>4) sEV-miRNA Expression Profiling of HUVECs Treated with DFO-sEVs.....</b>	<b>20</b>
<b>Discussion .....</b>	<b>28</b>
<b>Material and Methods .....</b>	<b>33</b>
Adipose Stem Cell Observation and Viability, DFO Treatment .....	33
ASCs derived DFO-sEVs isolation and characterization using Transmission Electron Microscopy (TEM), Tunable resistive pulse sensing (RPS) and Flow Cytometry.....	33
Endothelial Cell Treatment, Observation and Mitochondria Membrane Potential Analysis .....	34
RNA and miRNAs Sequencing, Data and Functional Enrichment Analysis .....	35
<b>Chapter 2: Complex Magnetic Fields act to reduce the Inflammation in Diabetic Derived Cells ...</b>	<b>37</b>
<b>Abstract:.....</b>	<b>37</b>
<b>Introduction: .....</b>	<b>38</b>
<b>Results: .....</b>	<b>43</b>
<b>1) Safety Test following International Standard Indication .....</b>	<b>43</b>
<b>2) ROS Production and Mitochondria Membrane Potential Analysis .....</b>	<b>44</b>
<b>3) Macrophages Polarization Analysis.....</b>	<b>48</b>
<b>4) Specific Inflammatory Markers analysis .....</b>	<b>50</b>
<b>5) Extracellular Matrix Genes Expression Profiling .....</b>	<b>51</b>
<b>6) Macrophages RNA sequencing analysis with IPA software and Enrichment analysis .....</b>	<b>52</b>
<b>7) Fibroblasts RNA sequencing analysis with IPA software and Enrichment analysis .....</b>	<b>58</b>
<b>Discussion:.....</b>	<b>64</b>
<b>Materials and Methods: .....</b>	<b>68</b>
Patients Recruitment and Samples Collection.....	68
Cell Isolation and Characterization .....	68
Cell Treatment .....	69
Cells Viability Test.....	71
Hemolysis Assay .....	71

Mutagenic Analysis with Ames Test.....	72
Scanning Electron Microscopy (SEM).....	72
RNA Extraction and Real-Time PCR Array .....	72
Reactive Oxygen Species (ROS) Analysis.....	73
Mitochondria membrane potential analysis.....	74
RNA sequencing and Analysis .....	74
Statistics.....	75
<b>References Chapter 1:</b> .....	<b>76</b>
<b>References Chapter 2:</b> .....	<b>82</b>

## Aims

This thesis is the result of a PhD in “Molecular Medicine” attended in “Tissue Engineering and Regenerative Medicine laboratory” leaded by Prof. Barbara Zavan.

Our laboratory is focused on the study of the stem cells, the design of novel bioactive scaffolds, the development of new approaches towards tissue regeneration and the study of the cell-to-cell communication. This laboratory works in and belong to Translational Medicine field that is a rapidly growing discipline in biomedical research and aims to expedite the discovery of new diagnostic tools and treatments by using a multi-disciplinary, highly collaborative, "bench-to bedside" approach.

During these three years of PhD, I focused my studies on regenerative medicine with the goal to find multiple approaches for innovative therapies development applicable to several pathologies. The regenerative medicine is the branch of the medicine that effectively uses stem cell therapy and tissue engineering strategies to lead healing or replacement of damaged tissues or organs. It represents the field of research using cells and their mediators or other materials to either enhance or replace biological tissues.

On these basis, two different approaches to develop innovative therapies are presented in this thesis. The first study (Chapter 1), is aimed to explore the potential use of Small Extracellular Vesicles (sEVs) as innovative treatment for multiple illness like here presented, Cardiovascular Diseases (CVDs) that represent a major health concern worldwide remaining a leading cause of death globally. In order to do that, Mesenchymal Stem Cells (MSCs) has been exposed to hypoxia condition, since it is well known that MSC subjected to hypoxia are able to produce mediators capable to enhance a regenerative effect, acting on biological processes that induce tissue regeneration. The sEVs-derived from MSC under hypoxia were investigated as possible therapy, using them as treatment on Human Umbilical Vein Endothelial Cells (HUVECs). The effect on this cellular model, was investigated using multiple laboratory techniques as the mitochondria membrane potential analysis and a complete transcriptomic analysis by Illumina RNA sequencing analysis of the HUVEC and HUVEC sEVs-derived miRNA-content sequencing.

The second study reported here (Chapter 2) represents a physical non-invasive approach that is aimed to investigate the effect of complex magnetic fields (CMFs) on fibroblasts and monocyte cultures (subsequently differentiated in macrophages) derived from diabetic patients, affected by Diabetic Foot Ulcers (DFUs), with the goal to evaluate their capacity to influence the ROS production and their effect on wound healing properties and processes

on these selected cells, as cellular models representing those tissues known as affected by the diabetes diseases during the advanced stages of the illness. In order to realize this study, ROS production analysis, mitochondria membrane potential analysis, morphology observation using scanning electron microscopy (SEM) and Illumina RNA sequencing analysis of fibroblast and monocyte cultures from diabetic patients were performed.

# **Chapter 1: Mesenchymal Stem Cell and deriving Extracellular Vesicles to induce a Regenerative Process in Endothelial Cells**

## **Abstract:**

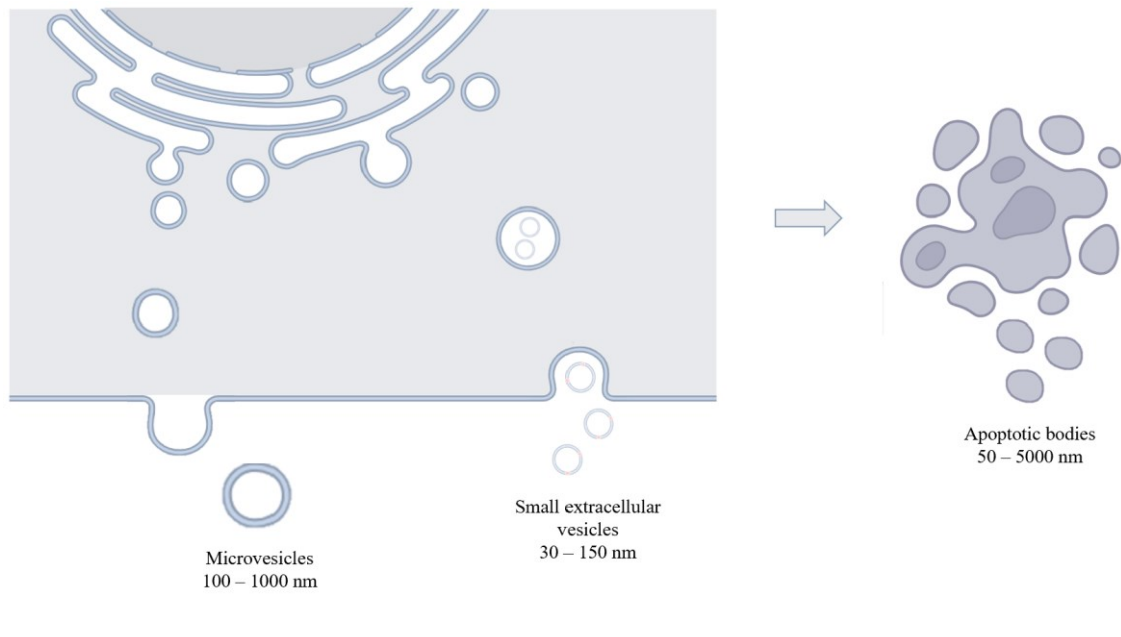
Small extracellular vesicles (sEVs) produced by mesenchymal stem cells (MSCs) have attracted growing interest as a possible novel therapeutic agent for an innovative treatment of different cardiovascular diseases (CVDs) that remains a major health concern worldwide. Currently, it is also well known that changing the extracellular environment of MSCs, it becomes possible to induce the production of different mediators in their secretome. It's reported that hypoxia condition significantly enhances the secretion of angiogenic mediators from MSCs as well as the production of sEVs. The iron-chelating deferoxamine mesylate (DFO) is used to push the cells in environmental hypoxia being a stabilizer of hypoxia-inducible factor 1 (HIF). The angiogenic factors are the main characters responsible for improving regenerative potential of DFO-treated MSCs, but the contribution of sEVs to this effect is still unknown and requires investigations. In the first chapter presented here, adipose-derived stem cells (ASCs) were treated using a nontoxic dose of DFO to produce and collect sEVs (DFO-sEVs). After the harvest, these DFO-sEVs were used to treat Human umbilical vein endothelial cells (HUVECs), subsequently analyzed performing mRNA sequencing and miRNA profiling of sEVs cargo (HUVEC-sEVs). Resulted transcriptomes showed upregulation of mitochondrial genes linked to oxidative phosphorylation. In addition, functional enrichment analysis on miRNAs of HUVEC-sEVs revealed a connection with the signaling pathways involved in cell proliferation and angiogenesis biological process.

Taken together, these data let to assume that mesenchymal stem cells treated with DFO release sEVs that are able to induce in the recipient endothelial cells molecular pathways and biological processes involved in the proliferation and angiogenesis too, allowing to envision a possible use of under hypoxia MSC sEVs derived as potential therapy on CVDs.

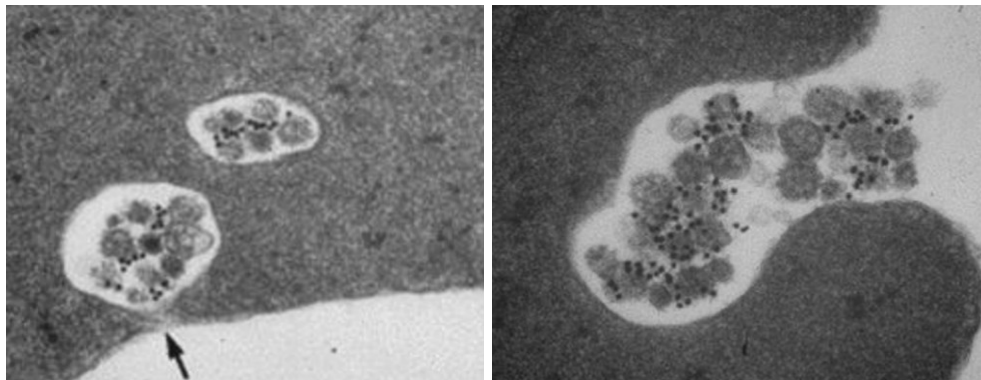
## Introduction

Therapies that exploit stem-cell-based strategies have recently gained popularity as a promising approach to support regenerative processes. Mesenchymal Stem Cells (MSCs) are multipotent cells that are easily isolated, easily cultured, and also readily expanded in the laboratory setting. For all these reasons they became an attractive cell source to be used in several clinical applications [1]. Furthermore, MSCs resulted interesting exhibiting a high self-renewal capacity, multilineage differentiation potential and immunomodulatory properties [2]. When we talk about MSCs we could think to many different tissues in which they reside, like bone marrow (BM), adipose tissue (AT), fetal lung, dental pulp, and umbilical cord (UC) [3]. Among these tissues, the adipose stem cells (ASCs) resulted very attractive due to the simple method to isolate and collect them and the remarkably high cell yield [4]. ASCs are mesenchymal stem cells identified in several tissues, within subcutaneous tissue at the base of the hair follicle (dermal papilla cells), in the dermal sheets (dermal sheet cells), in interfollicular dermis, and in the hypodermis tissue. These cells are known to proliferate and differentiate into skin cells to repair damaged or dead cells, but also act by an autocrine and paracrine pathway to activate cell regeneration and the healing process. Speaking about wound healing, ASCs have a great ability in migration to be recruited rapidly into wounded sites added to their differentiation towards dermal fibroblasts (DF), endothelial cells, and keratinocytes [5].

Nevertheless, there still are impediments and limits to achieve clinical translation of cell-based therapies. This reason makes the research increasingly focused on the paracrine mediators, like extracellular vesicles (EVs), capable to work between MSCs and multiple other target cells and tissues. Many studies have shifted from the use of transplanted stem cells to their secreted EVs. Extracellular vesicles can define basing on different considerations, like biogenesis (exosomes, apoptotic bodies etc.) or dimension (microvesicles or nanovesicles). Among these, we can find Small Extracellular Vesicles (sEVs) that are biological nanoparticles delimited by a lipid bilayer (with a nominal size ranging from 30 to 150 nm) that are released by cells to act as intercellular signaling mediators in both physiological and pathological conditions. They are vesicles of endosomal origin capable to bring RNAs, proteins, and lipids to recipient cells and thus have an important role in intercellular communication [6,7] (Figure 1a, 1b).



(a)



(b)

Figure 1: (a) Graphical sketch of the various types of extracellular vesicles biogenesis: exosomes, microvesicles, and apoptotic bodies; (b) exosome release with electron microscopy (Akers JC, Gonda D, Kim R, Carter BS, Chen CC. Biogenesis of extracellular vesicles (EV): exosomes, microvesicles, retrovirus-like vesicles, and apoptotic bodies. *J Neurooncol.* 2013 May;113(1):1-11. doi: 10.1007/s11060-013-1084-8. Epub 2013 Mar 2. PMID: 23456661; PMCID: PMC5533094.);

Contributing to cell-to-cell communication, sEVs have regenerative features like parenteral cells, and this reason may exceed the unwanted effects associated with stem cell transplantation. Indeed, sEVs have a lower possibility of immune rejection, and they are more stable and storable compared to the cells [8,9]. As well as the cells, even sEVs have been isolated from numerous sources of MSCs, and their regenerative potential has been investigated. Several examples are reported in literature like the sEVs obtained from bone marrow showed a prevalent effect on cell proliferation and viability, sEVs from dental-pulp-derived MSCs showed instead distinct transcriptomic signatures of neurogenesis, while sEVs from adipose tissue showed a significantly improved ability to promote endothelial cell migration and angiogenesis [10,11].

To date, MSC-derived sEVs have been attracting interest as a possible novel therapeutic agent being capable to manage different pathological condition like cardiovascular diseases (CVDs) that remain a major health concern worldwide and the leading cause of death globally. CVDs are defined by World Health Organization a group of disorders of the heart and blood vessels that can include:

- coronary heart disease (a disorder of the blood vessels supplying the heart muscle);
- cerebrovascular disease (a dysfunction of the blood vessels supplying the brain);
- peripheral arterial disease (a disease of blood vessels supplying the arms and legs);
- rheumatic heart disease (damage to the heart muscle and heart valves from rheumatic fever, caused by streptococcal bacteria);
- congenital heart disease (birth defects that affect the normal development and functioning of the heart caused by malformations of the heart structure from birth);
- deep vein thrombosis and pulmonary embolism (blood clots in the leg veins, which can dislodge and move to the heart and lungs);

Regarding heart attacks and strokes they are usually defined acute events and resulted mainly caused by a blockage that prevents blood from flowing to the heart or brain. Fatty deposits on the inner walls of the blood vessels that supply the heart or brain represents the most common reason for this is a build-up of. Strokes can even be caused by bleeding from a blood vessel in the brain or due to the presence of blood clots [12].

In this perspective, it's even more interesting to know that MSC-derived sEVs have shown beneficial outcomes similar to cell therapy concerning regenerative and neovascular actions in addition to their anti-apoptotic, anti-remodeling, and anti-inflammatory actions. In addition, sEVs secreted by MSCs have shown cytoprotection, stimulation of angiogenesis,

and they can even modulate macrophage infiltration in peripheral arterial diseases, atherosclerosis, and myocardial infarct [13-20].

In vivo, MSCs are located in niches characterized by low-oxygen conditions, and conversely, in vitro culture conditions are often at atmospheric oxygen tensions [21]. However, it has been observed that hypoxic culture condition could significantly enhance the secretion of angiogenic mediators from MSCs. Culturing MSCs under more physiologically relevant conditions of low-oxygen tension may uniquely benefit the expansion, differentiation, adhesion, growth factor secretion, and regenerative potential of ASCs (Figure 2) [22,23].

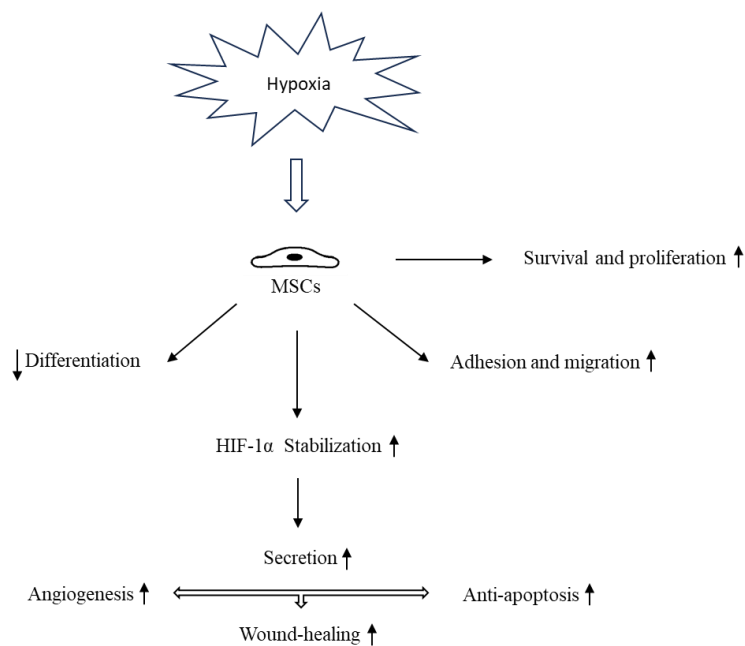


Figure 2: Responses of MSCs undergoing hypoxia condition;

As well as the cells, even the sEVs derived from MSCs preconditioned by hypoxia promote the angiogenesis, proliferation, and migration of endothelial cells in vivo and in vitro [20]. Besides, the overexpression of the hypoxia-inducible factor 1 $\alpha$  (HIF-1 $\alpha$ ) in MSCs in general and in ASCs in detail, improves angiogenesis in endothelial cells by the release of Jagged1-carrying sEVs [21]. Iron-chelating deferoxamine mesylate (DFO) can be added to the culture medium as a useful substitute to create a hypoxia condition. Several studies have also proved that compared with hypoxia, the hypoxia mimetic agent like DFO, could also induce related

hypoxic genes. DFO is a prolyl-4 hydroxylase inhibitor that stabilizes HIF-1 $\alpha$  under normoxic conditions through the inhibition of the prolyl hydroxylases enzyme. This enzyme targets the HIF-1 protein through degradation. As previously mentioned, hypoxic conditioning enhances the regenerative potential of ASCs through the upregulation of the transcription factor HIF-1 $\alpha$ , so the iron-chelating DFO can be used in order to mimic the increase in HIF-1 $\alpha$  expression [22]. DFO-treated ASCs showed an improved regenerative potential that has been attributed to the increased release of angiogenic factors [23]. If this effect is also mediated by the secreted sEVs has not yet been investigated.

On the basis of the above premises, the aim of this study was to investigate the biological effects of sEVs released from DFO-treated ASCs (DFO-sEVs) on human umbilical vein endothelial cells (HUVECs) as cellular model of a tissue involved in CVDs. Transcriptome sequencing and miRNA profiling of the sEV cargo (sEV-miRNA) of treated HUVECs have shown improvements in mitochondrial oxidative phosphorylation, as well as signaling pathways related to cell proliferation and angiogenesis.

## Results:

### 1) ASCs Morphology and Viability Analysis

The first evaluation was to observe the morphology and test the viability of the cells in order to understand if the DFO affects ASCs in a negative way. The ASCs showed a typical elongated morphology as reported in Figure 3 and the MTT test performed after 48 h of culture, demonstrated that there were no changes in the viability state of the cells with or without DFO treatment, showing a comparable absorbance between the samples.

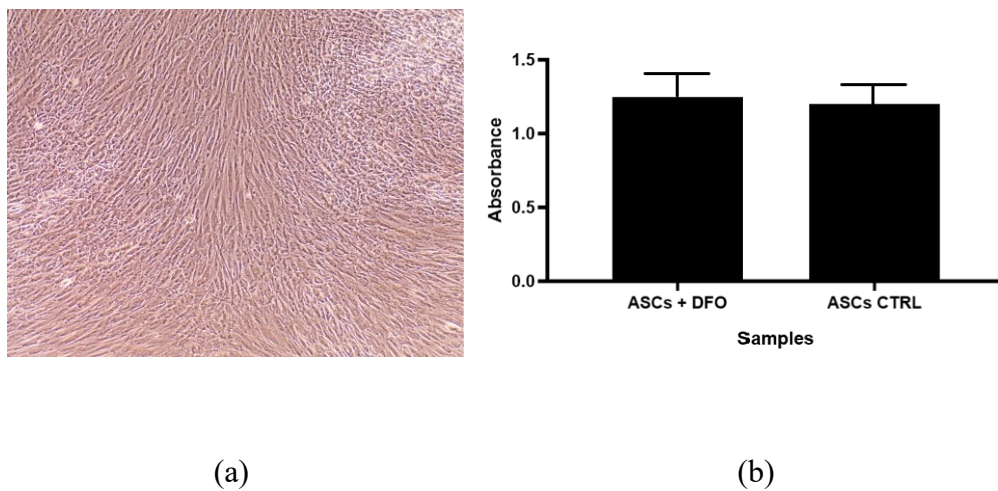


Figure 3: (a) Optic microscope picture of ASCs (magnification 10X) with elongated shape; (b) Viability test after 48 h of DFO treated and untreated cells; viability was measured as absorbance of the samples that was 1,246 nm and 1,202 nm respectively; data were obtained as the mean  $\pm$  standard deviation ( $n = 3$  per group).

### 2) DFO-sEVs Production and HUVEC Treatment

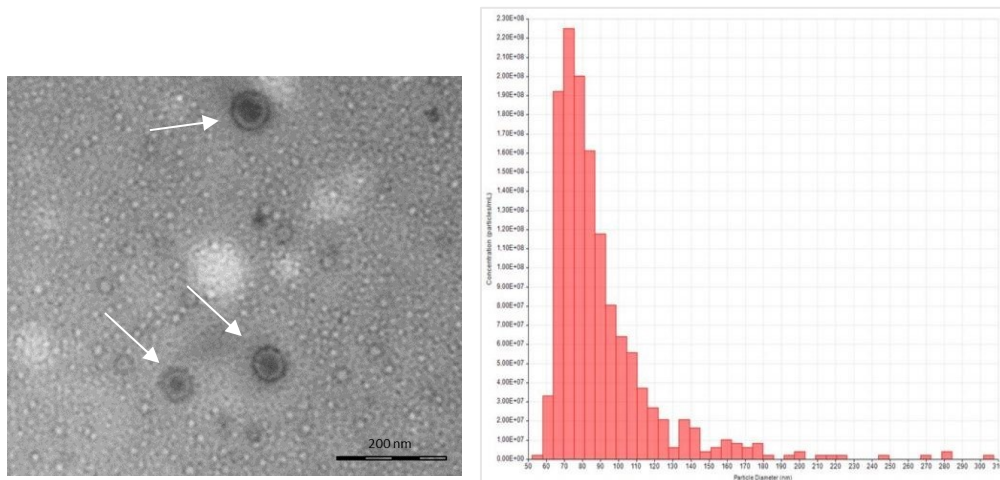
To create a right environment to collect sEVs for the following HUVEC treatment, human ASCs were treated with 100  $\mu$ M DFO to stabilize HIF-1 under normoxic conditions [24,25]. In detail, commercially available hASCs were used and seeded in a six-well plate at a density of  $4 \times 10^5$  hASCs/well in a complete medium added of FBS. The day after, cells were washed two times with phosphate-buffered saline (PBS, EuroClone) and then, incubated with 100  $\mu$ M deferoxamine mesylate (DFO; Thermo Fisher Scientific, Waltham, MA, USA) with a EV-depleted DMEM overnight. Conditional medium was harvested after the overnight

treatment, and the DFO-sEVs were isolated thanks to a Norgen's technology that exploits proprietary resin, which allows the purification of intact extracellular vesicles [2].

The DFO-sEVs appeared like rounded structures with a typical bilayer membrane, below 100 nm in the transmission electron microscopy (TEM) (Figure 4a). Using tunable resistive pulse sensing (RPS) analysis, it was confirmed the dimension of the vesicles with a mean diameter of  $90 \pm 30.9$  nm and mode of 73 nm. Particle size distribution of D10, D50, and D90 was 67 nm, 82 nm, and 121 nm, respectively whereas average concentration resulted to be  $1.33 \times 10^9$  particles/mL (Figure 4b). In addition, superficial membrane markers were analyzed using flow cytometry to verify sEVs nature. These DFO-sEVs, resulted positive for superficial markers CD81 and CD63, as shown in Figure 4c.

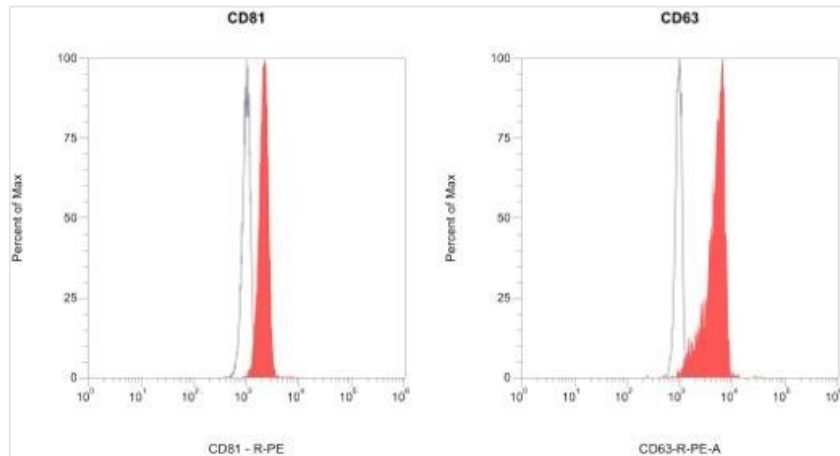
Speaking about the treatment, purified DFO-sEVs were added to HUVEC cultures for 24 h, and sEVs internalization was also detected thanks to the observation under confocal microscopy. As reported in Figure 4d, HUVECs incubated with PKH67 green fluorescent DFO-sEVs (on the left) are compared with cells incubated with the negative control (on the right), probe-labeled PBS. The red areas show a double magnification of the green areas. In addition, a double check was carried out in order to verify the internalization of the DFO-sEVs inside HUVECs. The sEVs were labeled with PKH26 and observed as red dots inside the cytoplasm of the cells, previously marked with the Phalloidin (Alexa Fluor™ 488) to highlight the actine filaments and the Hoechst 33342 to label the nuclei (Figure 4e).

HUVECs were then left for 72 h in an EV-depleted medium after which total RNA was isolated from the cells and conditioned medium was harvested for sEVs (HUVEC-sEVs) collection.

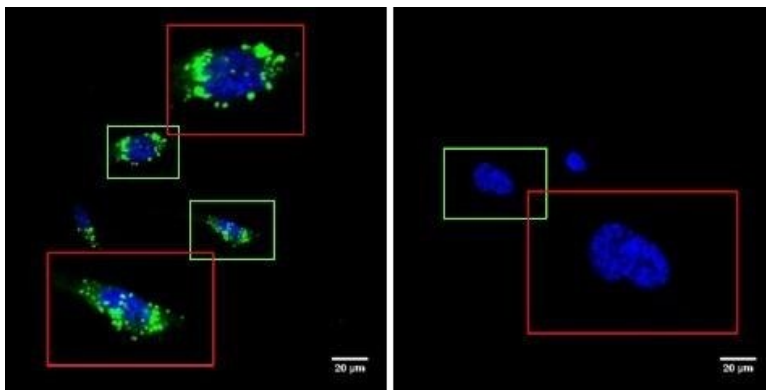


(a)

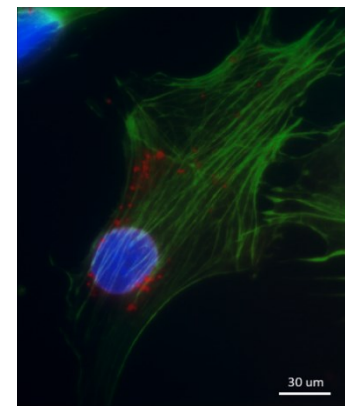
(b)



(c)



(d)

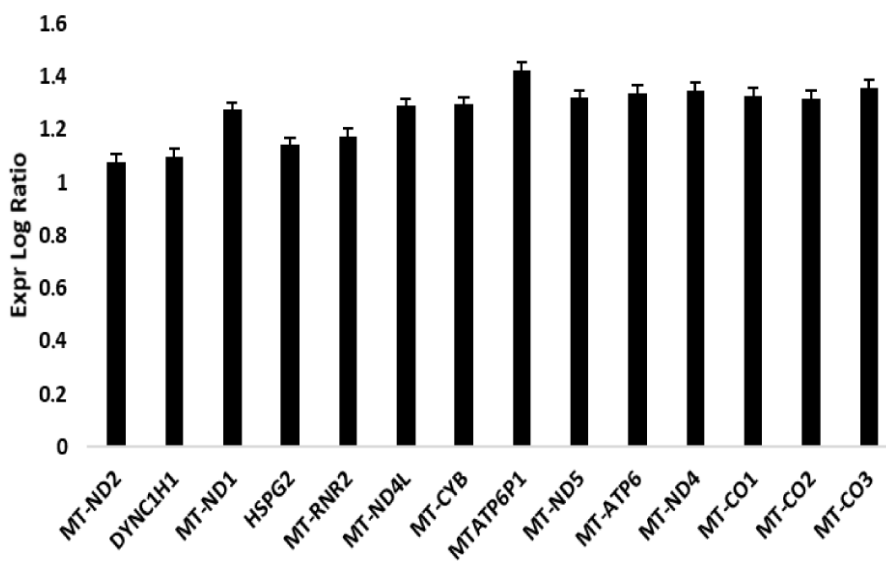


(e)

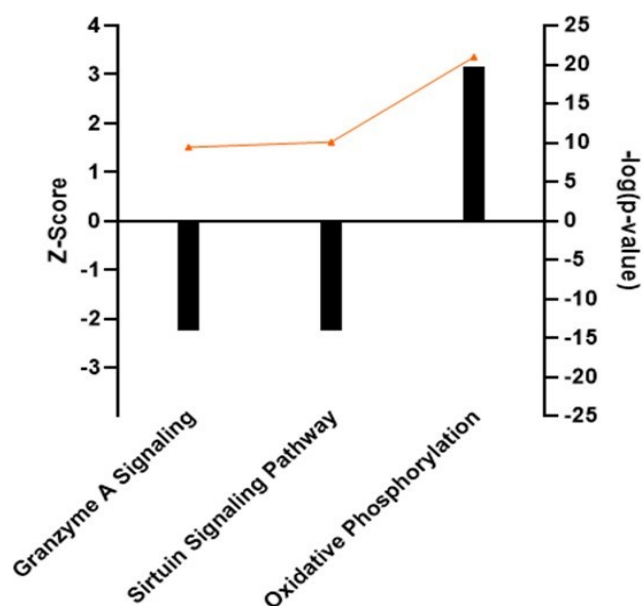
Figure 4. DFO-sEVs characterization and internalization by HUVEC observation. (a) Representative image of DFO-sEVs at TEM. The sEVs appear with the typical bilayer cup-shaped membrane structure (white arrows); (b) Particle size distribution and concentration of DFO-sEVs analyzed with tunable resistive pulse sensing: mean diameter of  $90 \pm 30.9$  nm, mode of 73 nm, and particle size distribution of D10 67, D50 81, and D90 121. The average concentration was  $1.33 \times 10^9$  particles/mL. (c) Flow cytometry of DFO-sEVs showing positivity to surface markers: CD81 and CD63 (DFO-sEVs in red, vehicle in gray). (d) Representative pictures of the uptake of PKH67-labeled green fluorescent DFO-sEVs (left) and of negative control, i.e., PKH67-labeled PBS, (right) after 24 h of incubation. Nuclei labeled with Hoechst 33342 (blue). Red areas are 2 $\times$  magnification of adjacent green area. (e) Confirmation representative image of DFO-sEVs internalization by HUVEC: sEVs with PKH26 internalized by HUVEC are visible as red spots inside cytoplasmic region of cells. Zeiss Axio-vert 200M Fluorescence Microscope was used to capture the images (63x oil objective). Nuclei of the cells are labeled in blue; Actin filaments are stained in green;

### 3) RNA Sequencing of HUVECs After Treatment with DFO-sEVs and Mitochondria Membrane Potential analysis

The total RNA extracted from DFO-sEVs-treated HUVECs and untreated HUVECs were sequenced, and ingenuity pathway analysis (IPA) was performed on differentially expressed genes (DEGs). Only fourteen genes were significantly upregulated in HUVECs treated with DFO-sEVs as reported in Figure 5a. Most of resulted significant DEGs were related to the mitochondria. Among these, there were genes encoding mitochondrially encoded NADH dehydrogenase (MT-ND1, MT-ND2, MT-ND4, MT-ND5, and MT-ND4L), mitochondrially encoded cytochrome c oxidase (MT-CO1, MT-CO2, and MT-CO3), mitochondrially encoded cytochrome b (MT-CYB), mitochondrially encoded ATP synthase 6 (MT-ATP6, MT-ATP6P1), dynein cytoplasmic 1 heavy chain 1 (DYNC1H1), and heparan sulfate proteoglycan 2 (HSPG2). Basing on the gene expression status, IPA is able to predict and perform a canonical pathways analysis. This prediction revealed that the deregulated genes are associated with three biological pathways: granzyme A signaling, the sirtuin signaling pathway, and oxidative phosphorylation (Figure 5b). The granzyme A and sirtuin pathways were significantly downregulated in HUVECs treated with DFO-sEVs (with a Z-score of -2.236; log (p-value) of - 9.43 and 10.1, respectively); meanwhile, oxidative phosphorylation pathway resulted significantly upregulated (with a Z-score of +3.162;  $-\log$  (p-value) of 21).



(a)

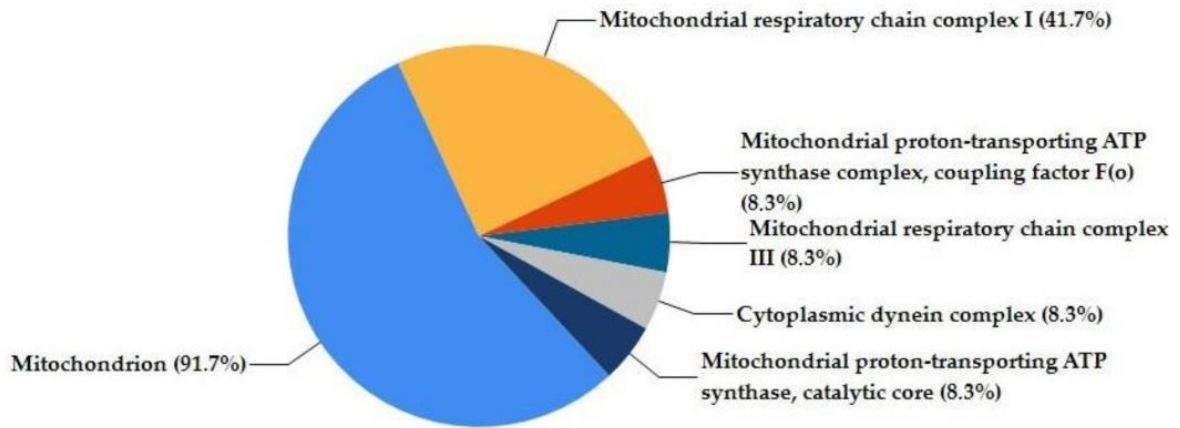


(b)

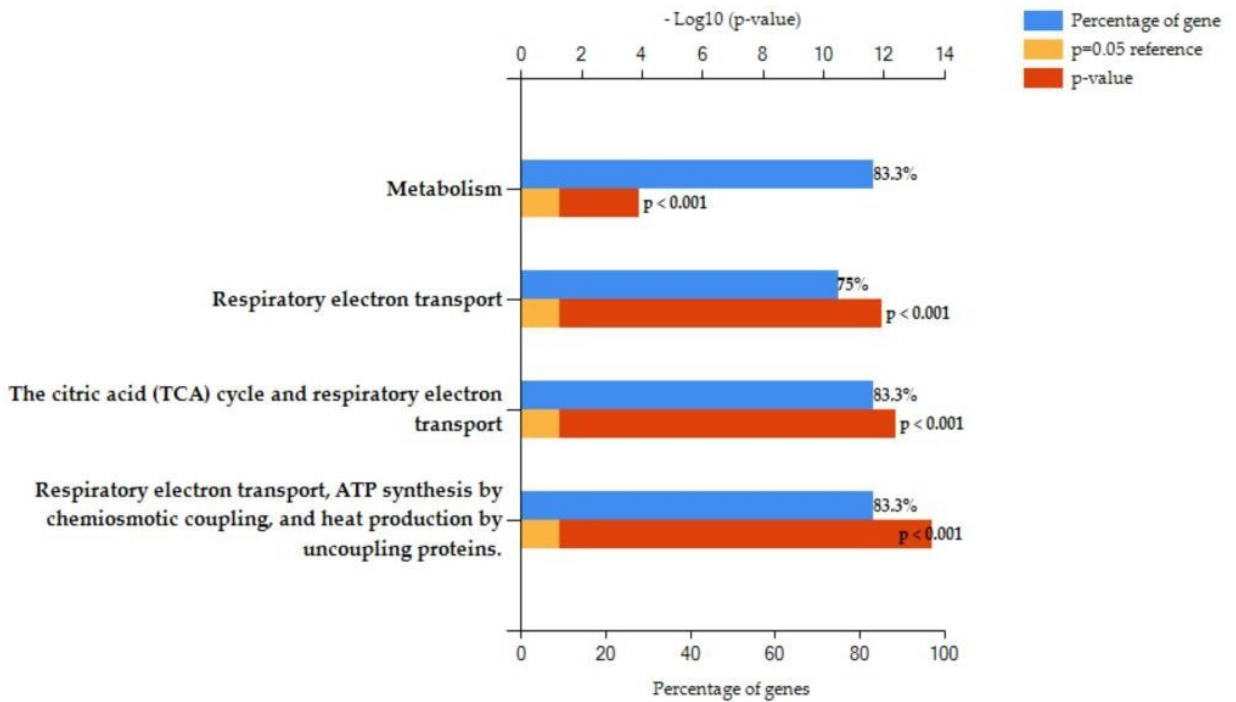
Figure 5. Ingenuity pathway analysis (IPA) on HUVECs treated with DFO-sEVs vs untreated HUVEC. (a) Gene expression reported as logarithmic ratios (Exp log ratio) of differentially regulated genes for treated HUVECs compared to untreated HUVECs. (b) IPA Canonical pathway analysis: predicted state of activation/inhibition of the molecular signaling is displayed as Z-Score (black bars), and the significance is expressed as  $-\log_{10}(\text{p-value})$  (orange line).

To further evaluate the molecular status of the treated cells with this gene expression profile, a functional enrichment analysis on the 14 significant genes was performed using FunRich software, that is able to provide enrichment studies for several categories like cellular component, biological pathway, and biological process (Figure 6). As mentioned before, significant upregulated genes were mostly mitochondrial components related, as shown in the pie chart (Figure 6a). Along the same line, even the biological pathways analysis were mitochondria related, resulting enriched with a significant  $p\text{-value} < 0,001$ . The specific resulting pathways enriched were the following: respiratory electron transport, ATP synthesis by chemiosmotic coupling, heat production by uncoupling proteins, the citric acid (TCA) cycle and respiratory electron transport, the respiratory electron transport, and

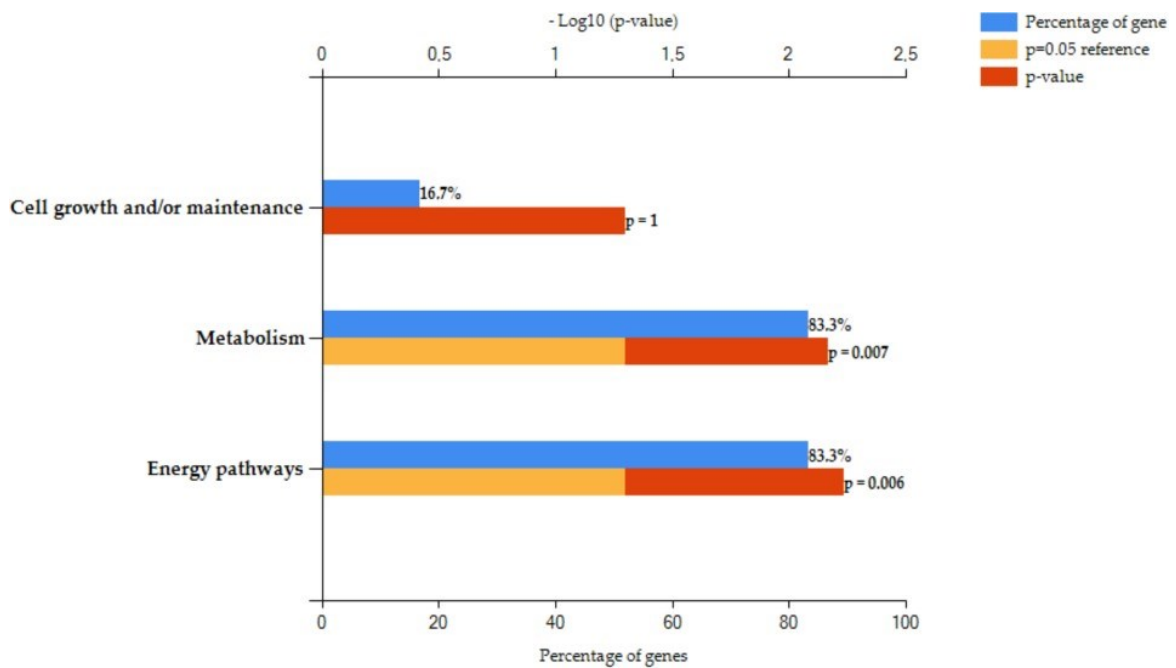
metabolism (Figure 6b). In addition, three biological processes resulted enriched in cell growth and maintenance, metabolism, and energy (Figure 6c).



(a)



(b)



(c)

Figure 6. Functional enrichment analysis with FunRich software version 3. (a) Pie chart of cellular component enrichment. (b) Biological pathway enrichment. (c) Biological process enrichment. Percentage of genes involved in each function (blue bar), p-value (red bar), and reference (orange bar).

Since the mitochondria activation resulted from the RNA sequencing and subsequently enrichment analyses performed on treated cells, another mitochondria parameter has been investigated. Indeed, HUVECs treated with DFO-sEVs showed amplified mitochondrial membrane potential compared to untreated cells, as displayed by the microscopy analysis with a fluorescent probe that accumulates in the mitochondria in a membrane-potential-dependent manner (Figure 4).

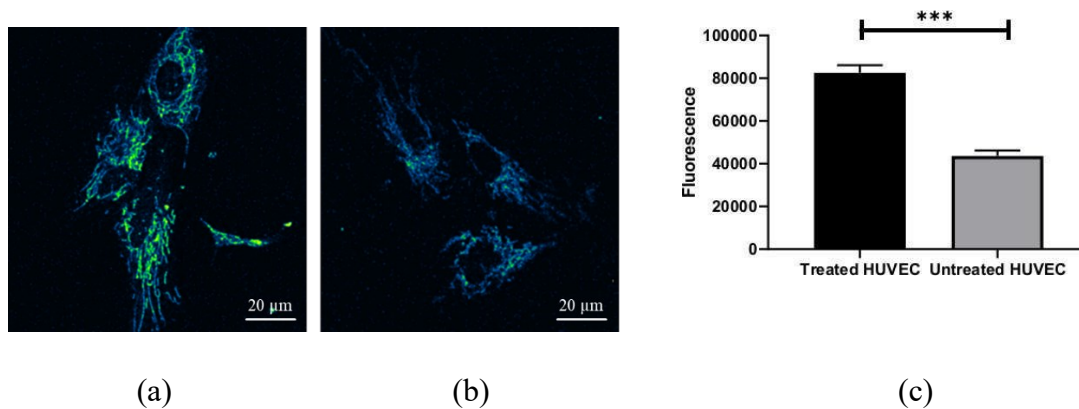


Figure 7. Mitochondrial membrane potential of HUVECs treated with DFO-sEVs compared to untreated cells. Representative images of (a) treated and (b) untreated HUVECs with confocal microscope. (c) Fluorescence intensity quantification with ImageJ software vs8. \*\*\* p-value < 0.001.

#### 4) sEV-miRNA Expression Profiling of HUVECs Treated with DFO-sEVs

In order to understand if even the mediators of the HUVECs after DFO-sEVs treatment can be affected, a HUVEC-sEVs complete analysis was executed. In details, a study of the size, concentration, the content (focusing on miRNAs) and a subsequent enrichment analysis of these vesicles compared to the control ones were performed.

After the HUVEC-sEVs isolation from the cells medium as previously described [26], the TEM image and tunable resistive pulse sensing analysis were performed. Resulting outputs showed the distinctive features of sEVs with a bilayer cup-shaped membrane structure as a result of dehydration during sample preparation (Figure 5a), and particle size dimension between 70–130 nm (Figure 5b).

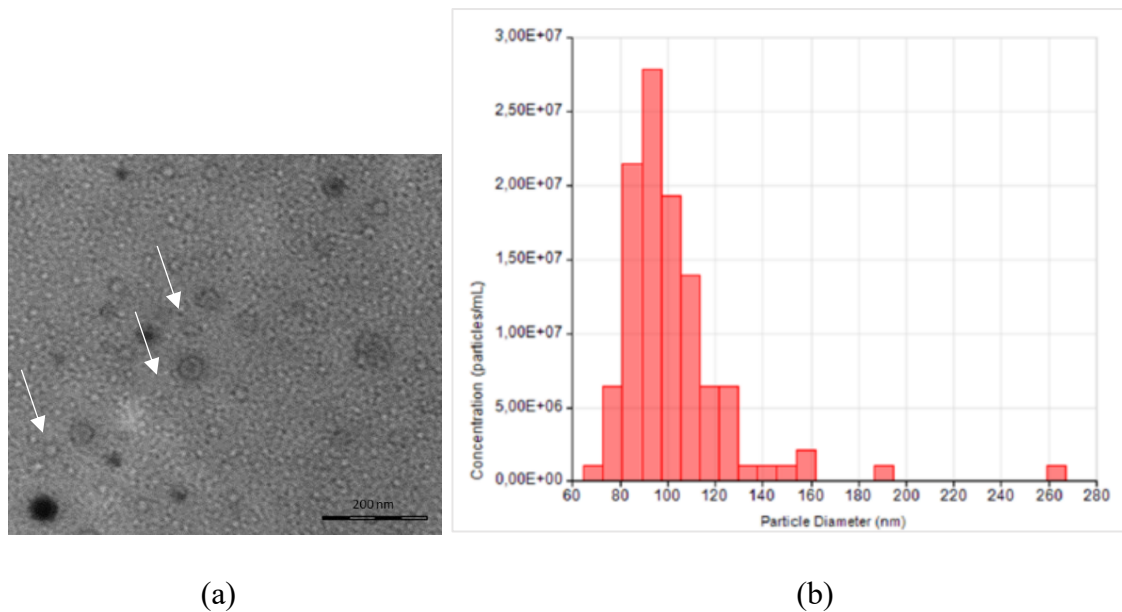


Figure 8. HUVEC-sEVs characterization. (a) Representative TEM image of the sEVs with a typical bilayer membrane (white arrows). (b) Size distribution and concentration using tunable resistive pulse sensing instrument qNano (iZON Science, Oxford, UK). sEVs show an average hydrodynamic diameter equal to  $102 \pm 24.9$  nm, with a mode of 93 nm, d10 83 nm, d50 97 nm, d90 123 nm. Average concentration was  $2.21 \times 10^7$  particles/mL.

To study sEVs content, Illumina sequencing and subsequent IPA analysis were performed on sEV-miRNAs of treated HUVECs. A total of 89 miRNAs were identified by the sequencing (Figure 6a). Among these miRNAs, a cluster of 18 miRNAs showed a significant fold-regulation value (with a cut-off  $> 2$  for upregulation and a cut-off  $< -2$  for down regulation). In detail, 11 miRNAs resulted up-regulated (has-let-7d-5p, has-miR-107, has-miR-143-3p, has-miR-191-5p, has-miR-196b-5p, has-miR-23b-3p, has-miR-27a-3p, has-miR-34a-5p, has-miR-361-5p, has-miR-423-3p, has-miR-9-5p) and the other remaining 7 miRNAs resulted down-regulated (has-miR-10a-5p, has-miR-10b-5p, has-miR-148a-3p, has-miR-151a-3p, has-miR-196a-5p, has-miR-29c-3p, has-miR-654-3p) (Figure 6b).

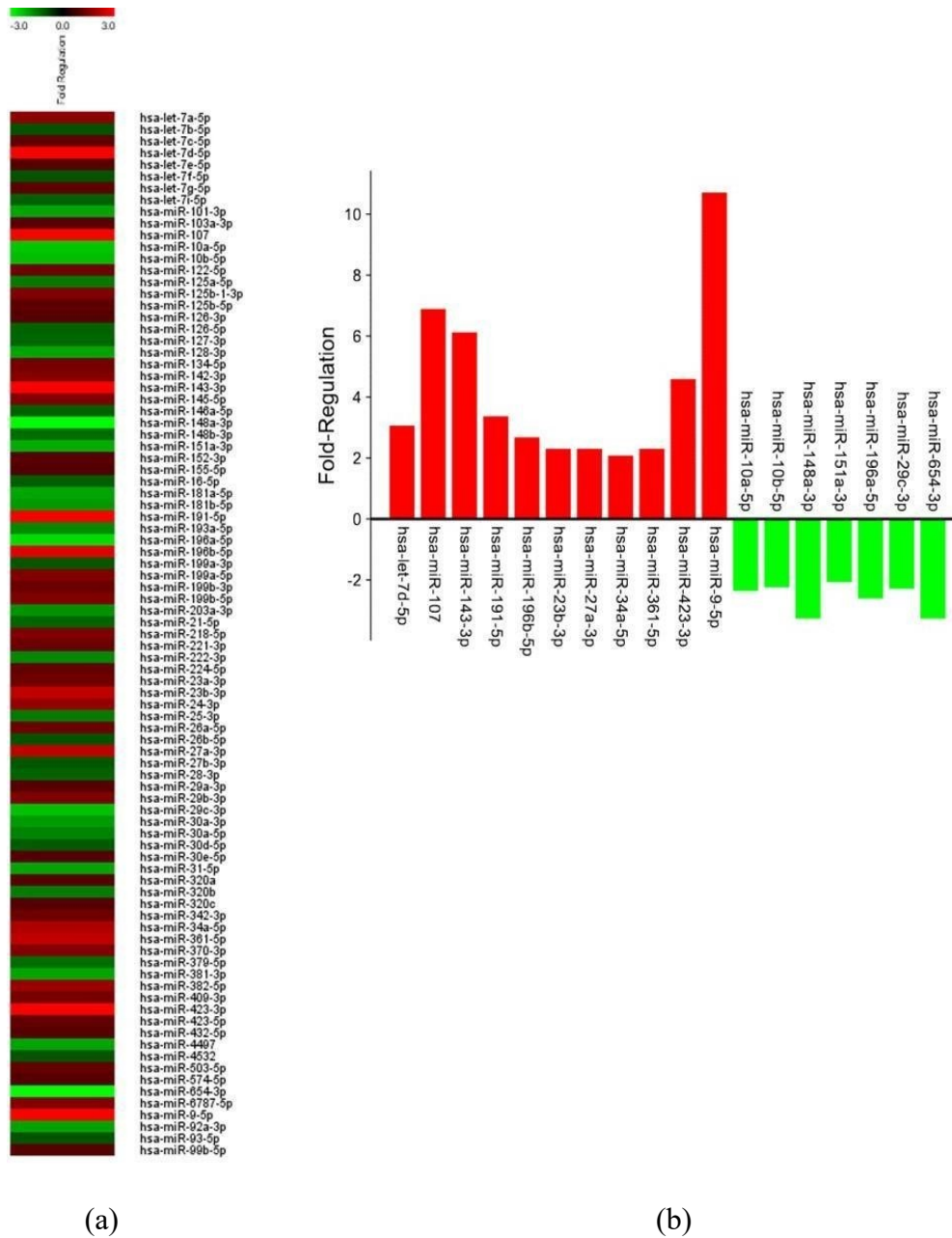
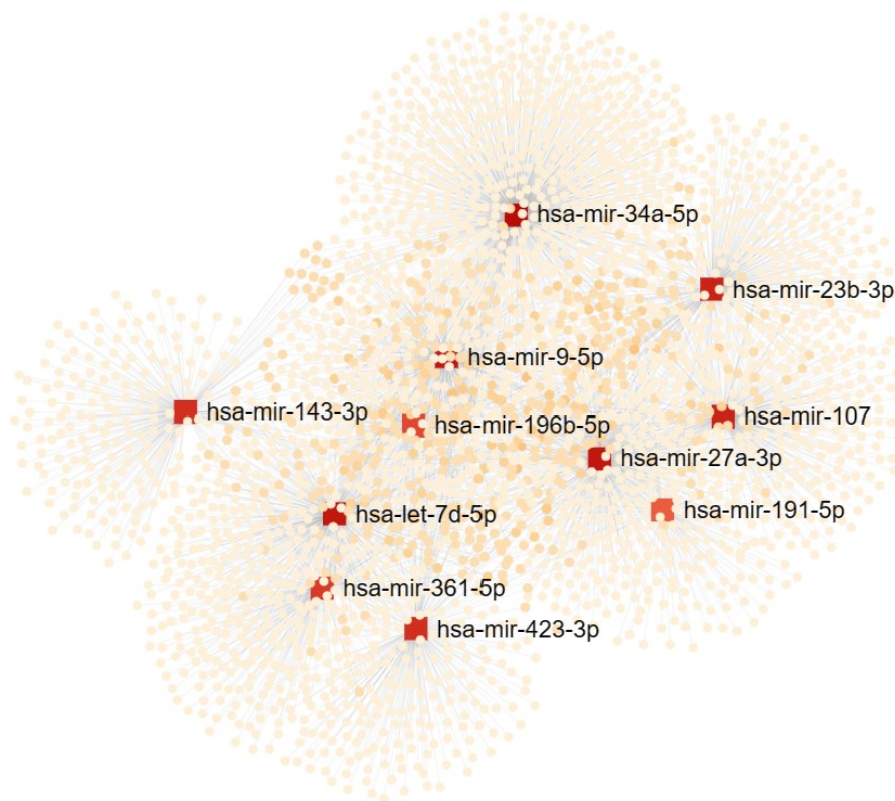


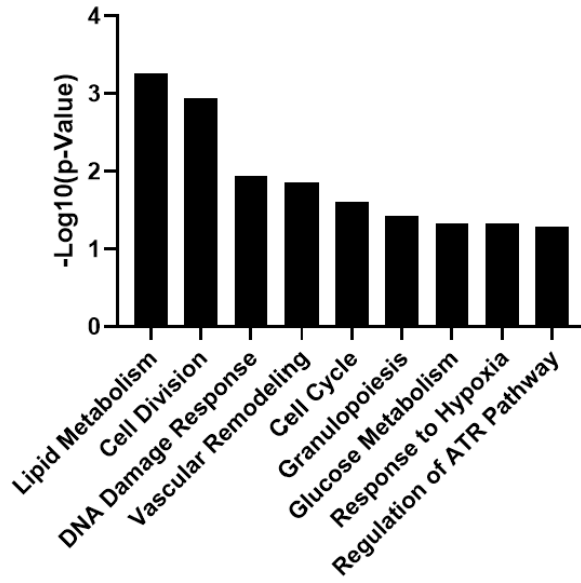
Figure 9. sEV-miRNA sequencing of HUVECs treated with DFO-sEVs. (a) Fold regulation of the totality of 89 significant identified miRNAs (b) 18 more significant miRNAs histogram: 11 up-regulated miRNAs with a fold regulation cut-off > 2 (red bars) and 7 down-regulated miRNAs with a fold regulation cut-off < -2 (green bars).

To make a prediction of the possible function and influence of the 18 significant miRNAs on possible target cells, a functional enrichment analysis on upregulated and downregulated

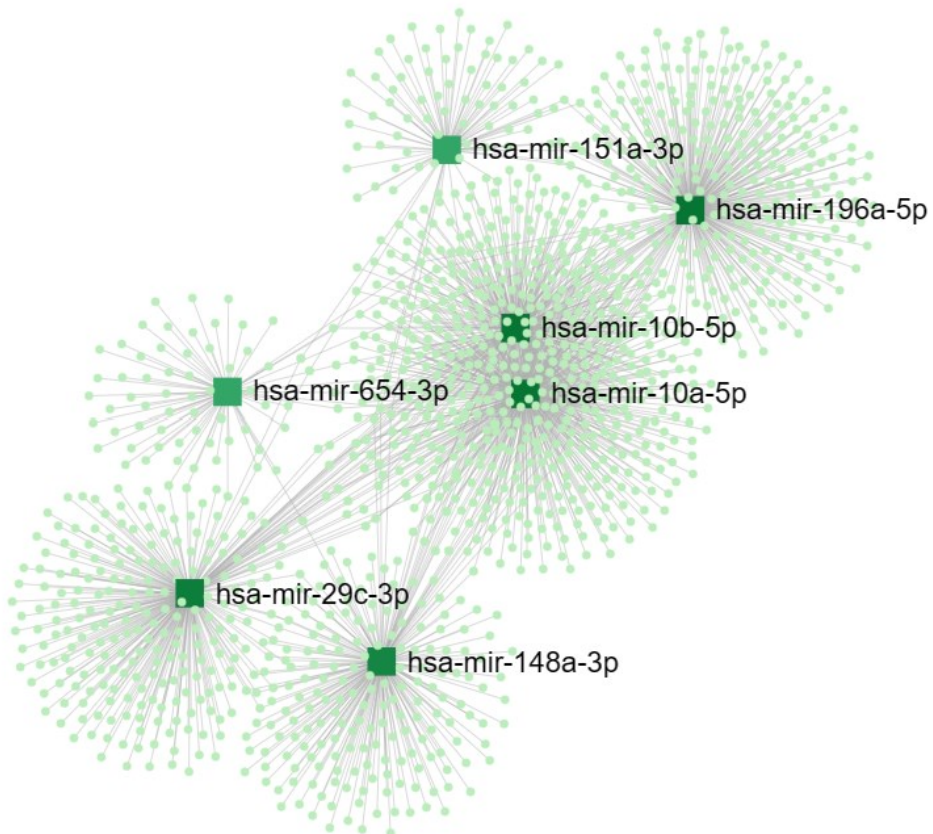
miRNAs was performed using the miRNet software Vs2 with miRTarBase v8.0 as reference database. From the analysis related to up-regulated miRNAs cluster, 9 molecular pathways resulted significantly enriched as reported in Figure 10b with a p-value < 0,05. Regarding the down-regulated cluster instead, 7 molecular pathways resulted significantly enriched with a p-value <0,05 as shown in Figure 10d.



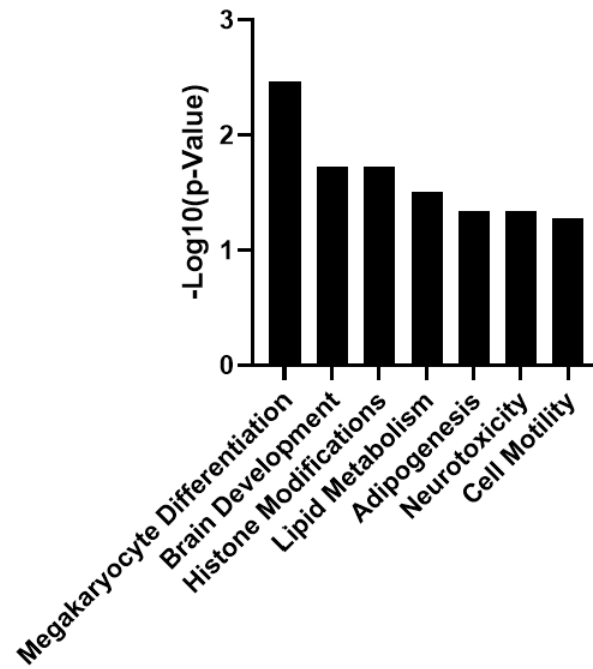
(a)



(b)



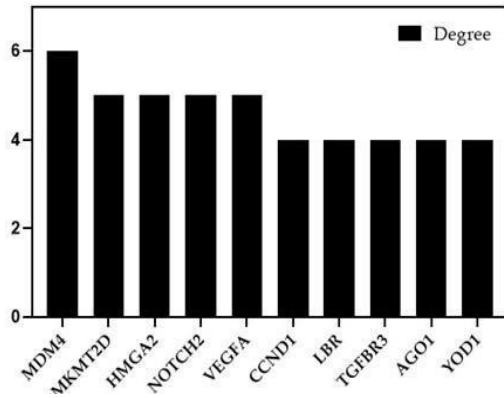
(c)



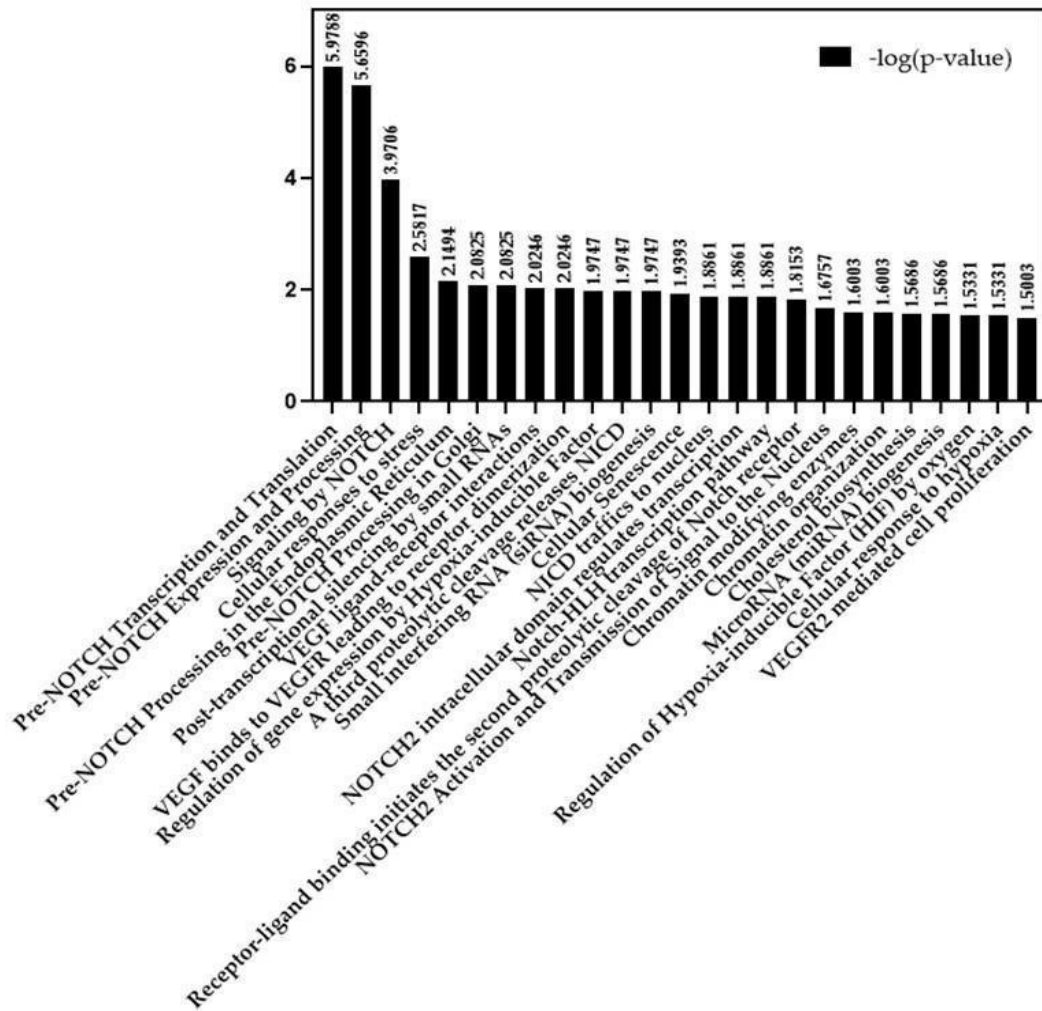
(d)

Figure 10: Functional enrichment analysis on 18 significant miRNAs; Representative network with the main target genes for up-regulated miRNAs (a) and down-regulated miRNAs (c); Significant molecular function enriched with a p-value < 0,05 (reported as -Log(p-value)) for the 11 up-regulated miRNAs (b) and the 7 down-regulated miRNAs (d);

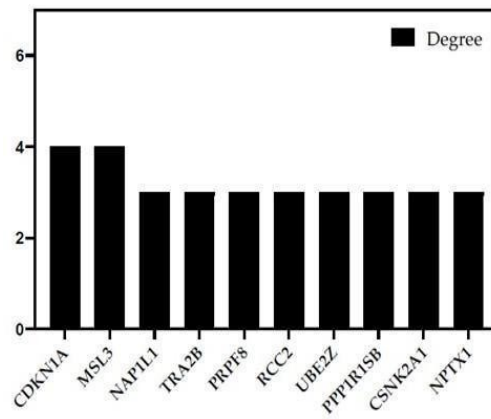
Subsequent to the enrichment on the miRNAs cluster, a functional enrichment analysis on the main target genes of each group was performed. In order to do that, Reactome was selected as reference database. In Figure 8a were shown the 10 main target genes of the 11 upregulated miRNAs, such as MDM4, NOTCH2, VEGFA, CCND1, and TGFBR3. All these target genes encoding proteins and receptors resulted related to several biological pathways of NOTCH, VEGFR, and HIF (Figure 8b). Speaking of the ten main target genes of the 7 downregulated miRNAs reported in Figure 8c (CDKN1A, MSL3, NAP1L1, TRA2B, PRPF8, RCC2, UBE2Z, PPP1R1SB, CSNK2A1 and NPTX1), they resulted related to cell proliferation and cell cycle progression (Figure 8d).



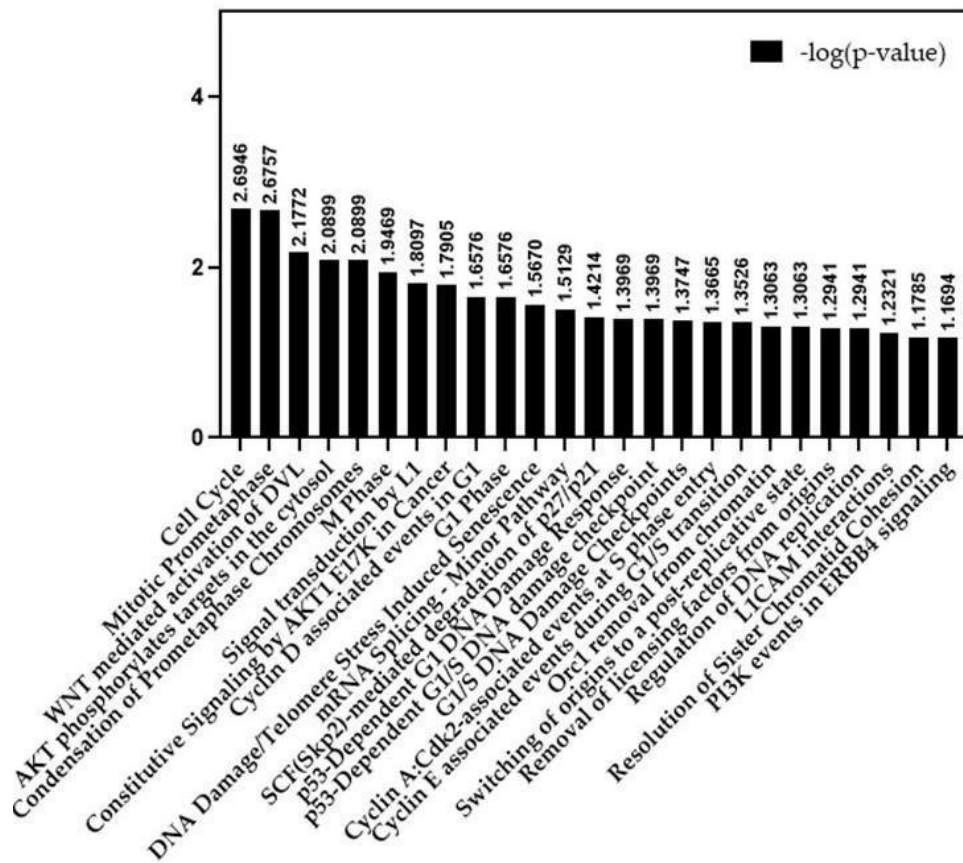
(a)



(b)



(c)



(d)

Figure 11. Functional enrichment analysis of sEV-miRNA target genes of treated HUVECs. (a) The 10 main target genes of the upregulated sEV-miRNAs. (b) Biological pathways enriched on these target genes. (c) The 10 main target genes of the downregulated sEV-miRNAs. (d) Biological pathways enriched on these target genes.

## Discussion

Small Extracellular Vesicles (sEVs) derived from MSCs grown under hypoxic conditions are able to induce desirable biological effects on multiple target cells, such as improvements in proliferation, angiogenesis and migration, giving a global regenerative result [20] (Figure 2). These promising effects seem to be related to hypoxia, which pushes HIF-1 $\alpha$  mRNA expression through PI3K/AKT pathway and the subsequently activation of NF $\kappa$ B [27]. Another research group reported that HIF-1 $\alpha$  overexpression in dental-pulp-derived MSCs, improves and enhance the angiogenesis in endothelial cells by the release of Jagged1-carrying exosomes [21]. CVDs represent a major health concern worldwide and the leading cause of death globally. For this reason, the research of innovative treatment of CVDs is constantly requested. MSC-derived sEVs have been attracting interest as a possible novel therapeutic agent being capable to manage different pathological condition like cardiovascular diseases.

On these bases, in the first chapter of the present study, ASCs were treated using the iron-chelating DFO to induce an increase in the HIF-1 expression. The action of DFO is to stabilize HIF-1 under normoxic conditions through the inhibition of the prolyl hydroxylases enzyme, which targets HIF-1 protein through degradation [27]. So, the increase of HIF-1 $\alpha$  expression in the cells was induced by the treatment with a molecule capable to stabilize HIF-1 protein through the block of its degradation. The treatment with DFO has been performed overnight and after that, the conditioned culture medium was harvested to collect and isolate sEVs using precipitation. A complete characterization and quantification of these sEVs were performed, with even the imaging by electron microscopy (TEM), particle tracking techniques, and flow cytometry for the membrane markers, following the guidelines of Minimal Information for Studies of Extracellular Vesicles [28] (Figure 4). In the TEM observation, sEVs appeared with a diameter of less than 100 nm and they showed the typical bilayer cup-shaped membrane structure, due to dehydration during sample preparation [29]. The qNano device was exploited to obtain particle size, particle size distribution, and particle concentration, using the tunable resistive pulse sensing (RPS) technique. In detail, particle mean diameter was 90 nm and the mode was 73 nm. The particle size distribution of D10, D50, and D90 was instead 67 nm, 82 nm, and 121 nm, respectively. Other research group like Connor et al., has previously analyzed EVs with a qNano device, defining the particles with the average size of 92 nm as small EVs [30]. In addition, the presence of sEVs markers was analyzed using the classical flow cytometry of bead-captured EVs [31]. To realize that, polystyrene beads (4.5  $\mu$ m diameter) coated with a primary monoclonal antibody specific

for the CD63 or CD81 membrane antigen were incubated overnight with DFO-sEVs. After the incubation, the bead-bound sEVs were labeled with a fluorescent-conjugated antibody for CD63 or CD81 markers. Taking together all these data allowed to define the particles isolated from DFO-treated MSCs as small EVs, because they showed a bilipid membrane vesicles and resulted with a mean diameter of 90 nm and positive to sEVs markers CD81 and CD63 (Figure 4). To investigate the possible effect of these vesicles on the main vessel's cells, with a view to their possible use in the CVDs treatment, DFO-sEVs were used to treat the recipient endothelial cells (HUVEC) prior to transcriptome sequencing and sEV-miRNA profiling (Figure 4d and 4e). Ingenuity Pathway Analysis software (IPA) of the QIAGEN, was used for studying transcriptome of HUVECs treated with DFO-sEVs. Despite the poor result of the RNA sequencing performed on HUVEC, fourteen genes resulted significantly upregulated. Among these, 12 were mitochondrial genes related to the oxidative phosphorylation, including MT-ND2, MT-ND1, MT-RNR2, MT-ND4L, MT-CYB, MT-ND5, MT-ATP6, MT-ATP6P1, MT-ND4, MT-CO1, MT-CO3, MT-CO2, and MTATP6P1. While the last two genes remaining, were DYNC1H1 and HSPG2 (Figure 5a). Specifically, DYNC1H1 encodes cytoplasmic dynein that acts as a motor for the intracellular retrograde motility of vesicles and organelles along microtubules. It is reported that the loss of function of this gene causes a significant decrease in cell viability and cell proliferative ability [32]. Speaking of HSPG2 gene, it encodes for "Perlecan", a proteoglycan key component of the vascular extracellular matrix, which is able to maintain the endothelial barrier function [33]. Observing the expression profile of DFO-sEV-treated HUVECs, it shown an enhanced mitochondrial activity by the overexpression of proactive genes that could improve several biological functions such as proliferation, development, and preservation of the extracellular matrix integrity. In addition to the RNA sequencing analysis, IPA software provides many different predictions, so it was even performed to identify the canonical pathways that result significant, basing on the transcriptome sequencing outcome and on categorize upregulated genes. Regarding treated HUVEC, three canonical pathways resulted with significant predictions: the granzyme A signaling and sirtuin signaling pathway resulted with an inactivated profile while oxidative phosphorylation pathway showed an activated profile (Figure 5b). Both the inactivated molecular pathways are responsible to induce bad effect on the cells. Indeed, Granzyme A signaling induces a caspase-independent cell death pathway [34], whereas sirtuin signaling can induce aging [35]. The only one resulted with an increased functionality was the oxidative phosphorylation, well known as the metabolic process that leads to ATP production inside cells [36]. Basing on these results, it was possible

to say that the canonical pathways identified by IPA highlighted a possible positive effect of DFO-sEVs on HUVECs, since they resulted increased in the expression of genes involved in oxidative phosphorylation and therefore the production of energy. On the contrary, it turned out that the treatment with DFO-sEVs reduced the expression of genes connected to cell death and aging. All these first data were then further verify performing a functional enrichment analysis using FunRich software and through mitochondrial membrane potential detection in order to evaluate a real increasing of the mitochondria activity of the treated cells. As expected, FunRich enrichment allowed to observe improvement in mitochondrial respiratory electron transport and ATP production, cell growth, and maintenance (Figure 6). Observing the enrichment analysis results, it was possible to see that IPA canonical pathway prediction and FunRich functional enrichment agreed in recognize same activated mitochondria related biological processes involved in mitochondria respiration.

Another way to investigate the activation state of the mitochondria is the evaluation of its membrane potential. This was analyzed using a probe (MitoTracker Red CMXRos, Thermo Fisher Scientific) that accumulates in the mitochondria in a membrane-potential- dependent manner. The microscopy analysis performed on *in vivo* cells, further confirmed that the mitochondrial activation increased for DFO-sEV-treated HUVECs compared to untreated cells (Figure 7). It could be interesting to plan another study of the mitochondria as a 3D imaging analysis using fluorescence probes in order to observe how the EVs treatment on the HUVECs can affect the general mitochondria network and turnover.

To implement the data about how the HUVEC response to DFO-sEVs treatment, a miRNA sequencing analysis of HUVEC-derived sEVs was performed. Again, even for this sequencing, IPA software was used to get the analysis and result. The sequencing on sEVs miRNAs content revealed 11 upregulated and 7 downregulated miRNAs in the treated HUVECs compared to untreated cells (Figure 9b and 10a). As reported in literature, the eleven upregulated miRNAs (hsa-let-7d-5p, hsa-mir-107, hsa-mir-143-3p, hsa-mir-191-5p, hsa-mir-196b-5p, hsa-mir-23b-3p, hsa-mir-27a-3p, hsa-mir-34a-5p, hsa-mir-361-5p, hsa-mir-423-3p, and hsa-mir-9-5p) have pro-angiogenesis and pro-proliferative action on cells. For instance, mir-9-5p can induce enhancement in angiogenesis, proliferation, and migration and prevent apoptosis in endothelial progenitor cells [37]. Whereas up-regulated miRNAs such as mir-107, mir-143-3p, mir-23b-3p, and mir-27a-3p are reported to have a pro-angiogenic function [38–40]. Furthermore, let- 7d-5p and mir-196b-5p miRNAs have proliferation-inducing functions [41,42]. To obtain a demonstration of this overall influence regulated by this up-regulated cluster of miRNAs, a functional enrichment analysis on them

was done. Using miRNet software to perform the analysis, 9 biological functions resulted enriched on the 11 up-regulated miRNAs of treated cells with a significant p-value  $< 0,05$ : lipid metabolism, cell division, DNA damage response, vascular remodeling, cell cycle, granulopoiesis, glucose metabolism, response to hypoxia and regulation of ATR pathway (Figure 10b). Taking together, all of them seem to be related to a proliferative pattern, with a specific biological pathway linked to the genome repair and protection such as DNA damage response and regulation of ATR pathway, well known as essential regulator for the genome integrity [43]. Moving on the down-regulated miRNAs cluster, seven downregulated miRNAs resulted from the sequencing of treated HUVEC derived sEVs compared to control: hsa-miR-10a-5p, hsa-miR-10b-5p, hsa-miR-148a-3p, hsa-miR-151a-3p, hsa-miR-196a-5p, hsa-miR-29c-3p, and hsa-miR-654-3p (Figure 9b and 10c). Regarding this group of miRNAs, if expressed, they have an anti-proliferative, anti-angiogenic, and pro-inflammatory action [44–48]. Again, miRNet software was exploited to perform a functional enrichment analysis on the down-regulated miRNAs of treated HUVEC-derived sEVs. Seven biological processes resulted enriched with a significant p-value  $< 0,05$ : megakaryocyte differentiation, brain development, histone modifications, lipid metabolism, adipogenesis, neurotoxicity and cell motility (Figure 10d). Showing a different pattern of influences on hypothetical target cells, such as pushing for differentiation like adipogenesis or even inducing bad effect for the cells like neurotoxicity, this enrichment confirmed that, if expressed, these down-regulated miRNAs could induce negative effect on target cells. On these data, it can be assumed that the downregulation of these miRNAs in HUVEC-sEVs could promote proliferation and prevent inflammation in the recipient cells. For another and deeper prediction of the possible influence of the treated-HUVEC-sEVs miRNAs content compared to control, a functional enrichment analysis on the ten main target genes of each up and down-regulated cluster of significant miRNAs was performed using miRNet software. The functional enrichment of the ten main target genes (Figure 11a) of upregulated miRNAs using Reactome as reference database, highlighted a link with the NOTCH, VEGFR, and HIF signaling pathways (Figure 11b), that are related to proliferation and angiogenesis [49]. On the contrary, the functional enrichment on the ten main target genes of downregulated miRNAs (Figure 11c) revealed enrichment of the biological pathways that control the cell cycle progression and AKT/PI3K signaling (Figure 11d) [50].

In the in vitro study here reported, the effects of DFO on ASCs were investigated, with a particular focus on the messages conveyed by the sEVs released after the treatment.

Specifically, human endothelial cells (HUVEC) were treated with sEVs derived from DFO-treated mesenchymal cells in order to evaluate the possible alteration and influence on cellular transcriptomes and miRNA cargo in sEVs. Treated HUVEC transcriptomic analysis revealed a downregulation of genes connected to cell death and aging and an upregulation of mitochondrial genes linked to oxidative phosphorylation. This potentiating effect of the treatment with DFO-sEVs ASCs-derived on endothelial cell mitochondria, was also highlighted by an increase in the mitochondrial membrane potential as proof of an enhanced functionality of mitochondria. In addition, the functional enrichment analysis on the significant deregulated sEV-miRNAs of treated HUVEC compared to control, showed a connection with the signaling pathways related to cell proliferation and angiogenesis.

In conclusion, all the data reported in this study support that adipose-derived mesenchymal cells treated with iron-chelating deferoxamine are able to release small extracellular vesicles capable to induce in the hypothetical recipient endothelial cells, important cells components of blood vessel, molecular pathways and biological processes strongly linked to energy storage, proliferation, and angiogenesis. Taking together, since the potential use of the sEVs as treatment for several kind of diseases, this chapter aims to hypothesize a smart modified sEVs use for CVDs therapy.

## **Material and Methods**

### Adipose Stem Cell Observation and Viability, DFO Treatment

Commercial human adipose stem cells (ASCs; purchased from ScienCell Research Laboratories, Inc., Carlsbad, CA, USA) were seeded with Dulbecco's Modified Eagle's Medium (DMEM, EuroClone, Milano, Italy) added with 10% fetal bovine serum (FBS, EuroClone, Milano, Italy) and 1% Antibiotic–Antimycotic (Thermo Fisher Scientific, Waltham, MA, USA) until the experiments were conducted. In a 6-well plate,  $4 \times 10^5$  hASCs/well (passages between 2 and 4) were seeded in the complete medium. All the cells were observed during all the experiment using EVOS™ XL Core Imaging System (Invitrogen, Waltham, Massachusetts, USA) equipped with a 4x objective. The following day, the cells were washed twice with phosphate-buffered saline (PBS, EuroClone) and then incubated with 100  $\mu$ M deferoxamine mesylate (DFO; Thermo Fisher Scientific, Waltham, MA, USA) in EV-depleted DMEM overnight. In order to evaluate the viability of the cells after the treatment with DFO, an MTT assay was performed.

### ASCs derived DFO-sEVs isolation and characterization using Transmission Electron Microscopy (TEM), Tunable resistive pulse sensing (RPS) and Flow Cytometry

The sEVs (DFO-sEVs) were isolated from the conditioned serum free medium of DFO-treated ASCs using a Cell Culture Media Exosome Purification Kit (Norgen Biotek Corp., Thorold, ON, Canada) according to the manufacturer's instructions. For transmission electron microscopy (TEM), the sEVs were fixed in a 2% glutaraldehyde solution in phosphate buffer (ratio 1:1). After that, sEVs were deposited, rinsed, and stained with heavy metal compounds onto a gridded slide according to the standard protocols. The slide was visualized with a TEM Zeiss EM 910 instrument (Zeiss, Oberkochen, Germany).

The distribution size and diameter of the sEVs were analyzed with a qNano platform (iZON Science, Oxford, UK) that exploits the RPS principle. The analyses were performed with NP150 nanopores and CPC200 calibration particles at 20 mbar pressure. The results were analyzed with the Izon control suite v3.4. Regarding the flow cytometry analysis, CD81-positive and CD63-positive sEVs were isolated with Exosome- Human CD81 Flow Detection (Thermo Fisher Scientific, Waltham, MA, USA) and Exosome- Human CD63 Isolation/Detection Reagent (Thermo Fisher Scientific, Waltham, MA, USA), respectively. Briefly, 100  $\mu$ L of an sEV suspension was incubated with 20  $\mu$ L of CD81 or CD63 magnetic

beads at 4 °C overnight. Bead-bound sEVs were washed twice with an Assay Buffer (0.1% BSA in PBS), and then labeled with 20 µL of mouse anti-human CD81-PE monoclonal antibody (BD Pharmingen™, BD Biosciences, San Jose, CA, USA) or 5 µL of mouse anti-human CD63-PE monoclonal antibody (eBioscience, San Diego, CA, USA). After incubation in an orbital shaker at 1000 rpm for 1 h, the bead-bound sEVs were washed twice with an Assay Buffer. Negative control was performed staining PBS (vehicle) instead of the sEVs. Flow cytometric detection was performed with an Attune™ N T Acoustic Focusing Cytometer (Life Technologies, Carlsbad, CA, USA), and the data were analyzed with the Attune N T Software version 2.5 (Life Technologies).

#### Endothelial Cell Treatment, Observation and Mitochondria Membrane Potential Analysis

Human umbilical vein endothelial cells (HUVECs; Thermo Fisher Scientific, MA, USA) were cultured in an EBMTM-2 basal medium (Lonza, Basel, Switzerland) completed with EGMTM-2 SingleQuots™ Supplements (Lonza). Into 6-well plates, HUVECs (passages between 2 and 4) at  $2 \times 10^5$  cells/well were seeded. After 24 h, 500 µL of DFO-sEVs at a concentration of  $1.33 \times 10^9$  particles/mL or an equal volume of PBS was added to the culture medium for 24 h. After 72 h of resting, the total RNA was isolated from the HUVECs using the Total RNA purification Plus kit (Norgen Biotek, Thorold, ON, Canada) according to the manufacturer's instructions. sEV-miRNA was collected from the conditional medium using Cell Culture Media Exosome Purification and an RNA Isolation Mini Kit (Norgen Biotek, Thorold, ON, Canada) according to the manufacturer's instructions.

For internalization detection and observation, the DFO-sEVs were stained with PKH67 (PKH67 Green Fluorescent, Sigma-Aldrich) for 20 min at 37 °C. An equal volume of PBS without sEVs was labeled with the green fluorescent probe and used as the negative control. Excess unincorporated dye was removed from the labeled solutions by using Exosome Spin Columns (MW 3000) (Thermo Fisher Scientific), following the manufacturer's instructions. Then, HUVECs were incubated with the labeled sEVs for 24 h. After washing with PBS, the nuclei were stained with Hoechst 33342 (ThermoFisher Scientific) for 10 min. The cells were observed with a laser scanning confocal microscopy system (Nikon A1 confocal microscope, Nikon Corporation, Tokyo, Japan) equipped with a 60 objective. The zoomed-in insets were produced with Fiji Vs4 software. In addition to that, another observation was performed using Zeiss Axiovert 200M Fluorescence Microscope (Zeiss, Oberkochen, Germany) to capture the images (63x oil objective). Stained sEVs with PKH26 were

internalized by HUVECs and resulted visible as red spots inside cytoplasmic region of cells. Nuclei of the cells was labeled again with Hoechst 33342 and actine filaments were stained with Alexa Fluor™ 488 Phalloidin (Thermo Fisher Scientific, Waltham, Massachusetts, USA).

In order to evaluate the mitochondrial membrane potential, the cells were incubated with MitoTracker Red CMXRos (Thermo Fisher Scientific) for 30 min at 37 °C. After washing, the cells were immediately observed on a Nikon LiveScan Swept Field Confocal Microscope (SFC) Eclipse Ti equipped with NIS-Elements microscope imaging software and on a confocal laser scanning Olympus FV3000 microscope both equipped with a 63X oil immersion objective (N.A. 1.4). The red signal colocalization rate was evaluated using the JACOP colocalization counter available in the Fiji software (ImageJ). For each condition, the signal was also determined by manually counting the fluorescent puncta. For each ROI, the Manders' parameter was calculated. For each condition, five replicates were observed, and four measurements were performed on each replicate.

#### RNA and miRNAs Sequencing, Data and Functional Enrichment Analysis

Both mRNA sequencing and miRNA profiling were carried out by Area Science Park (ASP, Trieste, Italy) with Illumina sequencing technology. The total RNA was evaluated using NanoDrop 2000 (Thermo Fisher Scientific, Waltham, MA, USA) and Agilent Bioanalyzer 2100 (Agilent, Santa Clara, CA, USA). Libraries were created with 1 µg of the total RNA with the TruSeq Sample Preparation RNA Kit (Illumina Inc., San Diego, CA, USA) according to the manufacturer's protocol. All libraries were quantified with the Qubit dsDNA BR Assay Kit (Thermo Fisher Scientific, Waltham, MA, USA) on a Qubit 2.0 Fluorometer (Thermo Fisher Scientific, Waltham, MA, USA). RNA sequencing was realized on a Novaseq 6000 sequencer (Illumina Inc., San Diego, CA, USA) according to the manufacturer's protocol. FASTQ files were output with the Illumina BCLFASTQ v2.20 software. All raw files' quality was verified with FASTQC software V4 (<http://www.bioinformatics.bbsrc.ac.uk/projects/fastqc>; accessed on 15 October 2022), and low-quality sequences were discarded from the analysis. Selected reads were aligned onto the complete human genome using Splices Transcripts Alignment to the Reference algorithm STAR version 2.7.3 using hg38 Genome Assembly and Genecode.v35 as the gene definition. The resulting mapped reads were included as the input for the feature count functions of the R subread packages and were used as gene counts for differential expression analysis using

the Deseq2 package. Reads comparison was performed between DFO-sEV-treated HUVECs and untreated HUVECs. Differentially expressed genes (DEGs) were selected for  $\log_2(\text{FR}) < 1$  or  $> 1$  and  $p\text{-value} < 0.05$ .

MiRNA-Seq libraries were prepared using the QIAseq miRNA Library Kit (QIAGEN; Hilden, Germany) and sequenced using Novaseq 6000 (Illumina; San Diego, CA, USA) in the 2 150 paired-end mode. Identification of miRNAs in the samples was performed using the QIAseq miRNA-NGS data analysis software V5 considering Single Read as the read type and Read 1 Cycles 75 as the read cycles.

All the datasets from RNA sequencing and miRNA sequencing were analyzed with the Qiagen Ingenuity Pathway Analysis (IPA) software. For the RNA sequencing analysis, IPA categorized all deregulated express genes (DEGs) in canonical pathways. IPA can make a prediction on possible diseases and functions, which were ranked based on their significance ( $p\text{-value}$ ) and predicted state of activation/inhibition ( $z\text{-Score}$ ). The  $Z\text{-score}$  value was set with cut-off  $< - 2$  or  $> +2$ . RNA sequencing was used to perform functional, biological pathway, biological process, and cellular component enrichment with the FunRich software [51], while MiRNet was used to analyze functional enrichment for miRNA sequencing. miRNet provided miRNA target gene data that were collected from four well-annotated miRTareBase v8.0 databases. Functional enrichment with miRNet was performed on the Reactome Biological Pathway database [52]. All miRNet enrichment was reported with a Prism 8.03 software graphical view (GraphPad Software Inc., Boston, MA, USA). The data are expressed as means SEM. Student's t-test was used for comparing single comparisons. For multiple comparisons, one-way analysis of variance (ANOVA) was performed. A value of  $p < 0.05$  was used as the benchmark for statistical significance.

## **Chapter 2: Complex Magnetic Fields act to reduce the Inflammation in Diabetic Derived Cells**

### **Abstract:**

Wound healing is a complex process that can be compromise by several factors like ischemia, infection and skin injury. One common feature of these different phenomena is that each of them resulted related to the reactive oxygen species (ROS), whose production plays a vital role in wound healing. From this point of view, multiple strategies have been developed in order to stimulate the activation of the antioxidative system, with the goal to reduce the damage caused by oxidative stress and to improve wound healing.

In this prospective, in this chapter complex magnetic fields (CMFs) were used on fibroblasts and monocyte cultures derived from diabetic patients, with the purpose to evaluate their capacity to influence the ROS production and related wound healing properties and processes. Different analyses were performed to evaluate biocompatibility, cytotoxicity, mitochondrial ROS production and gene expression profile. The results confirmed a complete biocompatibility of the treatment and the lack of side effects on cell physiology following the ISO standard indication. Furthermore, other outputs confirm that the CMF treatment was capable to induce a reduction in the ROS production, an increase in the macrophage M2 anti-inflammatory phenotype through the activation of miRNA 5591, a reduction in inflammatory cytokines, such as interleukin-1 (IL-1) and IL-6, an increase in anti-inflammatory ones, such as IL- 10 and IL-12 and an increase in the markers related to improved wound healing such as collagen type I and integrins. As last experiment, an RNA sequencing analysis on macrophages and fibroblasts under CMF treatment demonstrated and confirm that CMF treatment is able to influence macrophages through an anti-inflammatory phenotype and increase fibroblasts capacity to induce regenerative biological processes.

Taking together, all the data collected in this work highlight the beneficial potential of CMF treatment for those diabetic patients that develop diabetic foot.

## **Introduction:**

To date it is well known that Diabetes mellitus (DM) is defined as a chronic metabolic disorder, characterized by a persistent hyperglycemia. It occurs due to an impairment insulin secretion, resistance to peripheral actions of insulin, or both together. This chronic hyperglycemia condition in synergy with other metabolic aberrations in patients with diabetes mellitus can induce damage to various organ systems and tissues, promoting the development of disabling and life-threatening health complications, most prominent of which are microvascular such as retinopathy, nephropathy, and neuropathy and macrovascular complications leading to a 2-fold to 4-fold increased risk of cardiovascular diseases and even tissue damages like inducing the diabetic foot ulcers (DFU). Specifically, Type 1 diabetes mellitus (T1DM) accounts for 5% to 10% of DM and is characterized by autoimmune destruction of insulin-producing beta cells in the islets of the pancreas whereas Type 2 diabetes mellitus (T2DM) accounts for around 90% of all cases of diabetes [1]. Epidemiologic researches have definitively established the existence of an association between inflammatory biomarkers and the occurrence of T2DM and complications [2]. Focusing on diabetic foot, that is the most diffused cause of morbidity among diabetic patients, it is the result of functional and structural alterations such as ulcers often associated to osteomyelitis/gangrene resulting from chronic inflammation and endothelial dysfunction [3,4]. So far in this view, it is known that many cells result damaged by the global situation that occurs in diabetes pathology. In particular, endothelial cells, when under a hyperglycemic state, can change the utilization of nitric oxide to metabolize glucose and the depletion of which results in the inability to vasodilate [5]. The consequent inability to vasodilate of the vessels increases the intravascular pressure, causing injury and inflammation to the endothelial cells, which in turn causes the subintimal migration of inflammatory cells, thereby inducing the formation of atherogenic foam cells [6]. In addition, the inflammatory cells are able to release lytic enzymes that can damage even the extracellular matrix (ECM) and the vessels in general. This complex condition can induce an imbalance in free radicals and antioxidants, with an overproduction of reactive oxygen species (ROS), an enhanced inflammation and a decreased tissue regeneration process [7].

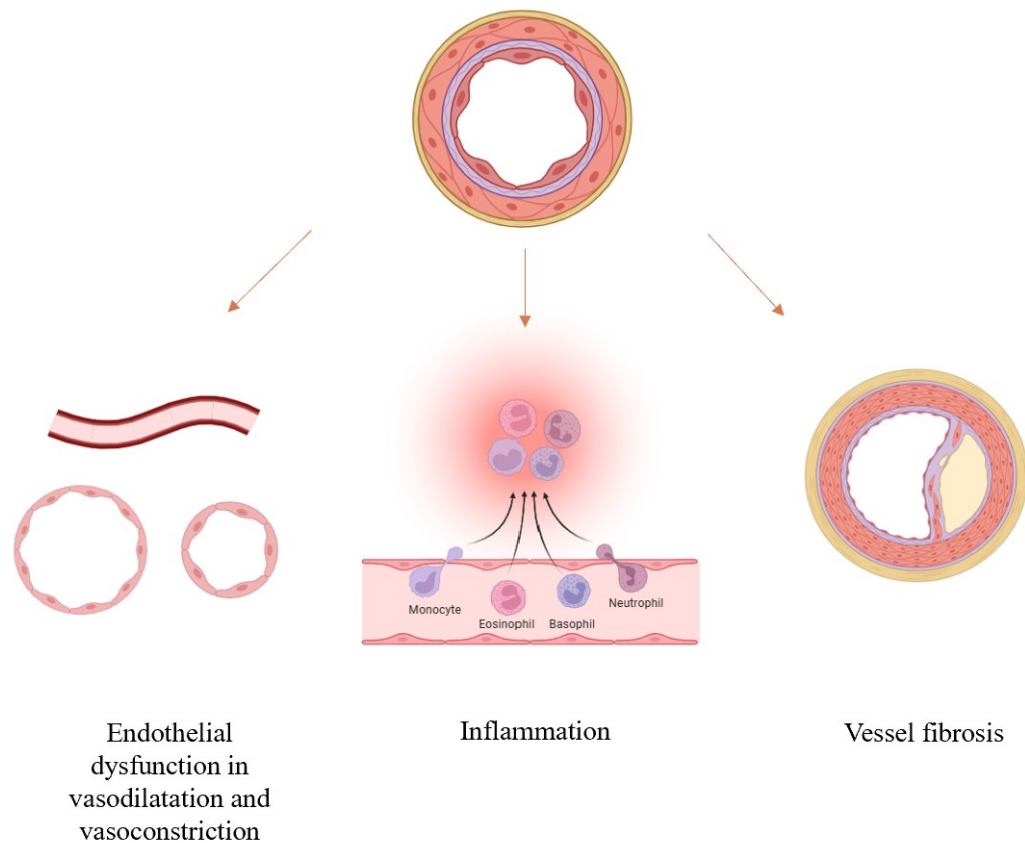


Figure 1: Diabetes main vessel damages;

The ROS can act as secondary messengers for immune-cells, influencing the recruitment and activity of monocytes to the wound site and subsequently regulate the angiogenesis process. All these just mentioned events can cause a vasculopathy, able to lead through an impaired healing and ulceration [8]. On these bases, ROS production control represents a promising strategy to improve wound healing responses, that involve multiple and complex processes as a result of distinct, but overlapping phases, like hemostasis, inflammation, proliferation and remodeling [9, 10].

On the base of these premises, to date, several non-invasive technologies have been developed [10–15]. In scientific literature, it has been reported that the exposition of biological tissues and cell models to a magnetic field, is able to promote anti-inflammatory molecular pathways and to decrease the production of the ROS [16]. It even has been reported that devices capable to produce electromagnetic fields (EMF) are able to affect

numerous biological processes, such as wound and bone healing, inflammation, osteoarthritis, post-operative edema, chronic/neuropathy pain and tissue regeneration [9–25]. This ability of EMF to affect biological processes depends by the complex composition of that. Indeed, the electromagnetic waves that are used in magnetic therapy, are the product of an electric field and a magnetic field that have a perpendicular direction (Figure 2). Those two physical fields can be modulated in wavelength and frequency in order to create a Complex Magnetic Field (CMF) basing on the membrane potential knowledges correlated to every kind of tissue [26].

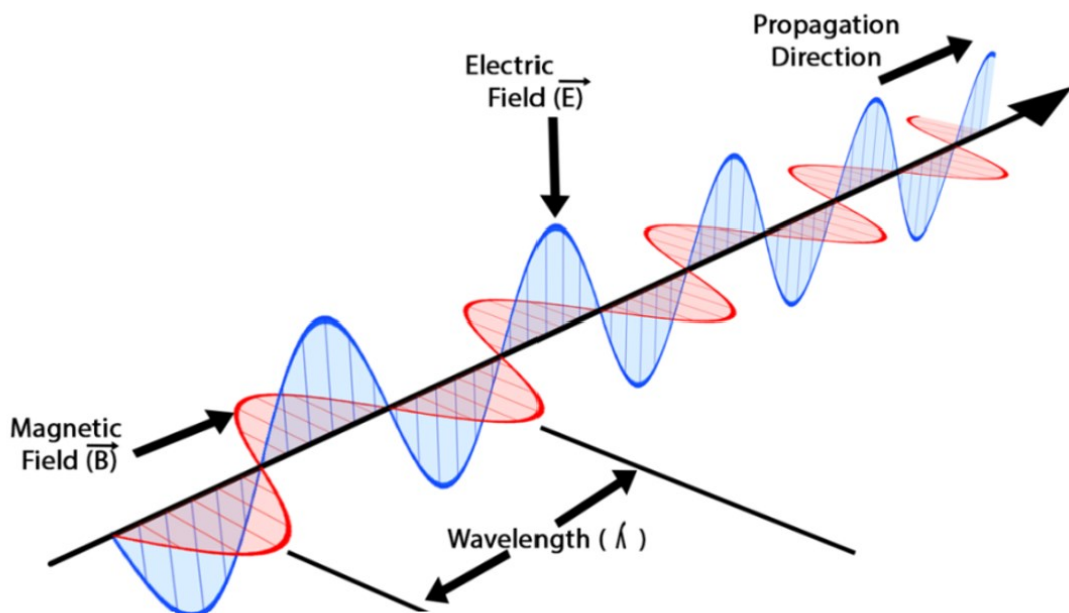


Figure 2: Electromagnetic wave compositions and elements;

To evaluate the safety of the exposition to CMF, exposure guidelines have been regularly developed and revised based on the available scientific knowledge such as the “exposure guidelines” that are published by the International Commission on Non-Ionizing Radiation Protection (ICNIRP). All these guidelines are made and exist for several frequency bands, including low-frequency electric and magnetic fields. The essential and unavoidable principle of these guidelines, is that EMFs exposition, in the frequency range of interest,

does not cause damaging effects to either the patient, the operator or any third party. The laboratory behind the work presented in this chapter, has been working on EMF for 10 years with different medical devices, studying different models, i.e., skin and bone [30–35], becoming able to confirm the safety of EMF and providing both preclinical and clinical data represented by the coherent data and useful interpretations capable to provide results and be able to replicate them in this fairly “risky” field of research. On these knowledges, a technology that exploits EMF can represent an important alternative compared to the classical approaches usually considered for all chronic wounds that are as highly invalidating for the patients as Diabetic foot ulcers (DFUs). As mentioned before DFU is one the most common complications of diabetes mellitus (DM), that can often result in disability and can be associated with an increased risk of mortality. All the complications from DFU are even associated with serious morbidity and overall reduction in quality of life. A lot of epidemiologist analyses confirmed that the annual incidence of DFU varies from 9.1 million to 26.1 million around the world. As previously reported, DFU development and pathogenesis can involve and induce peripheral nerve lesions and peripheral artery diseases. To date, the DFU is a complex situation that is managed using multiple approaches. A classical management of that includes standard care such as offloading, debridement, moisture-retentive dressings, infection management, tissue-based products, autologous platelet-rich gel and ozone therapy. Antibiotic treatment of invasive infection in conjunction with tissue debridement or amputation and off-loading foot pressure until healing is achieved are the essential management principles. In addition, specific adjunctive therapies have been shown to improve the ulcer/wound healing. These further therapies can be topical antimicrobial ointments (silver sulfadiazine, mupirocin), wound growth factors, biologic dressings, negative pressure wound therapy, and hyperbaric oxygen treatments [36-37]. To date there still is limited evidence to support the effectiveness and safety of using EMF as a treatment for DFU. The definition of its mode of action and its influence on mitochondrial activity is still unclear and has to be investigated. Due to the previous experience on diabetic cells physiology and about mitochondrial indolence on wound healing of the laboratory in which this work has been conducted [38–45], the presented chapter of the thesis was focused on testing the effect of a novel system based on complex magnetic fields (CMFs) which consist of a special symphony of waveforms that have been developed for the treatment of several biological alterations. Taking together these considerations, the present work aimed to testing the in vitro effects of CMFs on derived diabetics cells (macrophages and fibroblasts) and evaluating their effect on the mitochondrial

ROS production, its related anti-inflammatory activity and its ability to improve wound healing through multiple molecular test such as different ROS production assays, mitochondria membrane potential analysis, gene expression profiling of specific inflammatory markers and RNA sequencing, enrichment analysis and morphology analysis (SEM).

## Results:

### 1) Safety Test following International Standard Indication

Every time a medical device supposes to stay in contact with the human body and when its function can influence cellular behavior, a specific and accurate biocompatibility analysis is fundamental with the purpose of preventing any adverse effect. On these bases, the biocompatibility was tested and evaluated by studying the viability of fibroblastic cells line using a MTT assay, performed after 1, 3 and 5 days of treatments with a CMF (Figure 3). Cells cultured on plastic dish without treatment were used as a control. The mean standard deviation is the result of triplicates (n=3). The values resulted from the analysis were comparable between treated and untreated samples.

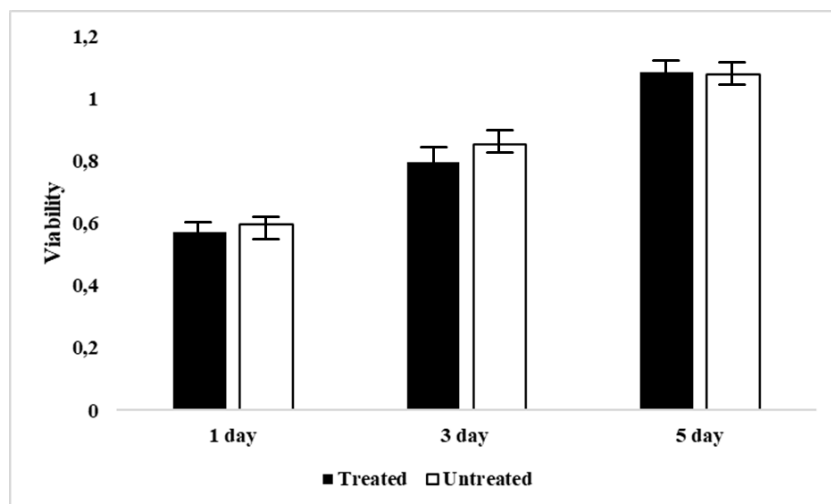


Figure 3: Viability test of fibroblasts after the CMF treatment with MTT assay at 1, 3 and 5 days. Cells on plastic dishes were used as control. Data are reported as the mean  $\pm$  standard deviation (n = 3 per group).

After the viability test, a second test was performed, in order to evaluate the blood compatibility with CMF treatment, by the hemolysis assay capable to quantify free hemoglobin released into the plasma subsequent a damage to the blood cells. No hemoglobin was released or detected, as reported in Table 1, confirming the absence of any hemolytic activity due to the CMF treatment.

Sample	OD	Hemolysis Index	Results
Positive control	0.834 +/- 0.011	100%	Hemolytic
Negative control	0.0103 +/- 0.023	0%	Non Hemolytic
CMF treatment	0.0142 +/- 0.018	0.031%	Non Hemolytic
No treatment	0.0131 +/- 0.022	0.045%	Non Hemolytic

Table 1: Hemolysis assay;

Furthermore, a mutagenic potential due to CMF treatment was excluded by performing the Ames test. A negative result (Table 2), indicated that the treatment is not able to induce any mutagenic event.

Sample	STDisc™ TA1535		STDisc™ TA1537		STDisc™ TA98		STDisc™ TA100	
	Revertant Colonies	Mutagenic						
Blank	4 ± 3	no	5 ± 3	no	4 ± 2	no	5 ± 2	no
Negative control	3 ± 2	no	3 ± 2	no	3 ± 2	no	2 ± 2	no
Positive control: ICR191	947 ± 85	yes	973 ± 66	yes	971 ± 79	yes	965 ± 69	yes
Positive control: Sodium Azide	853 ± 51	yes	876 ± 52	yes	893 ± 59	yes	879 ± 64	yes
CMF treatment	3 ± 2	no	2 ± 2	no	3 ± 2	no	3 ± 2	no
No treatment	3 ± 1	no	3 ± 2	no	2 ± 2	no	5 ± 2	no

Table 2: Ames test for mutagenic assay results;

## 2) ROS Production and Mitochondria Membrane Potential Analysis

Inflammatory condition and the subsequently resulting inflammatory environment, is able to induce every kind of cells including fibroblasts and macrophages, to produce the reactive oxygen species in a time dependent manner, as it's possible to observe in Figure 4. The OxiSelect ROS Assay Kit by Cell Biolabs Inc. was used to perform a ROS quantification of the cells under or not CMF treatment at different time points. When the cells have been exposed to CMF, they significantly resulted reduced in the ROS production basically for each time point analyzed.

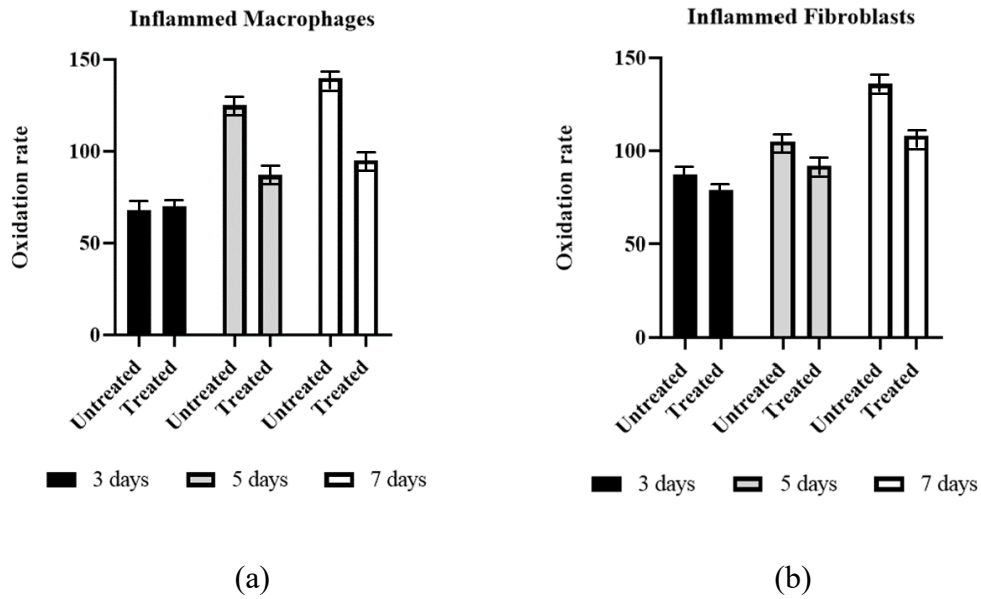


Figure 4: Effects of inflammation on the mitochondrial physiology evaluated by means of the oxidation process activation in inflamed macrophages and fibroblasts, in the presence or not of the CMF treatment (white bars) or in absence (untreated, black bars) with the CMF.

To further validate the ROS production previous data, another ROS assay was performed on macrophages and fibroblasts in normal condition, with or without the CMF treatment to analysis the mitochondria ROS production in vivo. The experiment exploited the MitoSox reagent, capable to label superoxide anion inside the cytoplasm of the cells. As it's possible to observe in Figure 5, two fields for sample were takes through the fluorescence detection. Both comparisons, showed that cells undergo CMF treatment product less superoxide anion compared to related controls.

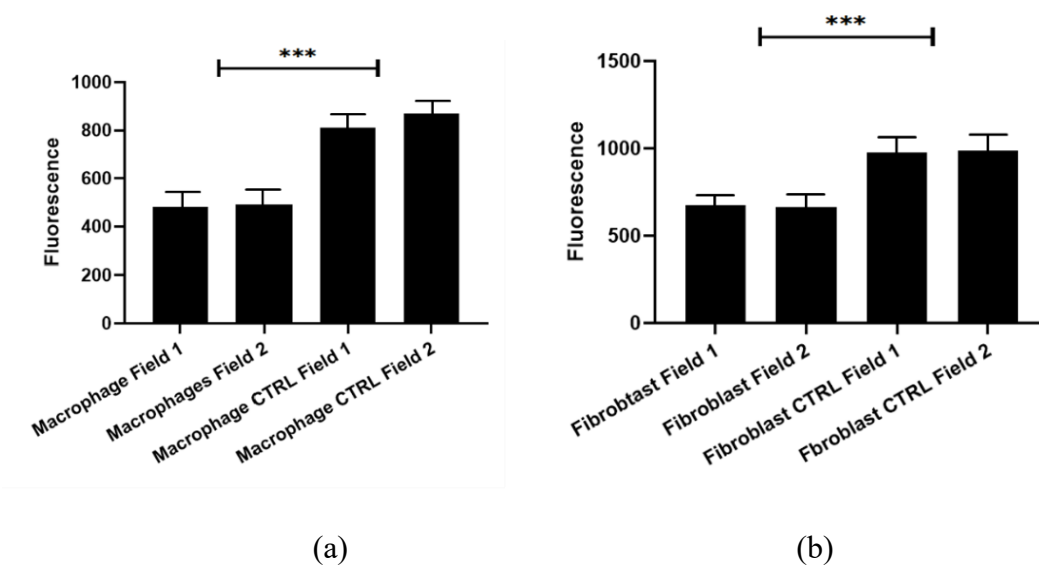
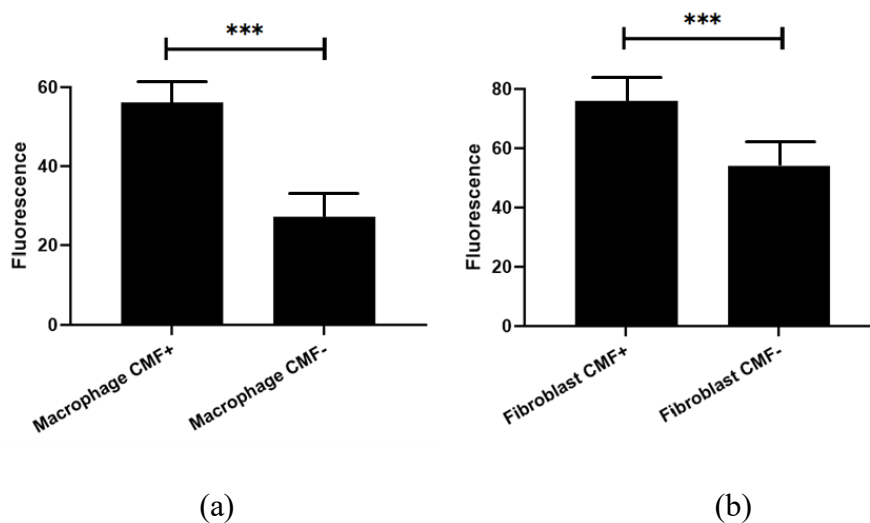
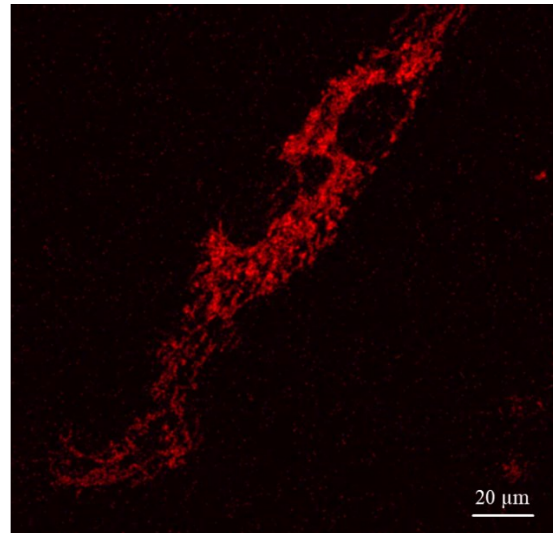
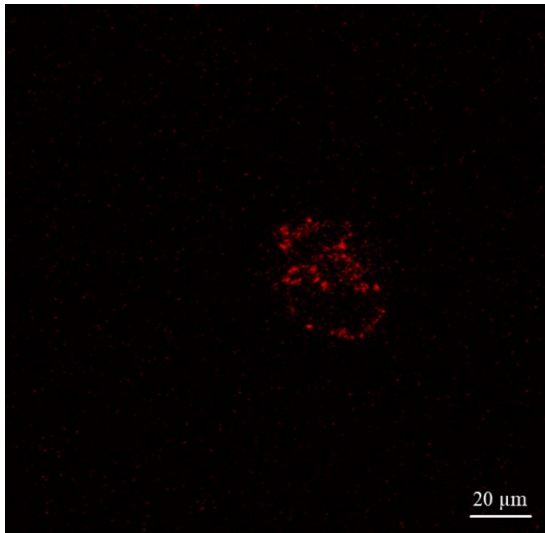


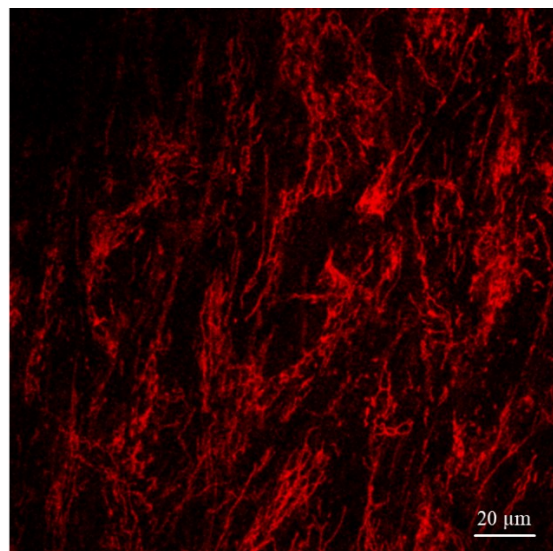
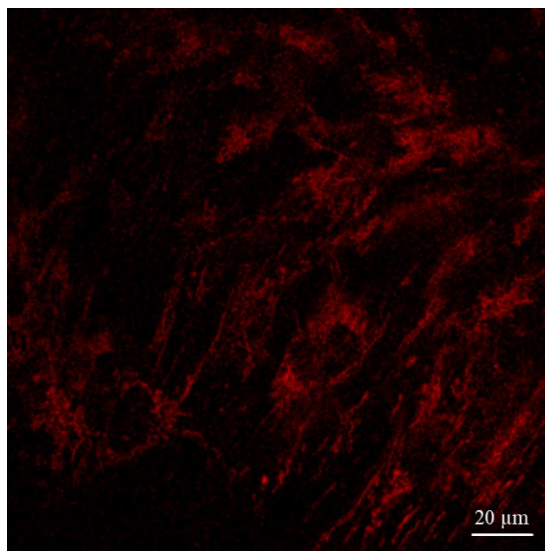
Figure 5: valuation of ROS production by mitochondria in vivo inside Macrophages (a) and fibroblasts (b) by using the MitoSox reagent capable to mark superoxide anion. \*\*\* p-value < 0.001.

Even mitochondria membrane potential was detected to deeply understand if the CMF treatment is able to induce changing to the mitochondria metabolism. Macrophages and fibroblasts treated with CMF resulted with high and amplified mitochondria membrane potential compared with their control samples as shown in Figure 6. Beyond the fluorescence intensity observed in the representative pictures below (Figure 6c and 6d), it's interesting to note the different shape of the macrophages with or without CMF treatment. Macrophages under CMF treatment resulted with an elongated shape compared to the untreated ones.





(c)



(d)

Figure 6: Fluorescence intensity quantification with ImageJ software vs8 of CMF treated and untreated macrophages and fibroblasts (a, b). \*\*\* p-value < 0,001. Mitochondrial membrane potential microscopy analysis of Macrophages (c) and Fibroblasts (d) representative pictures; all the untreated cells are reported on the left compared to treated cells on the right;

### 3) Macrophages Polarization Analysis

In order to evaluate the macrophages polarization in M1 or M2 phenotype under inflammatory condition (TNF- $\alpha$  treatment), when exposed to CMF treatment, a qPCR was performed to observe those genes and miRNAs related to the respective phenotypes. It is well known that an inflammatory environment is able to induce a commitment of the macrophages in M1 polarization, as it's possible to observe in Figure 7 in which high expression level of this M1 pathways related miRNAs and genes are reported: miR-181a, miR-155-5p, miR-204-5p, miR-451, miR-125b-5p, miR-21, miR-193b-3p, miR-125a-5p, Akt2, p110d, PTEN, TSC1, TSC2 and p85a. To support this observation, it's even possible to see that the gene expression of AKT1, p110a, p110b, p110g, TSC1 and rictor/mTORC2 related to the M2 phenotype was strongly reduced for untreated cells. On the contrary, it's interesting to observe how the expression profile rates of the respectively polarization phenotypes change when (white bars) or not (black bars) the cells were exposed to CMF treatment, pushing macrophages through a M2 phenotype.

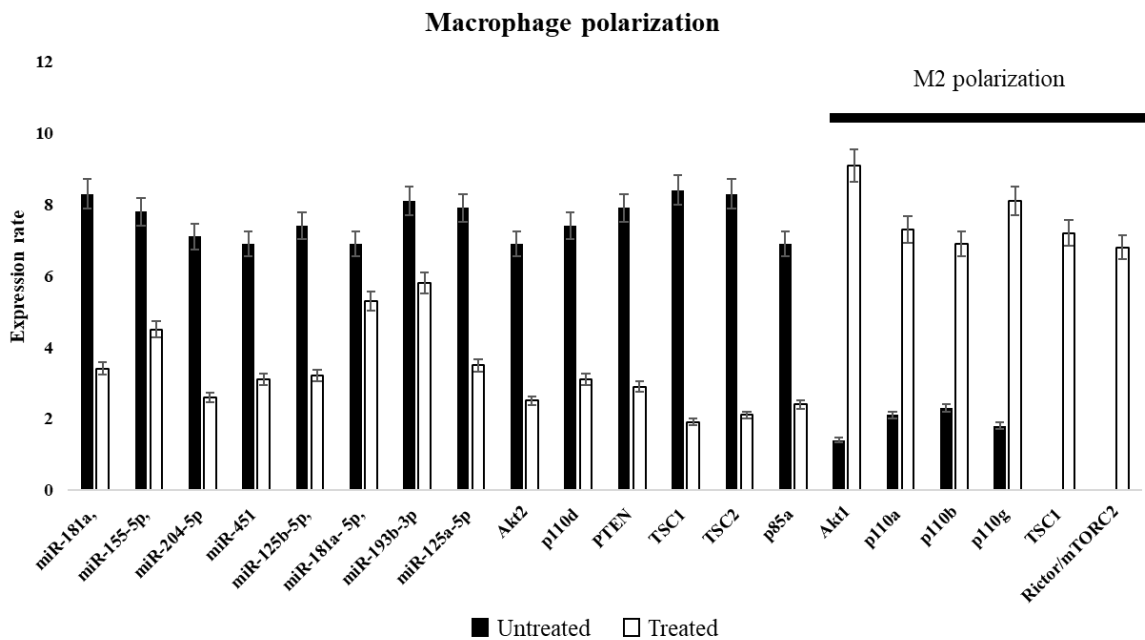
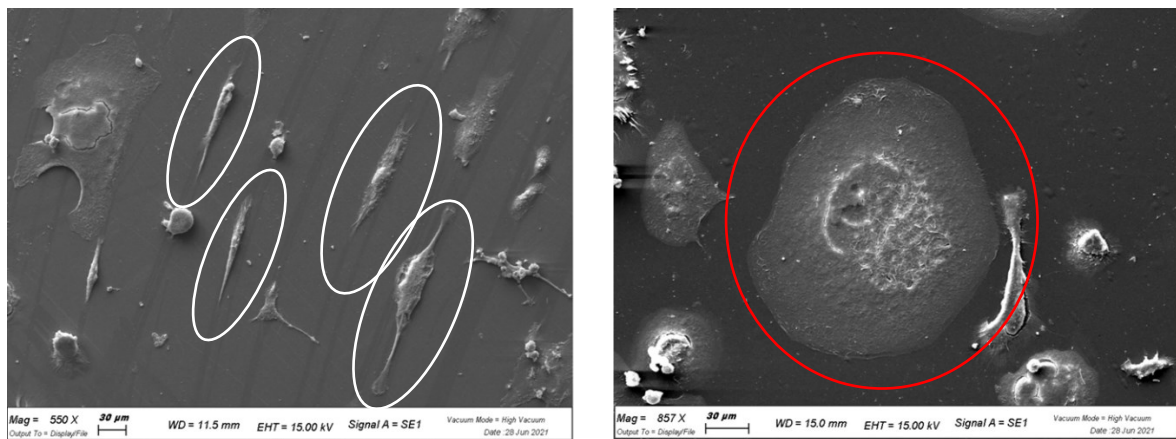
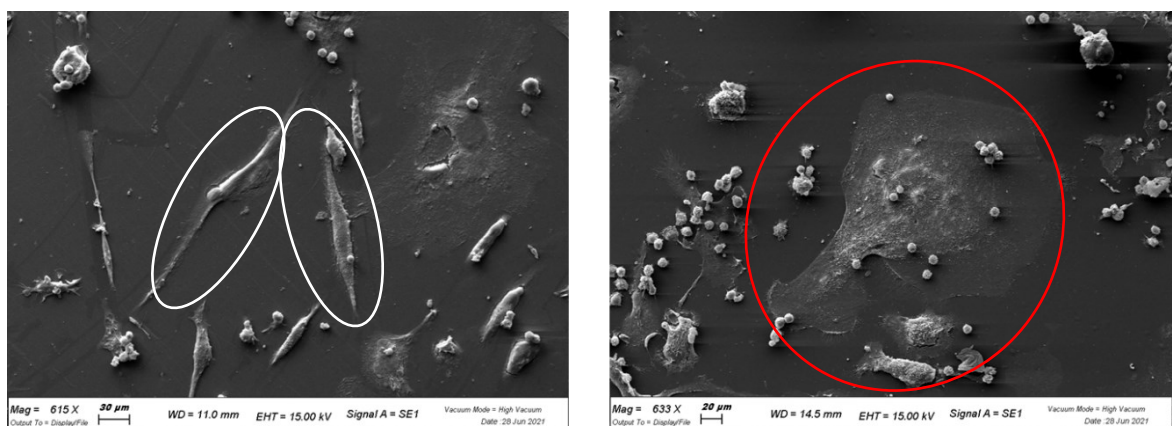


Figure 7: Expression profiles of the genes related to macrophages polarization. M2 phenotype genes are reported under the black bar on the right. Black bars represent gene expression in absence of the CMF and the white bars in the presence of the CMF;

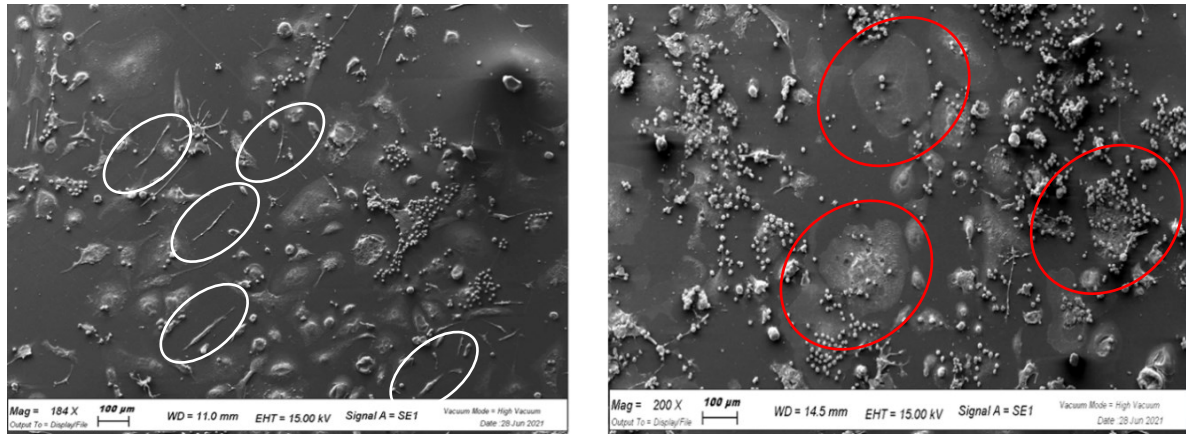
To date it is well known that the polarization state of the macrophages is reflected even in the morphology of the cells. So, in order to verify that, a morphology analysis of the macrophages with or without CMF treatment was performed using electron microscopy (SEM). The commitment of the cells in pro-inflammatory phenotype M1 (red circles) characterized from a rounded shape or anti-inflammatory phenotype M2 (elongated shape, white circles) are reported in representative pictures in in Figure 8. CMF treatment is able to increase the commitment of macrophages into the M2 anti-inflammatory polarization shape (pictures on the left, different magnitudes) compared to M1 pro-inflammatory polarization shape (pictures on the right, different magnitudes). This observation confirmed the previous different in macrophages shape detected also in the mitochondria membrane potential analysis in vivo through the confocal microscopy observation (Figure 6c).



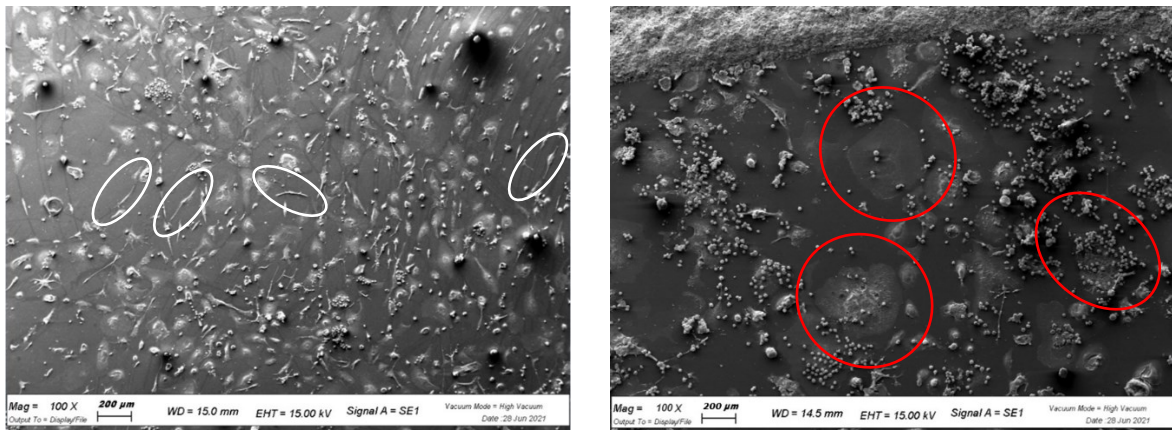
(a)



(b)



(c)



(d)

Figure 8: Scanning Electron Microscopy analyses of the macrophages with the CMF treatment (pictures on the left) with M2 anti-inflammatory phenotype characterized by a long fusiform shape (a, b, c, white circles) and without CMF treatment that acquires a M1 inflammatory rounded shape phenotype (a, b, c, red circles).

#### 4) Specific Inflammatory Markers analysis

To further confirm the data presented above, gene expression profiling of the main inflammatory cytokines such as IL1b, TNF- $\alpha$ , iNOS, IL6 and IL8, for a pro-inflammatory and IL-10 and IL-12 for an anti-inflammatory pattern, were detected on the macrophage cultures subjected to inflammatory condition (Figure 9). Cells involved in this situation without CMF treatment confirmed to have an increased level of the pro-inflammatory

cytokines (black bars Figure 9) compared to the cells under treatment that showed a decreased level of the pro-inflammatory cytokines and an increased level of the anti-inflammatory kind (white bars Figure 9).

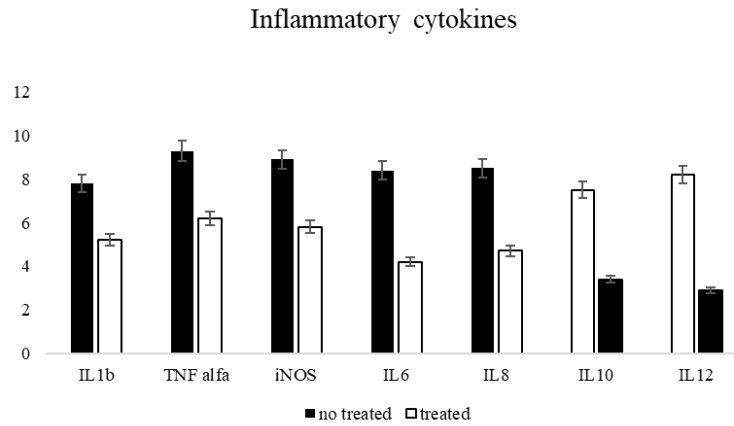


Figure 9: Macrophages inflammatory marker expression profiling. Untreated cells (black bars) and CMF treated cells (white bars);

### 5) Extracellular Matrix Genes Expression Profiling

In the same way with which macrophages-specific inflammatory markers were verified, the ability of fibroblasts to act on the wound healing process was evaluated in vitro making a gene expression profiling of some main extracellular matrix (ECM) was performed (Figure 10). The gene expression of the collagen fibers confirmed that, in the presence of an inflammation process, the fibroblasts resulted not able to produce a good ECM, showing a low level of important ECM components such as collagen fibers type I, III, IV, V, XIV and vitronectin (black bars). On the contrary, under the same inflammatory condition when in the presence of the CMF, the fibroblasts induced an increased amount of the ECM components (white bars).

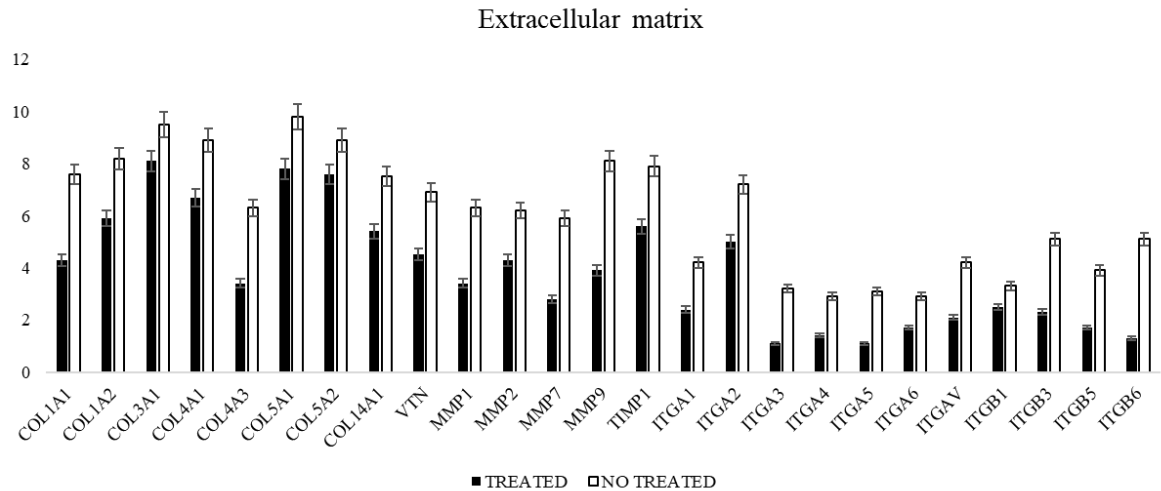
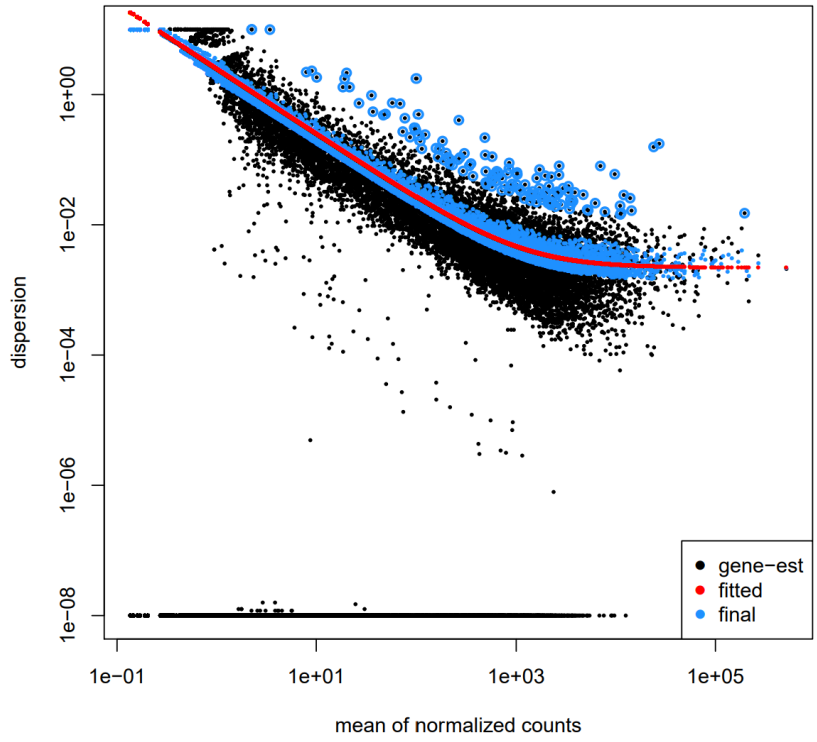


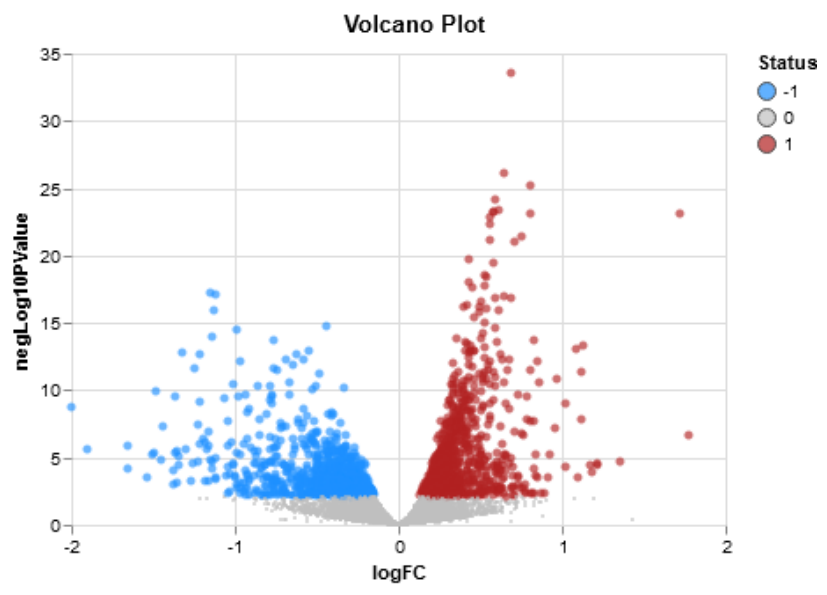
Figure 10: Extracellular matrix main components gene expression profiling. Untreated cells (black bars), CMF treated cells (white bar);

## 6) Macrophages RNA sequencing analysis with IPA software and Enrichment analysis

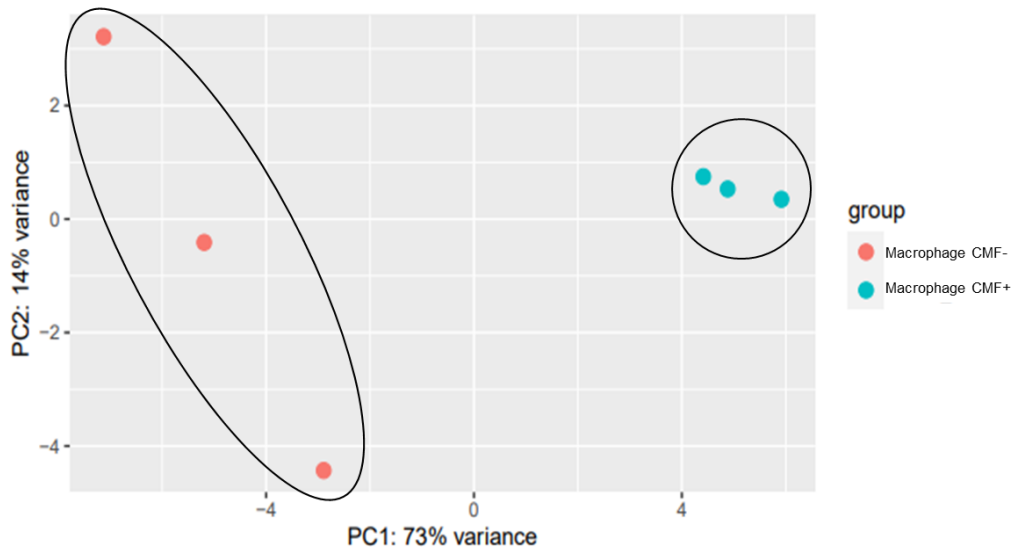
Basing on the above results in a second time, it was decided to performed an RNA sequencing analysis both on macrophages and fibroblasts derived from diabetes patients to confirm the pattern of gene expression observed under CMF treatment and evaluate the effect of an exposure to CMF for an extended time of 21 days. In order to do this, both the cellular population in normal culture condition were treated in parallel with related control. Starting from macrophages RNA sequencing output, 1921 significant genes resulted from the analysis (Figure 11a). Of these genes, 1071 were down-regulated and 850 were up-regulated as shown in the volcano plot in Figure 11b. Using IPA software, it's possible to obtain the PCA plot of the analyzed samples. As shown in Figure 11c, it's possible to observe the distribution of the samples considering the intrinsic variance inside the analyzed group. Macrophages without CMF treatment showed a major intrinsic variance compared to the treated sample.



(a)



(b)



(c)

Figure 11: Dispersion distribution plot of normalized counts from RNA sequencing of macrophages (a); Volcano plot of significant up (red dots) and down-regulated (blue dots) genes resulted from RNA sequencing of macrophages with CMF treatment compared to control analyzed with IPA software (b); PCA plot showing samples grouped on internal variance (c); macrophage minus CMF are reported in red, macrophages plus CMF are reported in blue;

Basing on the interest of the study about all genes resulting from the sequencing, the focus was on the most differentially regulated genes related to inflammation. From the resulted list, 53 genes were selected known to be involved in the inflammation mechanism. About these genes, 15 resulted down regulated and 38 resulted up regulated (Figure 12a) Among the up regulated genes were found 8 genes (EGR2, IL4R, STAT6, ILI41, PPARD, MRC1, IL10RA and FN1) related to M2 polarization while among the down regulated genes were found 5 genes (IRAK3, IRF8, DNMT1, TNFAIP2 and IL6R) related to M1 polarization (Figure 12b)

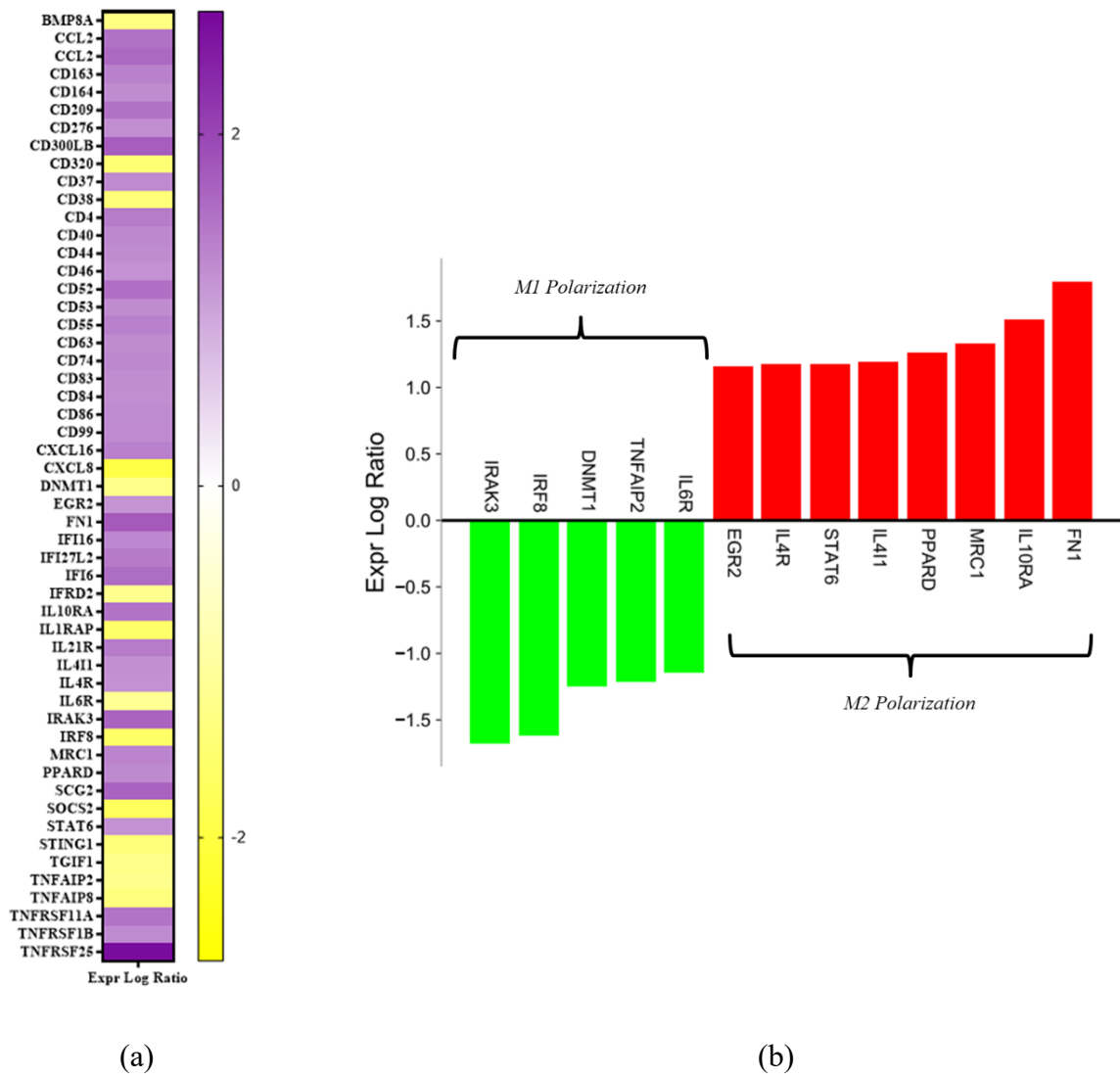
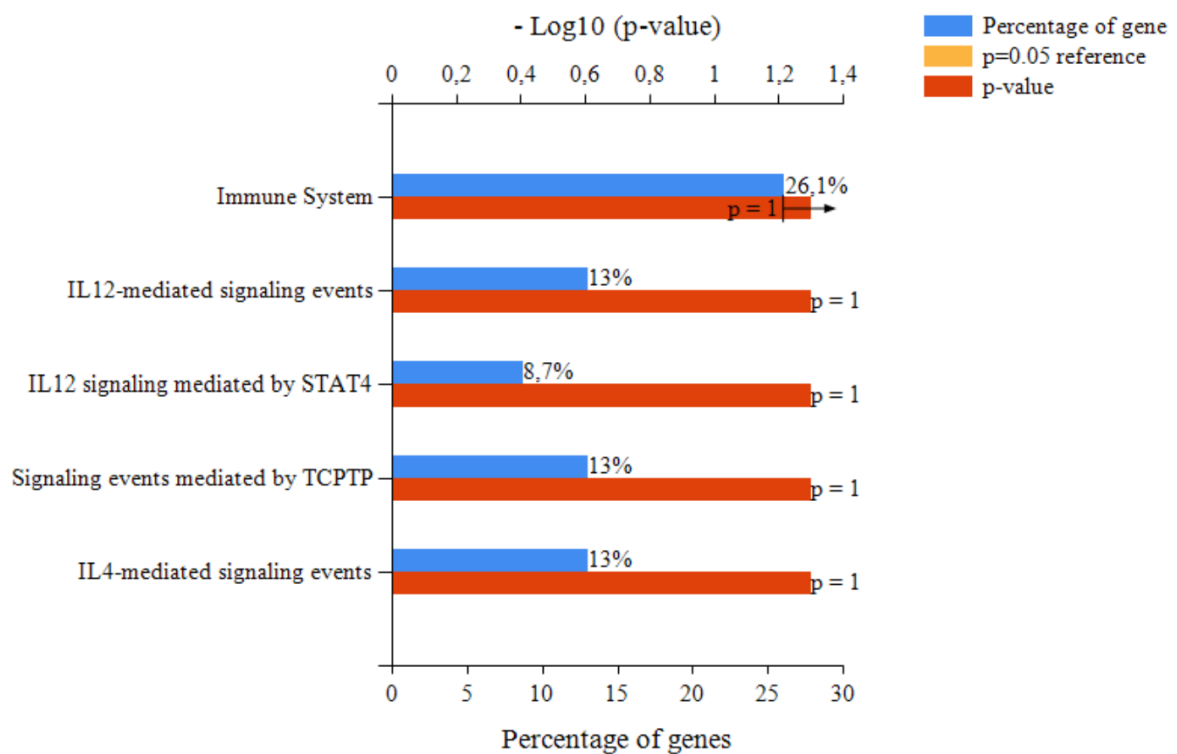


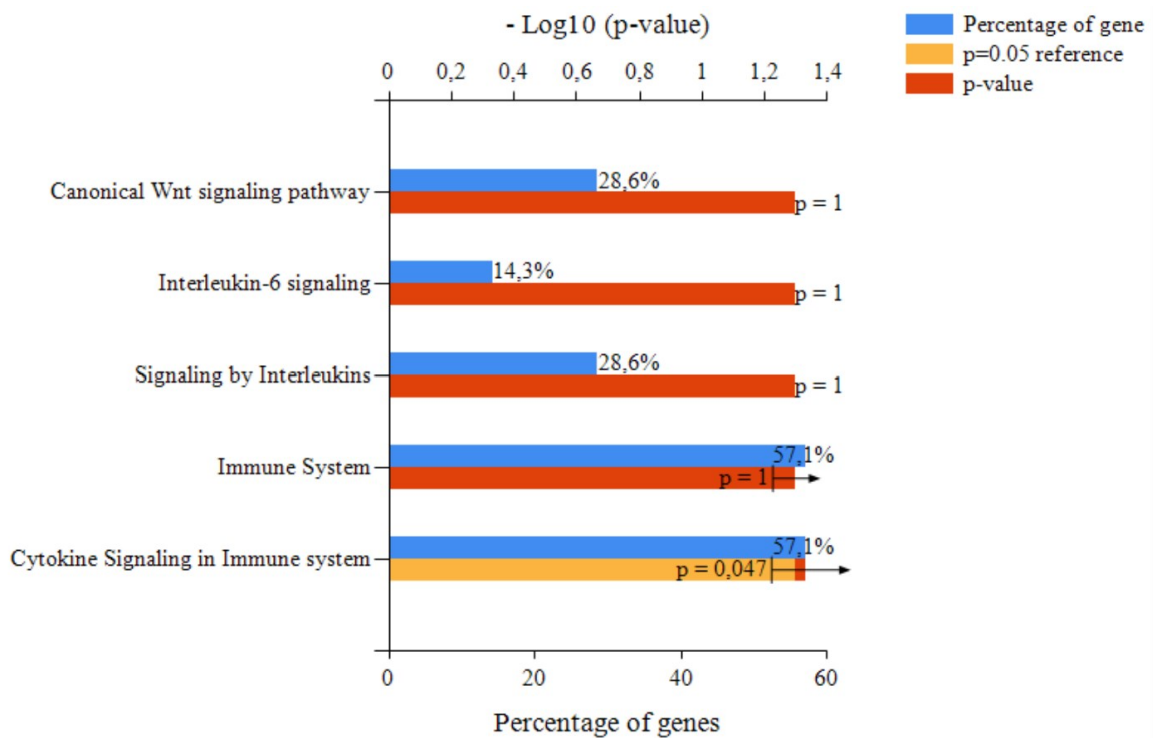
Figure 12: 53 differentially expressed genes selected related to the inflammation (up regulated genes in purple, down regulated genes in yellow) (a); Macrophage polarization related genes (b); 5 down regulated M1 polarization related genes (in green) and 8 up regulated M2 polarization related genes (in red); All reported genes was selected basing on an Expr. Log. Ratio  $-1 < \text{or} > 1$ ;

To further evaluate if the selected significant genes involved in inflammation with this expression status, are able to favor an anti-inflammatory phenotype of the treated macrophages compared with control sample, a biological pathway enrichment on up and down-regulated gene of the cells was performed using FunRich software (Figure 13). The software provides the most significant pathways basing on the percentage of the genes involved and p-value. Six pathways were selected for each group under analysis. On the up-

regulated genes the signaling enriched were: immune system, IL 12-mediated signaling events and signaling mediated by STAT4, signaling mediated by TCPTP and IL-4 mediated signaling events (Figure 13a). Whereas, the pathways enriched for the down-regulated genes were: canonical Wnt signaling pathways, interleukin 6 signaling, signaling by interleukin, immune system and cytokine signaling (Figure 13b).



(a)



(b)

Figure 13: FunRich Biological pathways enrichment on up (a) and down-regulated (b) genes belonging to selected inflammation cluster genes from the RNA sequencing analysis of CMF treated macrophages compared to control; Percentage of genes involved in each function (blue bar), p-value (red bar), and reference (orange bar).

With IPA software it was even possible to obtain a prediction about increased or decreased biological functions, basing on the expression status of the significant genes from the sequencing (Figure 14). This activation or inactivation, is expressed by a Z-Score. Two significant biological function (Z-score > 2) turned out to be increased (vasculogenesis and survival of organism) while three on them, resulted decreased with a Z-score < -2 (chemotaxis of leukocytes, inflammatory response and killing of bacteria).

## Biological Function

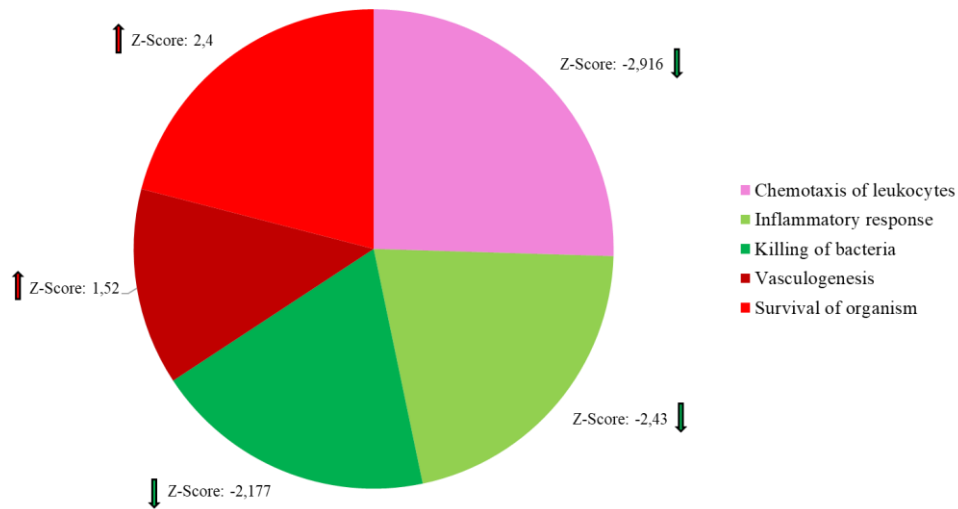
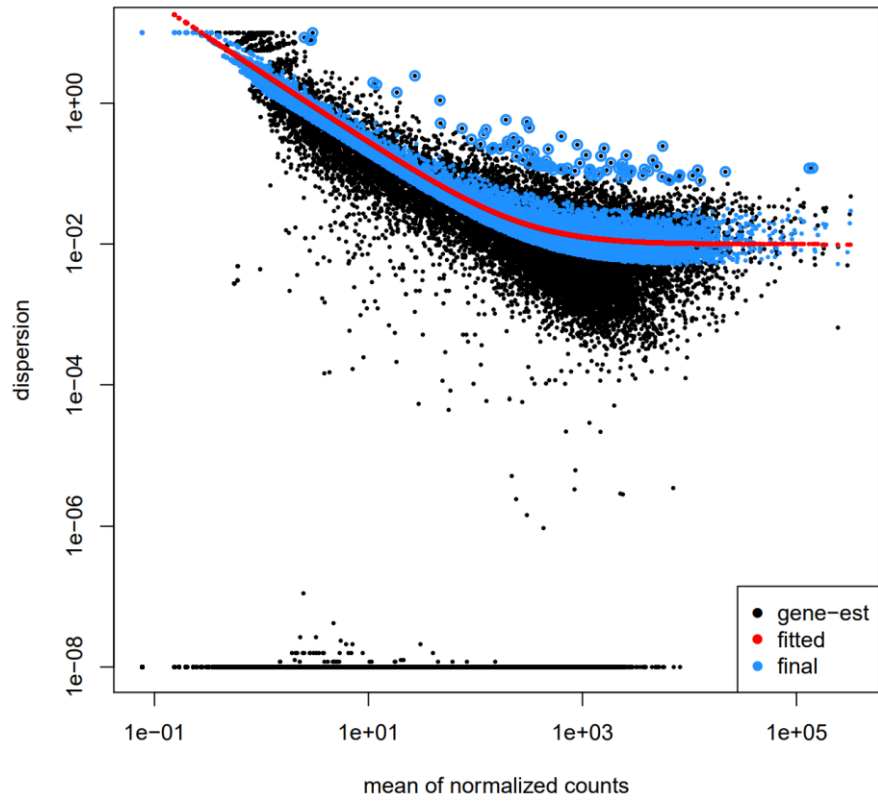


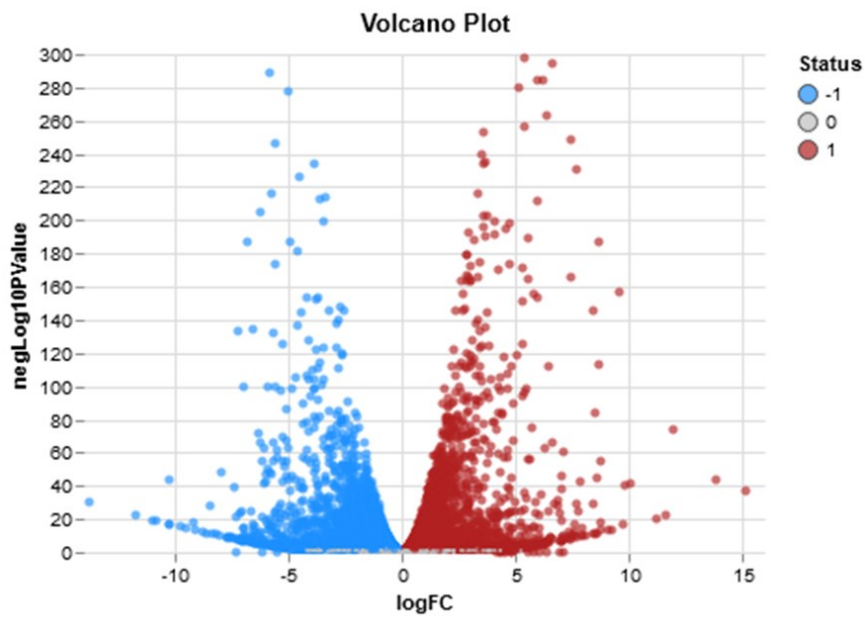
Figure 14: Significant Biological Function analysis by IPA software for CMF treated macrophages compared to untreated samples;

### 7) Fibroblasts RNA sequencing analysis with IPA software and Enrichment analysis

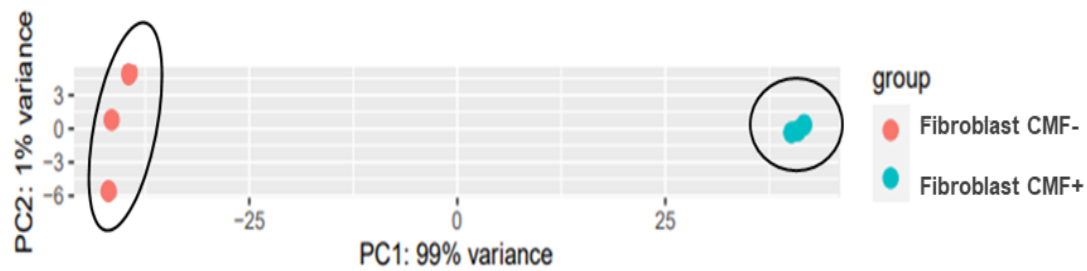
Moving on fibroblasts RNA sequencing results, a total of 8211 genes were significantly differentially expressed with a  $\log_{2}FC < -1$  or  $> 1$  after the normalization (Figure 15a). Of these genes, 4203 resulted down-regulated and 4008 resulted up-regulated (Figure 15b). Again, in the PCA plot provided from IPA software, it's reported the distribution of the samples considering the intrinsic variance inside the analyzed group. (Figure 15c). Even for fibroblasts sample there is a major variance among the untreated sample compared to treated one with CMF.



(a)



(b)



(c)

Figure 15: Dispersion distribution plot of normalized counts from RNA sequencing of fibroblasts (a); (b) Volcano plot of significant up (red dots) and down-regulated (blue dots) genes resulted from RNA sequencing of macrophages with CMF treatment compared to control, analyzed with IPA software; PCA plot showing samples grouped on internal variance (c); untreated fibroblasts are reported in red, while treated fibroblasts with CMF are reported in blue;

About the fibroblasts list of significant genes resulted from RNA sequencing, the focus was on the genes related to the extracellular matrix (ECM) components in order to verify if the fibroblasts under CMF treatment resulted more capable to induce regenerative mechanism by expressing ECM genes compared to untreated control. After the selection, 94 significant genes involved in the regulation of ECM turned out (Figure 16). Of these genes, 34 resulted up regulated and 60 were down regulated in the CMF treated fibroblasts compared to the control (untreated).

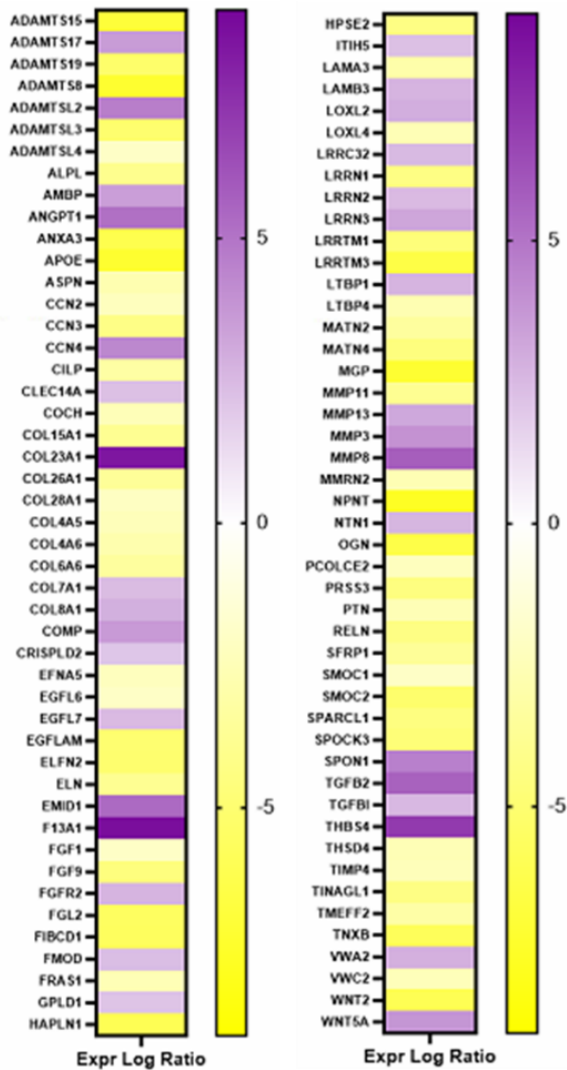
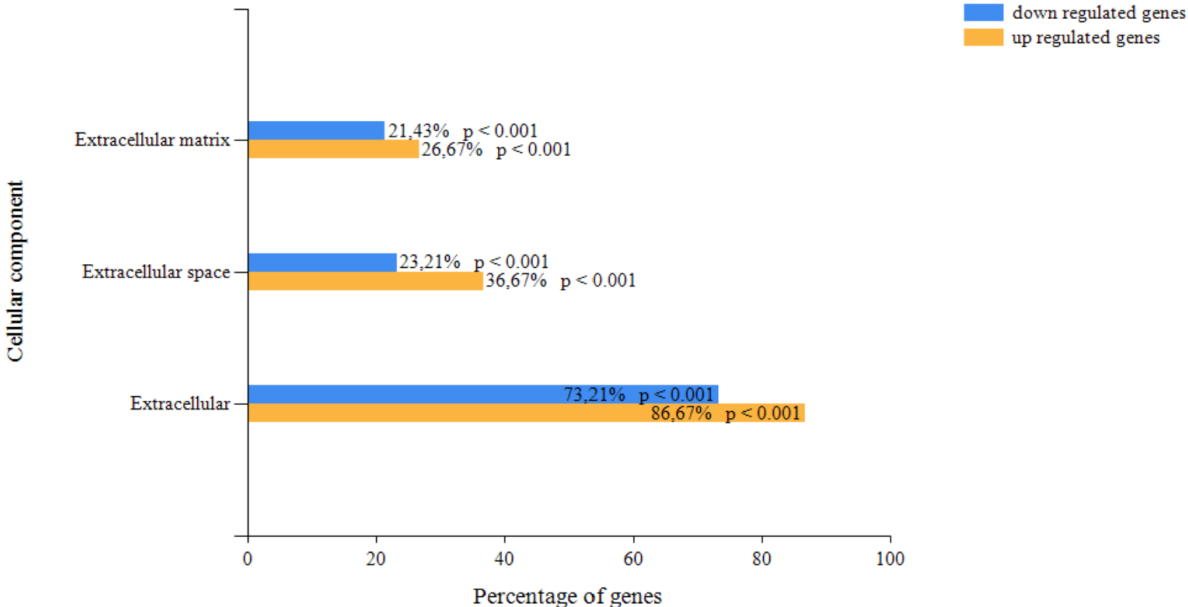


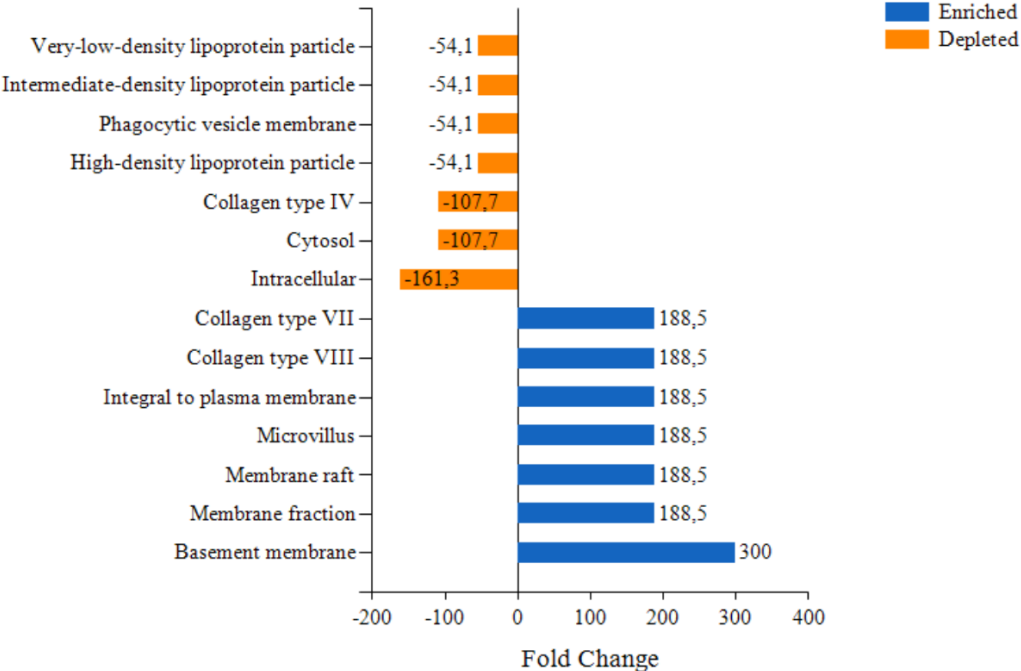
Figure 16: 94 differentially expressed genes selected related to the ECM regulation (up regulated genes in purple, down regulated genes in yellow). All reported genes were selected basing on an Expr. Log. Ratio  $-1 < \text{or} > 1$ ;

To evaluate how the resulting expression profiling of the selected genes related to the ECM, can influence the capacity of the cells under treatment compared to the untreated ones, to induce regenerative processes, a cellular component enrichment was performed exploiting FunRich software. First of all, a comparison analysis between up-regulated and down-regulated genes was done in order to verify which group were more enriched for ECM components (Figure 17a). The up-regulated cluster genes resulted enriched compared to the down-regulated cluster of genes. Subsequently, a specific cellular component analysis basing on the fold change of the genes, was performed (Figure 17b). Placing up-regulated vs down-

regulated cluster genes in the software, up-regulated group of genes resulted enriched for specific ECM components like, collagen type VII and VIII, and plasma membrane fraction, and depleted for intracellular fractions and functions.



(a)



(b)

Figure 17: FunRich cellular components enrichment on up and down-regulated genes related to ECM; (a) cellular component comparison; up-regulated genes (yellow bars), down-regulated genes (blue bars) (b) cellular component types and fold-change analysis of up-regulated vs down-regulated cluster genes;

Thanks to IPA software a list of Canonical pathways was predicted basing on the significant genes resulted from the sequencing. The most significant functions were selected basing on a Z-score  $< -2$  or  $> 2$  (Figure 18). Among the increased biological pathways, it's possible to observe many functions related to the tissue regeneration as activation of cells, proliferation of epithelial cells, chemotaxis, development of connective tissue cells, activation of blood cells, vascularization, growth of muscle tissue, proliferation of muscle cells and migration of vascular cells. Regarding instead the decreased canonical pathways, they resulted to be mostly correlated to cancer pathway as pelvic cancer, genital tract cancer, malignant neoplasm of male genital organ and prostate cancer.

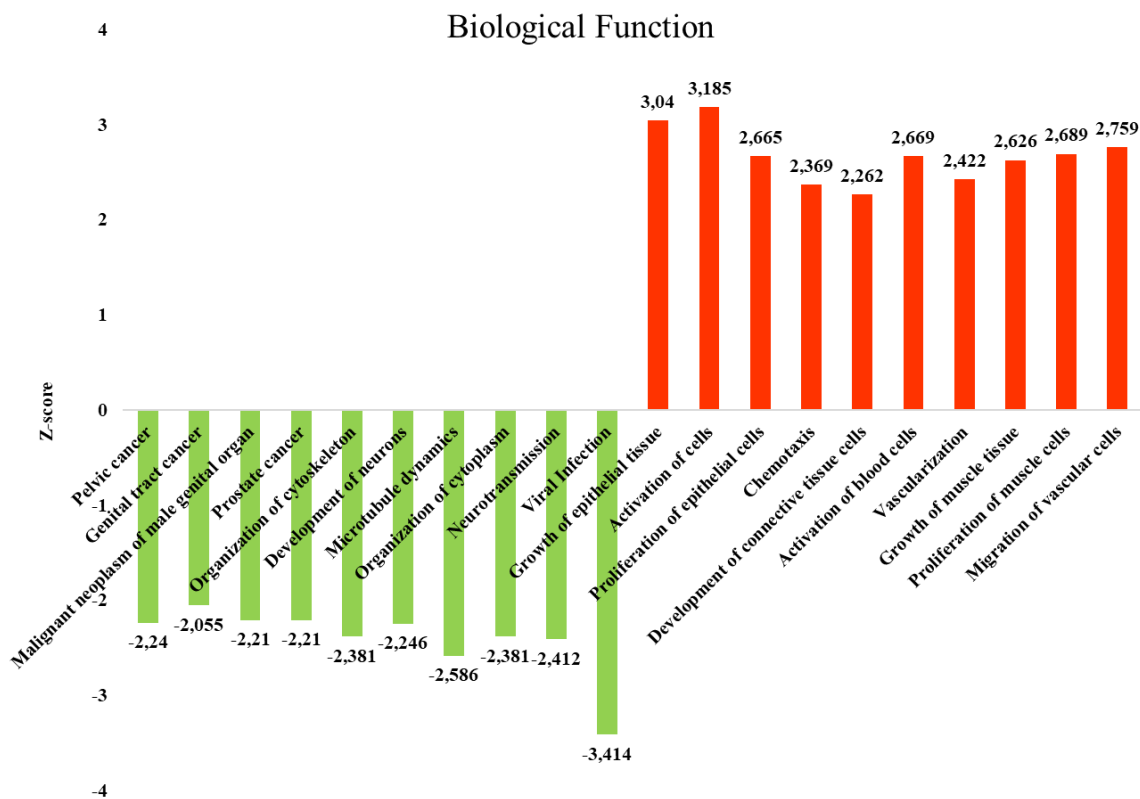


Figure 18: Significant Biological Function analysis by IPA software for treated with CMF fibroblasts compared to untreated samples;

## Discussion:

When we speak about a non-invasive therapy capable to promote healing approved by the U.S. FDA, Electromagnetic Fields (EMF), in this work called Complex Magnetic Field (CMFs), are inserted as a *non-thermal treatment* that uses an active electromagnetic waveform in order to treat damaged tissues. The emission of electromagnetic waveforms is able to penetrate completely any kind of tissues as previously reported by Dr. Mattsson M.O. et al. [46-51]. Due to this capacity, the CMF treatment can be performed and recognize as a non-invasive way therapy. The CMFs that work basing on biophysical energy of the specific tissue target of the treatment, was here used to be test using in vitro models, as therapy for diabetic foot ulcers with the goal to accelerate the healing process, evaluating the ROS production and correlated biological event during an inflammatory condition. When in presence of a chronic inflammation situation, the main associated factors with the failure of the healing of the diabetic foot ulcers are the high expression of the matrix metalloprotease instead of pro-ECM production factors, the ROS production in the wound tissue and a promotion of pro-inflammatory immune system cells and mediators. [52–57]. Indeed, the presence of the ROS is able to induce damage and to disrupt proteins, DNA and membrane phospholipids, and to induce the diabetic wound impairment, whether in the prolonged presence of the pro-inflammatory (M1) macrophages phenotype or the related failure of their transition to the regenerative (M2) macrophage phenotype [58–65]. Together to this, even the fibroblasts resulted no longer able to produce good ECM components for tissue regeneration when involved in an inflammatory process [66].

In this view, first resulted reported in second chapter of the thesis, is the set of the tests performed to verify the CMF treatment safety, by in vitro analysis, following the ISO requirements. Multiple tests were performed such as a cells viability with MTT, AMES test in order to observe the mutagenic effect of CMF using bacterial and the hemolysis assay. All the obtained results confirmed the total safety of the system used in this study. After this first evaluation, the second step was to look at the ability of CMF to contrast the ROS production, to induce an anti-inflammatory activity on biological models and enhance tissue regeneration making fibroblast more able to produce regenerative mediators and positive ECM factors. In order to verify the influence on the cell ROS production, several experiments were performed like: a ROS quantification using OxiSelect ROS Assay Kit performed at different time points (3, 5, and 7 days), a superoxide anion quantification inside the cytoplasm using MitoSox reagent and at last, a mitochondria membrane potential analysis in vivo, to detect how the mitochondria activation can be affected by CMF. Taking

together, all these data about ROS tests, confirmed that the CMF induced a reduction in these molecules, and an increased mitochondria activity as an improved metabolic activity of the cells. [67]. To investigate the impact of CMF on inflammatory cells like macrophages, a real time PCR in order to detect miRNAs and cytokines involved in the inflammatory and anti-inflammatory events was performed. The dysregulation of this macrophage plasticity was influenced by microRNAs (miRNAs) that are fundamental regulators of the transcriptome output. During wound healing, proinflammatory mediators such as lipopolysaccharide (LPS), TNF- $\alpha$  or IFN- $\gamma$  induced the polarization of the monocytes on the M1 macrophages phenotype. [68 PMID: 31178859] When in presence of a pathological condition, the polarization of macrophages in M1 and the subsequent inflammatory situations generated, are able to increase the expression of specific genes that favor extracellular matrix damage and the subsequent formation of ulcers such as in the DFU situation. In detail, all the pro-inflammatory mediators detected with the qPCR, miR-21, miR-155-5p, miR-204-5p, miR-451, miR-125b-5p, miR-181a-5p, miR-193b-3p, miR-125a-5p, Akt2, p110d, PTEN, TSC1, TSC2 and p85a resulted increased under inflammation. They play an essential role in the inflammatory immune response and as a support for this, the expression of the genes related to the M2 phenotype (AKT1, p110a, p110b, p110g, TSC1 and RICTOR/mTORC2) were strongly reduced during the inflammation. It was interesting to observe, that the CMF treatment in an inflamed tissue was able to strongly reduce the expression related to the M1 commitment and to increase the genes related to the M2 phenotype, with a general anti-inflammatory effect. Furthermore, inflammatory markers were analyzed to confirm previous data. The expression of these marker resulted higher under inflammatory environment, but decreased in the presence of a CMF. In particular, the cells (M1 polarized macrophages and fibroblasts) exhibited an upregulation of pro-inflammatory markers such as TNF $\alpha$ , IL-6, IL-1b, iNOS and IL-8 and a downregulation of anti-inflammatory marker as IL-10 well and IL-12, [69-73] in the presence of inflammation, but with opposite expression in the presence of an CMF.

To date it is even well known that the polarization of the macrophages can be observed in the morphology of the cells, recognizing the typical polarization-related shape of the these cells as reported in literature [74]. Since this awareness, a morphology analysis of the macrophages with or without CMF treatment was performed using electron microscopy (SEM). As shown in Figure 6, under CMF treatment the cells showed pro-inflammatory phenotype M1 characterized from a rounded shape and anti-inflammatory phenotype M2 whit an elongated shape. Even for the fibroblast main extracellular matrix

components were analyzed in order to verify the ability of the fibroblasts to induce regeneration of a damaged tissue. Such as macrophages results a same trend occurred when analyzed the extracellular matrix (ECM) components in the presence of the CMF in an inflammatory environment.

To confirm all the data above, an RNA sequencing analysis and multiple enrichment analysis were performed on macrophages and fibroblasts diabetic patients-derived. Looking for the inflammatory genes inside the macrophages RNA sequencing result, a commitment in up-regulation of M2 polarization genes was observed in the CMF treated cells with a down-regulation for M1 polarization genes when compared to the untreated cells (Figure 10). In order to obtain further demonstrations of this genome expression pattern and subsequently biological functions related, an enrichment analysis on the up and down regulated genes that belong to the inflammatory process was performed using FunRich software. From this analysis, regarding the up-regulated genes, the resulted signaling enriched were related to immune system with an increased commitment in anti-inflammatory signaling like IL12-mediated signaling events and IL-12 signaling mediated by STAT4 as previously reported as anti-inflammatory pathways, signaling mediated by TCPTP, that plays an anti-inflammatory role in the inflammation process when activated [75] and IL-4 mediated signaling events, knowing that IL-4 as an important anti-inflammatory mediator. [76] On the other hand, speaking about down-regulated genes among the resulting pathways enriched there were: canonical Wnt signaling pathways, which is a pathway mainly associated with oxidative stress, inflammation [77] and interleukin 6 signaling, that is one of the main pro-inflammatory mediators, belonging to pro-inflammatory cytokine family [78].

With the same mental approach, fibroblasts significant ECM-related genes from the RNA sequencing were used to make a prediction of the biological function that could be activated with this genome expression profile as a result of the CMF treatment. Thanks to IPA software biological function prediction, many signaling related to the tissue regeneration such as activation of cells, proliferation of epithelial cells, chemotaxis, development of connective tissue cells, activation of blood cells, vascularization, growth of muscle tissue, proliferation of muscle cells and migration of vascular cells has been predicted as activated function in those fibroblasts under CMF treatment compared to the untreated ones. To further confirm these patterns of activation/inactivation in the cells, a cellular component enrichment analysis was performed putting up-regulated versus down-regulated genes in FunRich software. The obtained output, confirmed that the cells subjected to CMF have an increased

commitment in multiple ECM factors like collagen type VII and VIII, able to contribute to the tissue regeneration and regenerative processes [79].

In light of these findings, it's possible to conclude that CMF are able to decrease ROS production both in macrophages and fibroblasts when exposed to an inflammatory environment, to increase the commitment in M2 polarized macrophages with an anti-inflammatory action, and to promote an enhanced ability of the fibroblasts to produce good extracellular matrix factors involved in tissue regeneration. Taking together, these data allow to say that in the presence of an acute inflammation situation, CMF can decrease the inflammatory process acting on the inflammation-related cells, and in the same time, they are able to improve the tissue regeneration process increasing the fibroblasts capacity to produce renewed ECM (Figure 19). In this view, CMF could strongly be considered as a non-invasive therapy able to support tissue regeneration of chronic and difficult wounds as those present in diabetic foot condition.

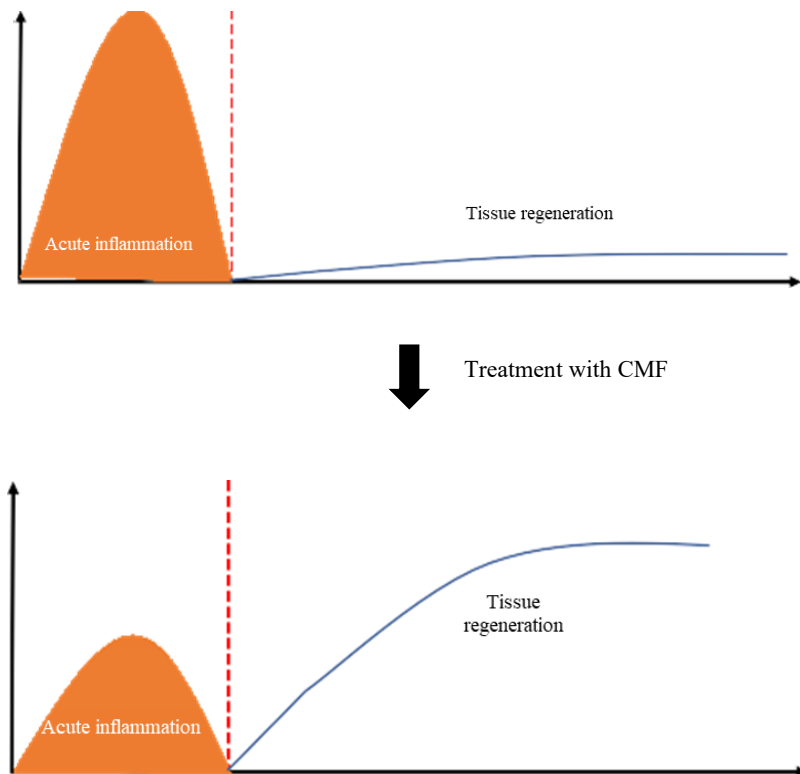


Figure 19. Potential effect of the CMF treatment on the wound healing process in diabetic foot condition;

## **Materials and Methods:**

### Patients Recruitment and Samples Collection

All the patients recruitment occurred thanks to the ECAD-CLI (NCT03636867) is an investigator-driven, single-center, prospective, single-arm study enrolling patients who are admitted to the Diabetic Foot Unit of the Maria Cecilia Hospital (Cotignola, Italy) with a diagnosis of diabetes mellitus and critical limb ischemia (CLI) with Diabetic Foot Ulcers (DFU) (consistent with the Rutherford classes 5 or 6). For the present work an overall of forty patients were recruited at Maria Cecilia Hospital (Cotignola, Ravenna, Italy). The entire study was conducted following the ethical principles for medical research involving human subjects from the World Medical Association Declaration of Helsinki. All the patients were involved inside the study after signing the consent form. All of them were included following these inclusion criteria: they suffered from type 2 diabetes for at least 5 years, the presence of a distal neuropathic ulcer on the foot larger than 1 cm<sup>2</sup> and appeared at least 6 weeks before, they had two palpable pulses at the ankle with a triphasic Doppler waveform and they were older than 18 years. Whereas, the exclusion criteria were chronic renal failure in dialytic treatment, local ischemia with an ankle-brachial pressure index (ABPI) < 0.9; infection according to the Infective Diseases Societies of the Americas (IDSA) guidelines, active or chronic Charcot's disease, HIV or any other systemic disease interfering with the immune system, steroid or cytostatic therapy, known or suspected cancer diagnosis and life expectancy of less than 1 year.

### Cell Isolation and Characterization

In order to collect the fibroblasts from the patients tissue samples, firstly the dermis was removed from biopsy, then washed in a phosphate-buffered saline (PBS, Euro-Clone, Milano, Italy) added with 1% antibiotic–antimycotic (AA, Thermo Fisher Scientific, Waltham, MA, USA), minced and digested with 200 U/mL collagenase type II (Gibco, Thermo Fisher Scientific) in Hanks' balanced salts solution (HBSS, Euroclone, Rome, Italy) at 37 °C for 16 h. The isolated cells were seeded at a density of 5x10<sup>4</sup> cells/cm<sup>2</sup> in Dulbecco's modified eagle medium (DMEM, EuroClone, Rome, Italy) added with 10% fetal bovine serum (FBS, EuroClone, Rome, Italy). Whereas, the isolation of the peripheral blood mononuclear cells (PBMCs) was performed using a Ficoll–Paque gradient method. Briefly,

the peripheral blood, freshly extracted from the patients, was carefully poured into a tube with the Ficoll at the blood/Ficoll 1:4 proportion, centrifuged at 591 g for 30 min at room temperature in order not to induce coagulation process. After that, the supernatant was discarded and the pellet containing the PBMCs was resuspended in 1 mL of PBS 1X for cell counting and viability tests. The cell cultures were maintained at 37 °C and 5% CO<sub>2</sub> and the medium was changed twice a week. PBMCs were then induced in Macrophages differentiation using 100 ng/mL of Phorbol 12-myristate 13-acetate (PMA) for a period of 24 h. To create and mimic an in vitro inflammatory condition, fibroblasts and macrophages were treated for 24 h with 0.1 mg/mL<sup>-1</sup> of the tumor necrosis factor-alpha (TNF- $\alpha$ , Celbio, Berlin, Germany). The TNF- $\alpha$  concentration used in the study was higher than in the physiologic conditions.

### Cell Treatment

The instrument used to create CMFs was Next sx version (M.F.I. Medicina Fisica Integrata, Rome, Italy), that is an electronic device able to emits innovative pulsed multi-frequency electromagnetic fields between 1 and 250 microT variable in intensity, frequency, complex wave form and time stimulation (Figure 17).



Figure 20: Next sx version (M.F.I. Medicina Fisica Integrata, Rome, Italy) electronic device used in the present work;

The generator of CMF provides different programs that work for and in relation to the configuration of the specific sector of the application. Every program is composed of several different steps with different intensities (from 1 to 250 microT), frequencies (1–250 Hz), interval times (1–4 min each steps) and forms of the complex multi-frequency waves with harmonic enrichments. All these four parameters, frequency, induction of intensity, wave form and time stimulation represent one of the steps of the machine program. A normal program is generally composed by 6 to 10 steps. The parameters used in this work were a frequency from 1 to 112 Hz, an induction intensity from 1 to 195  $\mu$ T, a time duration of the steps from 1 to 4 min each and impulsive waveforms with odd multiple harmonics. The treatment was performed on the cells once per day, for a total of three weeks after which every experiment has been realized. The position of every step inserted in the program followed for this study was chosen basing on physiological priority of the biological process that we wanted to induce promoting the wound healing. In the Table 3 below there are all the steps biological-process related used in the treatment in correlation with the articles that explain the choice of the order. For instance, if the goal is to treat wound healing, it's necessary to consider several biological conditions, including the inflammation status, the excess of free radicals in the ROS, the fungal and bacterial conditions, the lack of vascularization and the lack of free energy through which the body could recreate the conditions for regeneration.

<b>Mechanism of Action of Program: Wound Healing</b>		
<b>Program Step</b>	<b>Target</b>	<b>Bibliography</b>
1	Anti-inflammatory	[80-81]
2	Normalization Intracellular cell communication	[82-88]
3	Antibacterial and antifungal	[90-97]
4	ROS modulation	[98-100]
5	Normalization Intracellular cell communication	[82-88]
6	Vascularization and tissue engineering regeneration	[101-103]

Table 3: Steps and bibliography.

### Cells Viability Test

All the cytotoxicity of the treatment was evaluated in vitro using a mouse-derived established cell line of L929 fibroblasts (Cell bank Interlab Cell Line Collection, Genova, Italy) following the ISO 10993-5:2009 directions. The cells were seeded with a density of  $4 \times 10^4$ /well in 24-well plates for 24 h in the completed DMEM (cDMEM) medium. The cDMEM was created from Dulbecco's modified eagle medium (DMEM) (Lonza S.r.l., Milano, Italy), supplemented with 10% fetal bovine serum (FBS) (Bidachem S.p.A., Milano, Italy) and 1% P/S. Control sample consisted of fibroblasts seeded at the same concentration in absence of the treatment. Three samples were prepared for each group. All the cytotoxicity test was assessed after a 24 h, 72 h and 5 day of cells exposure. Briefly, after removing the medium, 1 mL of a 0.5 mg mL<sup>-1</sup> MTT solution was placed in each well. The MTT assay was then performed as previously explained. To determine the presence of viable cells, the MTT-based proliferation assay was performed according to the method of Denizot and Lang with minor modifications. The tissue samples were incubated for 3 h at 37 °C in 1 mL of a 0.5 mg mL<sup>-1</sup> MTT solution prepared in PBS. After the removal of the MTT solution by a pipette, 0.5 mL of 10% DMSO in isopropanol was added to extract the formazan in the samples for 30 min at 37 °C [16]. For each sample, the absorbance values was detected at 570 nm and recorded in duplicate on 200 µL aliquots deposited in the microwell plates using a multilabel plate reader (Victor 3, Perkin Elmer, Milano, Italy).

### Hemolysis Assay

The hemolysis assay was performed following the standard practices set forth in the ASTM F756 (Standard Practice for Assessment of Hemolytic Properties of Materials) for evaluating the blood compatibility of the cells after a treatment of the CMF and without treatment [34]. Thanks to the collaboration with another research group, the blood of three healthy New Zealand rabbits was pooled and diluted in a phosphate buffer saline (PBS; Lonza S.r.l., Milano, Italy) to achieve a total hemoglobin concentration of 101 mg/mL. While the samples were incubated with diluted blood, the blood cells could release hemoglobin into the plasma. The product of this reaction was quantified by measuring the OD at 540 nm with a spectrophotometer. The extraction conditions were 50 °C for 72 h. Each sample was incubated for 3 h at 37 °C, then centrifuged for 15 min at 800 g. One mL of the resulting supernatant from all the samples was added to 1 mL of Drabkin's reagent (Sigma-Aldrich,

St. Louis, MO, USA) and incubated at room temperature for 15 min. The reaction product was quantified with a multilabel plate reader (Victor 3, Perkin Elmer, Milano, Italy) by measuring the optical density (OD) at 540 nm. The hemolysis index (HI) was then calculated using the mean OD for each group as follows.  $HI(\%) = \frac{OD(\text{test material}) \times OD(\text{negative control})}{OD(\text{positive control}) \times OD(\text{negative control})} \times 100$ . With a HI 2%, the sample was considered nonhemolytic whereas with a HI > 2%, the sample was considered hemolytic.

#### Mutagenic Analysis with Ames Test

Mutagenic potential of the CMF treatment was evaluated exploiting the Ames test by using the Salmonella mutagenicity complete test kit (Moltox, Molecular toxicology Inc., Boone, NC, USA), as described in Ferroni et al. [36]. Four different strains of Salmonella were incubated for 48 h at 37 °C with the different extracts, then the number of the revertant colonies per plate was counted. Three replicates were performed for each sample. If the number of the reverted colonies was equivalent to those observed with the blank and negative control, the sample was considered not mutagenic. If the number of the reverted colonies was equivalent to those observed with positive controls, the sample was considered mutagenic.

#### Scanning Electron Microscopy (SEM)

Macrophages and fibroblasts samples were preserved in a 2.5% glutaraldehyde/0.1 M sodium cacodylate buffer overnight at 4 °C, treated with a 1% Osmio O4/0.1 M sodium cacodylate buffer and dehydrated using ethanol solutions of increasing concentrations. The samples have been analyzed using SEM (Electronic Microscopy Service, Department of Biology, University of Ferrara, Ferrara, Italy) with a SEM Zeiss EVO 40. The image acquisition system consisted of a Tietz video camera (Tietz Video and Image Processing Systems GmbH, Gauting, Germany) and the TIA FEI imaging software 6 (FEI Company).

#### RNA Extraction and Real-Time PCR Array

Cells total RNA was extracted using the RNeasy Mini Kit (Qiagen, Hilden, Germany). For every sample, 500 ng of the total RNA was reverse-transcribed with the RT2 First Strand

Kit (Qiagen) in a SimpliAmp™ Thermal Cycler (Applied Biosystems™, Rome, Italy) Thermo Fisher Scientific, Berlin, Germany) following the manufacture indications. The resulting cDNA was stored at -20 °C until the next step. A human wound healing RT2 Profiler PCR Array (Qiagen) was performed in accordance with the manufacture protocol. Shortly, cDNA samples were mixed with RT2 SYBR Green Mastermix (Qiagen) and then aliquoted into the wells of the RT2 Profiler PCR Array. The real-time PCR system (Applied Biosystems™) was set up with the following thermal cycling conditions: denaturation at 95 °C for 10 min followed by 40 cycles of denaturation at 95 °C for 15 s and annealing and elongation at 60 °C for 1 min. A dissociation curve for each well was performed by running the following program: 95 °C for 1 min, 65 °C for 2 min and 65 °C to 95 °C at 2 °C/min. The relative expression was determined using the  $2^{-\Delta\Delta CT}$  method. All the Ct values of the target genes were then normalized to the geometric mean Ct values of the housekeeping gene (ACTB). The results were reported as a fold regulation of the target genes in the test group (treated with CMF) compared with the control group (untreated). The statistical significance was set at  $p < 0.05$ .

#### Reactive Oxygen Species (ROS) Analysis

OxiSelect ROS Assay Kit (Cell Biolabs Inc., San Diego, CA, USA) is a cell-based assay for measuring the intracellular activity of hydroxyls, peroxy radicals and other ROSs employing the cell-permeable fluorogenic probe DCFHDA. This probe diffuses into the cells and is deacetylated by the cellular esterase into a non-fluorescent DCFH. When in presence of the ROS, the DCFH is rapidly oxidized generating highly fluorescent DCF. Fluorescence signal was detected using a standard fluorometric plate reader. In addition to this previous detection, even the production of superoxide anion inside mitochondria was evaluated. This superoxide anion can be visualized using a fluorescence microscopy that works on using MitoSOX™ Red Mitochondrial Superoxide Indicators label (Invitrogen, ThermoFisher, cat number M36008) that can be detected in live cells. The obtained output from this assay is related to fluorescence, higher is the production of superoxide anion, higher is the fluorescence.

### Mitochondria membrane potential analysis

To measure mitochondrial membrane potential, the cells were incubated with MitoTracker Red CMXRos (Thermo Fisher Scientific) for 30 min at 37 °C and after one washing phase they were immediately observed with a Nikon LiveScan Swept Field Confocal Microscope (SFC) Eclipse Ti equipped with NIS-Elements microscope imaging software and on a confocal laser scanning Olympus FV3000 microscope both equipped with a 63X oil immersion objective (N.A. 1.4). The red signal colocalization rate was evaluated using the JACOP colocalization counter available in the Fiji software (ImageJ). For each condition, the signal was also determined by manually counting the fluorescent puncta. For every ROI obtained, the Manders' parameter was calculated. For each condition, five replicates were observed, and four measurements were performed on each replicate.

### RNA sequencing and Analysis

Again, the mRNA sequencing was performed by Area Science Park (ASP, Trieste, Italy) using Illumina sequencing technique. Total RNA was quantified using NanoDrop 2000 (Thermo Fisher Scientific, Waltham, MA, USA) and also Agilent Bioanalyzer 2100 (Agilent, Santa Clara, CA, USA). All the libraries were created with 1 µg of the total RNA using the TruSeq Sample Preparation RNA Kit (Illumina Inc., San Diego, CA, USA) according to the manufacturer's protocol. They were then quantified with the Qubit dsDNA BR Assay Kit (Thermo Fisher Scientific, Waltham, MA, USA) on a Qubit 2.0 Fluorometer (Thermo Fisher Scientific, Waltham, MA, USA). RNA sequencing was realized on a Novaseq 6000 sequencer (Illumina Inc., San Diego, CA, USA) according to the manufacturer's protocol. The final output from Illumina BCLFASTQ v2.20 software was given in FASTQ files. Raw files' quality was checked using FASTQC software V4 (<http://www.bioinformatics.bbsrc.ac.uk/projects/fastqc>; accessed on 15 October 2022), and all the low-quality sequences were discarded from the analysis. After this, all the selected reads were aligned onto the complete human genome using Splices Transcripts Alignment to the Reference algorithm STAR version 2.7.3 using hg38 Genome Assembly and Genecode.v35 as the gene definition. The resulting mapped reads were included as the input for the feature count functions of the R subread packages and were used as gene counts for differential expression analysis using the Deseq2 package. Reads comparison was performed

between DFO-sEV-treated HUVECs and untreated HUVECs. Differentially expressed genes (DEGs) were selected for  $\log_2(\text{FR}) < 1$  or  $> 1$  and  $p\text{-value} < 0.05$ .

### Statistics

The datasets from RNA sequencing were analyzed with the Qiagen Ingenuity Pathway Analysis (IPA) software. This provides a list of significant genes and is able to categorize all differentially expressed genes (DEGs) in canonical pathways. Doing this IPA can make a prediction on possible diseases and functions, which were ranked based on their significance (p-value) and predicted state of activation/inhibition expressed in Z-Score. The Z-score value used in this study was set with cut-off  $< -2$  or  $> +2$ . RNA sequencing was used to perform functional, biological pathway, biological process, and cellular component enrichment with the FunRich software. Multiple results are reported using a Prism 8.03 software graphical view (GraphPad Software Inc., Boston, MA, USA). The data are expressed as means SEM. Student's t-test was used for comparing single comparisons. For multiple comparisons, one-way analysis of variance (ANOVA) was performed. A value of  $p < 0.05$  was used as the benchmark for statistical significance. The repeatability was calculated as the standard deviation of the difference between the measurements. All the testing was performed in the SPSS 16.0 software (SPSS Inc., Chicago, IL, USA; license of the University of Ferrara, Ferrara, Italy).

## References Chapter 1:

1. Casadei A, Epis R, Ferroni L, Tocco I, Gardin C, Bressan E, Sivolella S, Vindigni V, Pinton P, Mucci G, Zavan B. Adipose tissue regeneration: a state of the art. *J Biomed Biotechnol.* 2012;2012:462543. doi: 10.1155/2012/462543. Epub 2012 Oct 3. PMID: 23193362; PMCID: PMC3488420.
2. Mushahary D, Spittler A, Kasper C, Weber V, Charwat V. Isolation, cultivation, and characterization of human mesenchymal stem cells. *Cytometry A.* 2018 Jan;93(1):19-31. doi: 10.1002/cyto.a.23242. Epub 2017 Oct 26. PMID: 29072818
3. Wang ZG, He ZY, Liang S, Yang Q, Cheng P, Chen AM. Comprehensive proteomic analysis of exosomes derived from human bone marrow, adipose tissue, and umbilical cord mesenchymal stem cells. *Stem Cell Res Ther.* 2020 Nov 27;11(1):511. doi: 10.1186/s13287-020-02032-8. PMID: 33246507; PMCID: PMC7694919
4. Seo, Y.; Shin, T.H.; Kim, H.S. Current Strategies to Enhance Adipose Stem Cell Function: An Update. *Int. J. Mol. Sci.* 2019, 20, 3827. [CrossRef]
5. Mazini L, Rochette L, Admou B, Amal S, Malka G. Hopes and Limits of Adipose-Derived Stem Cells (ADSCs) and Mesenchymal Stem Cells (MSCs) in Wound Healing. *Int J Mol Sci.* 2020 Feb 14;21(4):1306. doi: 10.3390/ijms21041306. PMID: 32075181; PMCID: PMC7072889
6. Gardin, C.; Ferroni, L.; Leo, S.; Tremoli, E.; Zavan, B. Platelet-Derived Exosomes in Atherosclerosis. *Int. J. Mol. Sci.* 2022, 23, 12546. [CrossRef]
7. Bellin, G.; Gardin, C.; Ferroni, L.; Chachques, J.C.; Rogante, M.; Mitrecic, D.; Ferrari, R.; Zavan, B. Exosome in Cardiovascular Diseases: A Complex World Full of Hope. *Cells* 2019, 8, 166. [CrossRef] [PubMed]
8. Ferroni, L.; Gardin, C.; D'Amora, U.; Calzà, L.; Ronca, A.; Tremoli, E.; Ambrosio, L.; Zavan, B. Exosomes of mesenchymal stem cells delivered from methacrylated hyaluronic acid patch improve the regenerative properties of endothelial and dermal cells. *Biomater. Adv.* 2022, 139, 213000.
9. Trentini, M.; Zanotti, F.; Tiengo, E.; Camponogara, F.; Degasperi, M.; Licastro, D.; Lovatti, L.; Zavan, B. An Apple a Day Keeps the Doctor Away: Potential Role of miRNA

146 on Macrophages Treated with Exosomes Derived from Apples. *Biomedicines* 2022, 10, 415.

10. Pomatto, M.; Gai, C.; Negro, F.; Cedrino, M.; Grange, C.; Ceccotti, E.; Togliatto, G.; Collino, F.; Tapparo, M.; Figliolini, F.; et al. Differential Therapeutic Effect of Extracellular Vesicles Derived by Bone Marrow and Adipose Mesenchymal Stem Cells on Wound Healing of Diabetic Ulcers and Correlation to Their Cargoes. *Int. J. Mol. Sci.* 2021, 22, 3851.

11. Terunuma, A.; Yoshioka, Y.; Sekine, T.; Takane, T.; Shimizu, Y.; Narita, S.; Ochiya, T.; Terunuma, H. Extracellular vesicles from mesenchymal stem cells of dental pulp and adipose tissue display distinct transcriptomic characteristics suggestive of potential therapeutic targets. *J. Stem Cells Regen. Med.* 2021, 17, 56–60.

12. Francula-Zaninovic S, Nola IA. Management of Measurable Variable Cardiovascular Disease' Risk Factors. *Curr Cardiol Rev.* 2018;14(3):153-163. doi: 10.2174/1573403X14666180222102312. PMID: 29473518; PMCID: PMC6131408

13 Ahmed, L.; Al-Massri, K. New Approaches for Enhancement of the Efficacy of Mesenchymal Stem Cell-Derived Exosomes in Cardiovascular Diseases. *Tissue Eng. Regen. Med.* 2022, 19, 1129–1146.

14. Brunello, G.; Zanotti, F.; Trentini, M.; Zanolli, I.; Pishavar, E.; Favero, V.; Favero, R.; Favero, L.; Bressan, E.; Bonora, M.; et al. Exosomes Derived from Dental Pulp Stem Cells Show Different Angiogenic and Osteogenic Properties in Relation to the Age of the Donor. *Pharmaceutics* 2022, 14, 908.

15. Chachques, J.C.; Gardin, C.; Lila, N.; Ferroni, L.; Migonney, V.; Falentin-Daudre, C.; Zanotti, F.; Trentini, M.; Brunello, G.; Rocca, T.; et al. Elastomeric Cardiowrap Scaffolds Functionalized with Mesenchymal Stem Cells-Derived Exosomes Induce a Positive Modulation in the Inflammatory and Wound Healing Response of Mesenchymal Stem Cell and Macrophage. *Biomedicines* 2021, 9, 824.

16. Bosco, G.; Paganini, M.; Giacon, T.A.; Oppio, A.; Vezzoli, A.; Dellanoce, C.; Moro, T.; Paoli, A.; Zanotti, F.; Zavan, B.; et al. Oxidative Stress and Inflammation, MicroRNA, and Hemoglobin Variations after Administration of Oxygen at Different Pressures and Concentrations: A Randomized Trial. *Int. J. Environ. Res. Public Health* 2021, 18, 9755.

17. Chung, H.M.; Won, C.H.; Sung, J.H. Responses of adipose-derived stem cells during hypoxia: Enhanced skin-regenerative potential. *Expert Opin. Biol. Ther.* 2009, 9, 1499–1508.
18. Trentini, M.; Zanolta, I.; Zanotti, F.; Tiengo, E.; Licastro, D.; Dal Monego, S.; Lovatti, L.; Zavan, B. Apple Derived Exosomes Improve Collagen Type I Production and Decrease MMPs during Aging of the Skin through Downregulation of the NF- $\kappa$ B Pathway as Mode of Action. *Cells* 2022, 11, 3950.
19. Liu, W.; Li, L.; Rong, Y.; Qian, D.; Chen, J.; Zhou, Z.; Luo, Y.; Jiang, D.; Cheng, L.; Zhao, S.; et al. Hypoxic mesenchymal stem cell-derived exosomes promote bone fracture healing by the transfer of miR-126. *Acta Biomater.* 2020, 103, 196–212.
20. Gonzalez-King, H.; García, N.A.; Ontoria-Oviedo, I.; Ciria, M.; Montero, J.A.; Sepúlveda, P. Hypoxia Inducible Factor-1 $\alpha$  Potentiates Jagged 1-Mediated Angiogenesis by Mesenchymal Stem Cell-Derived Exosomes. *Stem Cells* 2017, 35, 1747–1759.
21. Karuppagounder, S.S.; Ratan, R.R. Hypoxia-inducible factor prolyl hydroxylase inhibition: Robust new target or another big bust for stroke therapeutics? *J. Cereb. Blood Flow Metab.* 2012, 32, 1347–1361.
22. Mehrabani, M.; Najafi, M.; Kamarul, T.; Mansouri, K.; Iranpour, M.; Nematollahi, M.H.; Ghazi-Khansari, M.; Sharifi, A.M. Deferoxamine preconditioning to restore impaired HIF-1 $\alpha$ -mediated angiogenic mechanisms in adipose-derived stem cells from STZ-induced type 1 diabetic rats. *Cell Prolif.* 2015, 48, 532–549.
23. Fisher, S.A.; Brunskill, S.J.; Doree, C.; Gooding, S.; Chowdhury, O.; Roberts, D.J. Desferrioxamine mesylate for managing transfusional iron overload in people with transfusion-dependent thalassaemia. *Cochrane Database Syst. Rev.* 2013, 8, CD004450.
24. Davis, C.K.; Jain, S.A.; Bae, O.N.; Majid, A.; Rajanikant, G.K. Hypoxia Mimetic Agents for Ischemic Stroke. *Front. Cell Dev. Biol.* 2018, 6, 175.
25. Gardin, C.; Ferroni, L.; Erdog˘ an, Y.K.; Zanotti, F.; De Francesco, F.; Trentini, M.; Brunello, G.; Ercan, B.; Zavan, B. Nanostructured Modifications of Titanium Surfaces Improve Vascular Regenerative Properties of Exosomes Derived from Mesenchymal Stem Cells: Preliminary In Vitro Results. *Nanomaterials* 2021, 11, 3452.
26. Belaiba, R.S.; Bonello, S.; Zähringer, C.; Schmidt, S.; Hess, J.; Kietzmann, T.; Görlach, A. Hypoxia up-regulates hypoxia-inducible factor-1 $\alpha$  transcription by involving

phosphatidylinositol 3-kinase and nuclear factor kappaB in pulmonary artery smooth muscle cells. *Mol. Biol. Cell* 2007, 18, 4691–4697. [CrossRef]

27. Théry, C.; Witwer, K.W.; Aikawa, E.; Alcaraz, M.J.; Anderson, J.D.; Andriantsitohaina, R.; Antoniou, A.; Arab, T.; Archer, F.; Atkin-Smith, G.K.; et al. Minimal information for studies of extracellular vesicles 2018 (MISEV2018): A position statement of the International Society for Extracellular Vesicles and update of the MISEV2014 guidelines. *J. Extracell. Vesicles* 2018, 7, 1535750.

28. Chuo, S.T.; Chien, J.C.; Lai, C.P. Imaging extracellular vesicles: Current and emerging methods. *J. Biomed. Sci.* 2018, 25, 91.

29. O'Brien, C.G.; Ozen, M.O.; Ikeda, G.; Vaskova, E.; Jung, J.H.; Bayardo, N.; Santoso, M.R.; Shi, L.; Wahlquist, C.; Jiang, Z.; et al. Mitochondria-Rich Extracellular Vesicles Rescue Patient-Specific Cardiomyocytes From Doxorubicin Injury: Insights Into the SENECA Trial. *JACC CardioOncol.* 2021, 3, 428–440.

30. Witwer, K.W.; Van Balkom, B.W.M.; Bruno, S.; Choo, A.; Dominici, M.; Gimona, M.; Hill, A.F.; De Kleijn, D.; Koh, M.; Lai, R.C.; et al. Defining mesenchymal stromal cell (MSC)-derived small extracellular vesicles for therapeutic applications. *J. Extracell. Vesicles* 2019, 8, 1609206.

31. Pan, H.; Chai, W.; Liu, X.; Yu, T.; Sun, L.; Yan, M. DYNC1H1 regulates NSCLC cell growth and metastasis by IFN- $\gamma$ -JAK-STAT signaling and is associated with an aberrant immune response. *Exp. Cell Res.* 2021, 409, 112897.

32. Martinez, J.R.; Dhawan, A.; Farach-Carson, M.C. Modular Proteoglycan Perlecan/HSPG2: Mutations, Phenotypes, and Functions. *Genes* 2018, 9, 556.

33. Fan, Z.; Beresford, P.J.; Oh, D.Y.; Zhang, D.; Lieberman, J. Tumor suppressor NM23-H1 is a granzyme A-activated DNase during CTL-mediated apoptosis, and the nucleosome assembly protein SET is its inhibitor. *Cell* 2003, 112, 659–672.

34. Tang, B.L. Sirt1 and the Mitochondria. *Mol. Cells* 2016, 39, 87–95.

35. Dietrich, M.O.; Horvath, T.L. The role of mitochondrial uncoupling proteins in lifespan. *Pflüg. Arch. Eur. J. Physiol.* 2010, 459, 269–275.

36. Zhu, J.; Sun, L.L.; Li, W.D.; Li, X.Q. Clarification of the Role of miR-9 in the Angiogenesis, Migration, and Autophagy of Endothelial Progenitor Cells Through RNA Sequence Analysis. *Cell Transplant* 2020, 29, 963689720963936.
37. Khor, E.S.; Wong, P.F. Endothelial replicative senescence delayed by the inhibition of MTORC1 signaling involves MicroRNA-107. *Int. J. Biochem. Cell Biol.* 2018, 101, 64–73.
38. Wang, R.; Zhang, H.; Ding, W.; Fan, Z.; Ji, B.; Ding, C.; Ji, F.; Tang, H. miR-143 promotes angiogenesis and osteoblast differentiation by targeting HDAC7. *Cell Death Dis.* 2020, 11, 179.
39. Santoro, M.M.; Nicoli, S. miRNAs in endothelial cell signaling: The endomiRNAs. *Exp. Cell Res.* 2013, 319, 1324–1330.
40. Gao, X.; Liu, H.; Wang, R.; Huang, M.; Wu, Q.; Wang, Y.; Zhang, W.; Liu, Y. Hsa-let-7d-5p Promotes Gastric Cancer Progression by Targeting PRDM5. *J. Oncol.* 2022, 2022, 2700651.
41. Wen, J.; Huang, Y.; Li, H.; Zhang, X.; Cheng, P.; Deng, D.; Peng, Z.; Luo, J.; Zhao, W.; Lai, Y.; et al. Over-expression of miR-196b-5p is significantly associated with the progression of myelodysplastic syndrome. *Int. J. Hematol.* 2017, 105, 777–783.
42. Jiang, H.; Toscano, J.F.; Song, S.S.; Schlick, K.H.; Dumitrascu, O.M.; Pan, J.; Lyden, P.D.; Saver, J.L.; Gonzalez, N.R. Differential expression of circulating exosomal microRNAs in refractory intracranial atherosclerosis associated with antiangiogenesis. *Sci. Rep.* 2019, 9, 19429.
43. [(Cimprich KA, Cortez D. ATR: an essential regulator of genome integrity. *Nat Rev Mol Cell Biol.* 2008 Aug;9(8):616-27. doi: 10.1038/nrm2450. Epub 2008 Jul 2. PMID: 18594563; PMCID: PMC2663384.)].
44. You, J.; Wang, X. Circ\_HIPK3 Knockdown Inhibits Cell Proliferation, Migration and Invasion of Cholangiocarcinoma Partly via Mediating the miR-148a-3p/ULK1 Pathway. *Cancer Manag. Res.* 2021, 13, 3827–3839.
45. Yoshioka, H.; Ramakrishnan, S.S.; Suzuki, A.; Iwata, J. Phenytoin Inhibits Cell Proliferation through microRNA-196a-5p in Mouse Lip Mesenchymal Cells. *Int. J. Mol. Sci.* 2021, 22, 1746.

46. Chen, C.; Huang, Z.; Mo, X.; Song, Y.; Li, X.; Zhang, M. The circular RNA 001971/miR-29c-3p axis modulates colorectal cancer growth, metastasis, and angiogenesis through VEGFA. *J. Exp. Clin. Cancer Res.* 2020, 39, 91.
47. Ni, J.; Huang, Z.; Wang, D. LncRNA TP73-AS1 promotes oxidized low-density lipoprotein-induced apoptosis of endothelial cells in atherosclerosis by targeting the miR-654-3p/AKT3 axis. *Cell. Mol. Biol. Lett.* 2021, 26, 27.
48. Fu, Y.; Xu, Y.; Chen, S.; Ouyang, Y.; Sun, G. MiR-151a-3p Promotes Postmenopausal Osteoporosis by Targeting SOCS5 and Activating JAK2/STAT3 Signaling. *Rejuvenation Res.* 2020, 23, 313–323.
49. Ramasamy, S.K.; Kusumbe, A.P.; Wang, L.; Adams, R.H. Endothelial Notch activity promotes angiogenesis and osteogenesis in bone. *Nature* 2014, 507, 376–380.
50. Li, W.; Du, D.; Wang, H.; Liu, Y.; Lai, X.; Jiang, F.; Chen, D.; Zhang, Y.; Zong, J.; Li, Y. Silent information regulator 1 (SIRT1) promotes the migration and proliferation of endothelial progenitor cells through the PI3K/Akt/eNOS signaling pathway. *Int. J. Clin. Exp. Pathol.* 2015, 8, 2274–2287.
51. Fonseka, P.; Pathan, M.; Chitti, S.V.; Kang, T.; Mathivanan, S. FunRich enables enrichment analysis of OMICs datasets. *J. Mol. Biol.* 2021, 433, 166747.
52. Chang, L.; Xia, J. *MicroRNA Regulatory Network Analysis Using miRNet 2.0*; Springer: New York, NY, USA, 2023; Volume 2594, pp. 185–204.

## References Chapter 2:

1. Zheng Y, Ley SH, Hu FB. Global aetiology and epidemiology of type 2 diabetes mellitus and its complications. *Nat Rev Endocrinol.* 2018 Feb;14(2):88-98. doi: 10.1038/nrendo.2017.151. Epub 2017 Dec 8. PMID: 29219149.
2. Lontchi-Yimagou E, Sobngwi E, Matsha TE, Kengne AP. Diabetes mellitus and inflammation. *Curr Diab Rep.* 2013 Jun;13(3):435-44. doi: 10.1007/s11892-013-0375-y. PMID: 23494755.
3. Dixon, D.; Edmonds, M. Managing Diabetic Foot Ulcers: Pharmacotherapy for Wound Healing. *Drugs* 2021, 81, 29–56.
4. Berlanga-Acosta, J.A.; Guillén-Nieto, G.E.; Rodríguez-Rodríguez, N.; Mendoza-Mari, Y.; Bringas-Vega, M.L.; Berlanga-Saez, J.O.; García Del Barco Herrera, D.; Martínez-Jimenez, I.; Hernandez-Gutierrez, S.; Valdés-Sosa, P.A. Cellular Senescence as the Pathogenic Hub of Diabetes-Related Wound Chronicity. *Front. Endocrinol.* 2020, 11, 573032.
5. Gardin, C.; Bressan, E.; Ferroni, L.; Nalesso, E.; Vindigni, V.; Stellini, E.; Pinton, P.; Sivolella, S.; Zavan, B. In vitro concurrent endothelial and osteogenic commitment of adipose-derived stem cells and their genomical analyses through comparative genomic hybridization array: Novel strategies to increase the successful engraftment of tissue-engineered bone grafts. *Stem Cells Dev.* 2012, 21, 767–777.
6. Gil, C.L.; Hooker, E.; Larrivée, B. Diabetic Kidney Disease, Endothelial Damage, and Podocyte-Endothelial Crosstalk. *Kidney Med.* 2020, 3, 105–115.
7. Deng, L.; Du, C.; Song, P.; Chen, T.; Rui, S.; Armstrong, D.G.; Deng, W. The Role of Oxidative Stress and Antioxidants in Diabetic Wound Healing. *Oxidative Med. Cell. Longev.* 2021, 2021, 8852759.
8. Packer, C.F.D.U.; Ali, S.A.; Manna, B. *StatPearls*; StatPearls Publishing: Treasure Island, FL, USA, 2021.
9. Enoch, S.; Grey, J.E.; Harding, K.G. ABC of wound healing: Recent advances and emerging treatments. *Br. Med. J.* 2006, 332, 962–965.

10. Di Virgilio F. New pathways for reactive oxygen species generation in inflammation and potential novel pharmacological targets. *Curr Pharm Des.* 2004;10(14):1647-52. doi: 10.2174/1381612043384727. PMID: 15134562.
11. Tiengo, E.; Fermi, E.; Zanolli, I.; Zanotti, F.; Trentini, M.; Pasquino, E.; Palmieri, M.C.; Soliani, G.; Leo, S.; Tremoli, E.; et al. In Vitro Model for the Evaluation of Innovative Transcatheter Debridement Device (TDD): Pericardium-Based Scaffold and Stem Cells to Reproduce Calcificated Valves. *Biomedicines* 2022, 10, 2352.
12. Elpomme, D.; Irigaray, P. Why electrohypersensitivity and related symptoms are caused by non-ionizing man-made electromagnetic fields: An overview and medical assessment. *Environ. Res.* 2022, 212 Pt A, 113374.
13. Markov, M.S. Expanding use of pulsed electromagnetic field therapies. *Electromagn. Biol. Med.* 2007, 26, 257–274.
14. Panagopoulos, D.J.; Karabarbounis, A.; Margaritis, L.H. Mechanism for action of electromagnetic fields on cells. *Biochem. Biophys. Res. Commun.* 2002, 298, 95–102.
15. Funk, R.H.W.; Monsees, T.; Özkucur, N. Electromagnetic effects—From cell biology to medicine. *Prog. Histochem. Cytochem.* 2009, 43, 177–264.
16. Chalidis, B.; Sachinis, N.; Assiotis, A.; Maccauro, G. Stimulation of bone formation and fracture healing with pulsed electromagnetic fields: Biologic responses and clinical implications. *Int. J. Immunopathol. Pharmacol.* 2011, 24 (Suppl. 2), 17–20.
17. Game, F.L.; Apelqvist, J.; Attinger, C.; Hartemann, A.; Hinchliffe, R.J.; Löndahl, M.; Price, P.E.; Jeffcoate, W.J.; International Working Group on the Diabetic Foot. Effectiveness of interventions to enhance healing of chronic ulcers of the foot in diabetes: A systematic review. *Diabetes Metab. Res. Rev.* 2016, 32, 154–168.
18. Thomas, A.W.; Graham, K.; Prato, F.S.; McKay, J.; Forster, P.M.; Moulin, D.E.; Chari, S. A randomized, double-blind, placebo-controlled clinical trial using a low-frequency magnetic field in the treatment of musculoskeletal chronic pain. *Pain Res. Manag.* 2007, 12, 249–258.
19. Zavan, B.; Gardin, C.; Guarino, V.; Rocca, T.; Maya, I.C.; Zanotti, F.; Ferroni, L.; Brunello, G.; Chachques, J.C.; Ambrosio, L.; et al. Electrospun PCL-Based Vascular Grafts: In Vitro Tests. *Nanomaterials* 2021, 11, 751.

20. Brunello, G.; Zanotti, F.; Trentini, M.; Zanolla, I.; Pishavar, E.; Favero, V.; Favero, R.; Favero, L.; Bressan, E.; Bonora, M.; et al. Exosomes Derived from Dental Pulp Stem Cells Show Different Angiogenic and Osteogenic Properties in Relation to the Age of the Donor. *Pharmaceutics* 2022, 14, 908.
21. Merighi, S.; Gessi, S.; Bencivenni, S.; Battistello, E.; Vincenzi, F.; Setti, S.; Cadossi, M.; Borea, P.A.; Cadossi, R.; Varani, K. Signaling pathways involved in anti-inflammatory effects of Pulsed Electromagnetic Field in microglial cells. *Cytokine* 2020, 125, 154777.
22. Lv, H.; Liu, J.; Zhen, C.; Wang, Y.; Wei, Y.; Ren, W.; Shang, P. Magnetic fields as a potential therapy for diabetic wounds based on animal experiments and clinical trials. *Cell Prolif.* 2021, 54, e12982.
23. Peng, L.; Fu, C.; Wang, L.; Zhang, Q.; Liang, Z.; He, C.; Wei, Q. The Effect of Pulsed Electromagnetic Fields on Angiogenesis. *Bioelectromagnetics* 2021, 42, 250–258.
24. Hu, H.; Yang, W.; Zeng, Q.; Chen, W.; Zhu, Y.; Liu, W.; Wang, S.; Wang, B.; Shao, Z.; Zhang, Y. Promising application of Pulsed Electromagnetic Fields (PEMFs) in musculoskeletal disorders. *Biomed. Pharm.* 2020, 131, 110767.
25. Lullini, G.; Cammisa, E.; Setti, S.; Sassoli, I.; Zaffagnini, S.; Muccioli, G.M.M. Role of pulsed electromagnetic fields after joint replacements. *World J. Orthop.* 2020, 11, 285–293.
26. Markov MS. Magnetic field therapy: a review. *Electromagn Biol Med.* 2007;26(1):1-23. doi: 10.1080/15368370600925342. PMID: 17454079.
27. Zhang, B.; Xie, Y.; Ni, Z.; Chen, L. Effects and Mechanisms of Exogenous Electromagnetic Field on Bone Cells: A Review. *Bioelectromagnetics* 2020, 41, 263–278.
28. Bressan, E.; Carraro, A.; Ferroni, L.; Gardin, C.; Sbricoli, L.; Guazzo, R.; Stellini, E.; Roman, M.; Pinton, P.; Sivoletta, S.; et al. Nanotechnology to drive stem cell commitment. *Nanomedicine* 2013, 8, 469–486.
29. Ehnert, S.; Schröter, S.; Aspera-Werz, R.H.; Eisler, W.; Falldorf, K.; Ronniger, M.; Nussler, A.K. Translational Insights into Extremely Low Frequency Pulsed Electromagnetic Fields (ELF-PEMFs) for Bone Regeneration after Trauma and Orthopedic Surgery. *J. Clin. Med.* 2019, 8, 2028.
30. Ferroni, L.; Bellin, G.; Emer, V.; Rizzuto, R.; Isola, M.; Gardin, C.; Zavan, B. Treatment by Therapeutic Magnetic Resonance (TMR™) increases fibroblastic activity and

keratinocyte differentiation in an in vitro model of 3D artificial skin. *J. Tissue Eng. Regen. Med.* 2017, 11, 1332–1342.

31. Barak, S.; Matalon, S.; Dolkart, O.; Zavan, B.; Mortellaro, C.; Piattelli, A. Miniaturized Electromagnetic Device Abutment Improves Stability of the Dental Implants. *J. Craniofac. Surg.* 2019, 30, 1055–1057.

32. Ferroni, L.; Gardin, C.; De Pieri, A.; Sambataro, M.; Seganfredo, E.; Goretti, C.; Iacopi, E.; Zavan, B.; Piaggese, A. Treatment of diabetic foot ulcers with Therapeutic Magnetic Resonance (TMR®) improves the quality of granulation tissue. *Eur. J. Histochem.* 2017, 61, 2800.

33. Ferroni, L.; Gardin, C.; Dolkart, O.; Salai, M.; Barak, S.; Piattelli, A.; Amir-Barak, H.; Zavan, B. Pulsed electromagnetic fields increase osteogenetic commitment of MSCs via the mTOR pathway in TNF- $\alpha$  mediated inflammatory conditions: An in-vitro study. *Sci. Rep.* 2018, 8, 5108.

34. Zhou, J.; Wang, J.; Qu, M.; Huang, X.; Yin, L.; Liao, Y.; Huang, F.; Ning, P.; Zhong, P.; Zeng, Y. Effect of the Pulsed Electromagnetic Field Treatment in a Rat Model of Senile Osteoporosis In Vivo. *Bioelectromagnetics* 2022, 43, 438–447.

35. Ferroni, L.; Tocco, I.; De Pieri, A.; Menarin, M.; Fermi, E.; Piattelli, A.; Gardin, C.; Zavan, B. Pulsed magnetic therapy increases osteogenic differentiation of mesenchymal stem cells only if they are pre-committed. *Life Sci.* 2016, 152, 44–51.

36. Lim JZ, Ng NS, Thomas C. Prevention and treatment of diabetic foot ulcers. *J R Soc Med.* 2017 Mar;110(3):104-109. doi: 10.1177/0141076816688346. Epub 2017 Jan 24. PMID: 28116957; PMCID: PMC5349377.

37. Bandyk DF. The diabetic foot: Pathophysiology, evaluation, and treatment. *Semin Vasc Surg.* 2018 Jun-Dec;31(2-4):43-48. doi: 10.1053/j.semvascsurg.2019.02.001. Epub 2019 Feb 6. PMID: 30876640.

38. Ferroni, L.; Gardin, C.; Paola, L.D.; Campo, G.; Cimaglia, P.; Bellin, G.; Pinton, P.; Zavan, B. Characterization of Dermal Stem Cells of Diabetic Patients. *Cells* 2019, 8, 729.

39. Morganti, C.; Missiroli, S.; Lebiezinska-Arciszewska, M.; Ferroni, L.; Morganti, L.; Perrone, M.; Ramaccini, D.; Occhionorelli, S.; Zavan, B.; Wieckowski, M.R.; et al. Regulation of PKC $\beta$  levels and autophagy by PML is essential for high-glucose-dependent mesenchymal stem cell adipogenesis. *Int. J. Obes.* 2019, 43, 963–973.

40. Giorgi, C.; Agnoletto, C.; Baldini, C.; Bononi, A.; Bonora, M.; Marchi, S.; Missiroli, S.; Patergnani, S.; Poletti, F.; Rimessi, A.; et al. Redox control of protein kinase C: Cell- and disease-specific aspects. *Antioxid. Redox Signal.* 2010, 13, 1051–1085.
45. Aguiari, P.; Leo, S.; Zavan, B.; Vindigni, V.; Rimessi, A.; Bianchi, K.; Franzin, C.; Cortivo, R.; Rossato, M.; Vettor, R.; et al. High glucose induces adipogenic differentiation of muscle-derived stem cells. *Proc. Natl. Acad. Sci. USA* 2008, 105, 1226–1231.
46. Mijiritsky, E.; Ferroni, L.; Gardin, C.; Peleg, O.; Gultekin, A.; Saglanmak, A.; Delogu, L.G.; Mitrecic, D.; Piattelli, A.; Tatullo, M.; et al. Presence of ROS in Inflammatory Environment of Peri-Implantitis Tissue: In Vitro and In Vivo Human Evidence. *J. Clin. Med.* 2019, 9, 38.
47. Bressan, E.; Ferroni, L.; Gardin, C.; Bellin, G.; Sbricoli, L.; Sivoletta, S.; Brunello, G.; Schwartz-Arad, D.; Mijiritsky, E.; Penarrocha, M.; et al. Metal Nanoparticles Released from Dental Implant Surfaces: Potential Contribution to Chronic Inflammation and Peri-Implant Bone Loss. *Materials* 2019, 12, 2036.
48. Giorgi, C.; Marchi, S.; Simoes, I.C.M.; Ren, Z.; Morciano, G.; Perrone, M.; Patalas-Krawczyk, P.; Borchard, S.; Jeđrak, P.; Pierzynowska, K.; et al. Mitochondria and Reactive Oxygen Species in Aging and Age-Related Diseases. *Int. Rev. Cell Mol. Biol.* 2018, 340, 209–344.
49. Ferroni, L.; Zago, M.; Patergnani, S.; Campbell, S.E.; Hébert, L.; Nielsen, M.; Scarpa, C.; Bassetto, F.; Pinton, P.; Zavan, B. Fluorescent Light Energy (FLE) Acts on Mitochondrial Physiology Improving Wound Healing. *Clin. Med.* 2020, 9, 559.
50. Mattsson, M.O.; Simkó, M.; Scarfi, M.R.; Zeni, O. Editorial: Effects of combined EMF exposures and co-exposures, volume II. *Front. Public Health* 2022, 10, 1052639.
51. Scarfi, M.R.; Mattsson, M.O.; Simkó, M.; Zeni, O. Special Issue: Electric, Magnetic, and Electromagnetic Fields in Biology and Medicine: From Mechanisms to Biomedical Applications. *Int. J. Environ. Res. Public Health* 2019, 16, 4548.
52. Mattsson, M.O.; Simkó, M. Emerging medical applications based on non-ionizing electromagnetic fields from 0 Hz to 10 THz. *Med. Devices* 2019, 12, 347–368.
53. Simkó, M.; Mattsson, M.O. 5G Wireless Communication and Health Effects—A Pragmatic Review Based on Available Studies Regarding 6 to 100 GHz. *Int. J. Environ. Res. Public Health* 2019, 16, 3406.

54. Simkó, M.; Mattsson, M.O. Activation of the intracellular temperature and ROS sensor membrane protein STIM1 as a mechanism underpinning biological effects of low-level low frequency magnetic fields. *Med. Hypotheses* 2019, 122, 68–72.
55. Mattsson, M.O.; Zeni, O.; Simkó, M.; Scarfi, M.R. Editorial: Effects of Combined EMF Exposures and Co-exposures. *Front. Public Health* 2018, 6, 230.
56. Rosado, M.M.; Simkó, M.; Mattsson, M.O.; Pioli, C. Immune-Modulating Perspectives for Low Frequency Electromagnetic Fields in Innate Immunity. *Front. Public Health* 2018, 6, 85.
57. Zeni, O.; Simkó, M.; Scarfi, M.R.; Mattsson, M.O. Cellular Response to ELF-MF and Heat: Evidence for a Common Involvement of Heat Shock Proteins? *Front. Public Health* 2017, 5, 280.
58. Herb, M.; Schramm, M. Functions of ROS in Macrophages and Antimicrobial Immunity. *Antioxidants* 2021, 10, 313.
59. Muri, J.; Kopf, M. Redox regulation of immunometabolism. *Nat. Rev. Immunol.* 2020, 21, 363–381.
60. Magnani, N.D.; Marchini, T.; Calabró, V.; Alvarez, S.; Evelson, P. Role of Mitochondria in the Redox Signaling Network and Its Outcomes in High Impact Inflammatory Syndromes. *Front. Endocrinol.* 2020, 11, 568305.
61. Rendra, E.; Riabov, V.; Mossel, D.M.; Sevastyanova, T.; Harmsen, M.C.; Kzhyshkowska, J. Reactive oxygen species (ROS) in macrophage activation and function in diabetes. *J. Immunobiol.* 2019, 224, 242–253.
62. Romano, M.; De Francesco, F.; Pirozzi, G.; Gringeri, E.; Boetto, R.; Di Domenico, M.; Zavan, B.; Ferraro, G.A.; Cillo, U. Expression of cancer stem cell biomarkers as a tool for a correct therapeutic approach to hepatocellular carcinoma. *Oncoscience* 2015, 2, 443–456.
63. Scialò, F.; Fernández-Ayala, D.J.; Sanz, A. Role of Mitochondrial Reverse Electron Transport in ROS Signaling: Potential Roles in Health and Disease. *Front. Physiol.* 2017, 8, 428.
64. Dong, R.; Zhang, B.; Tan, B.; Lin, N. Long non-coding RNAs as the regulators and targets of macrophage M2 polarization. *Life Sci.* 2021, 266, 118895.

65. Ferroni, L.; Gardin, C.; Sivoilella, S.; Brunello, G.; Berengo, M.; Piattelli, A.; Bressan, E.; Zavan, B. A hyaluronan-based scaffold for the in vitro construction of dental pulp-like tissue. *Int. J. Mol. Sci.* 2015, 16, 4666–4681.
66. Pasca, S.; Jurj, A.; Petrushev, B.; Tomuleasa, C.; Matei, D. microRNA-155 Implication in M1 Polarization and the Impact in Inflammatory Diseases. *Front. Immunol.* 2020, 11, 625.
67. Curtale, G.; Rubino, M.; Locati, M. MicroRNAs as Molecular Switches in Macrophage Activation. *Front. Immunol.* 2019, 10, 799.
68. Trentini, M.; Zanotti, F.; Tiengo, E.; Camponogara, F.; Degasperi, M.; Licastro, D.; Lovatti, L.; Zavan, B. An Apple a Day Keeps the Doctor Away: Potential Role of miRNA 146 on Macrophages Treated with Exosomes Derived from Apples. *Biomedicines* 2022, 10, 415.
69. Li, H.; Jiang, T.; Li, M.Q.; Zheng, X.L.; Zhao, G.J. Transcriptional Regulation of Macrophages Polarization by MicroRNAs. *Front. Immunol.* 2018, 9, 1175.
70. Li, C.; Xu, M.M.; Wang, K.; Adler, A.J.; Vella, A.T.; Zhou, B. Macrophage polarization and meta-inflammation. *Trans. Res.* 2018, 191, 29–44.
71. Croft AP, Campos J, Jansen K, Turner JD, Marshall J, Attar M, Savary L, Wehmeyer C, Naylor AJ, Kemble S, Begum J, Dürholz K, Perlman H, Barone F, McGettrick HM, Fearon DT, Wei K, Raychaudhuri S, Korsunsky I, Brenner MB, Coles M, Sansom SN, Filer A, Buckley CD. Distinct fibroblast subsets drive inflammation and damage in arthritis. *Nature.* 2019 Jun;570(7760):246-251. doi: 10.1038/s41586-019-1263-7. Epub 2019 May 29. PMID: 31142839; PMCID: PMC6690841.
72. De Biasi S, Simone AM, Bianchini E, Lo Tartaro D, Pecorini S, Nasi M, Patergnani S, Carnevale G, Gibellini L, Ferraro D, Vitetta F, Pinton P, Sola P, Cossarizza A, Pinti M. Mitochondrial functionality and metabolism in T cells from progressive multiple sclerosis patients. *Eur J Immunol.* 2019 Dec;49(12):2204-2221. doi: 10.1002/eji.201948223. Epub 2019 Aug 16. PMID: 31373677.
73. Orecchioni M, Ghosheh Y, Pramod AB, Ley K. Macrophage Polarization: Different Gene Signatures in M1(LPS+) vs. Classically and M2(LPS-) vs. Alternatively Activated Macrophages. *Front Immunol.* 2019 May 24;10:1084. doi: 10.3389/fimmu.2019.01084. Erratum in: *Front Immunol.* 2020 Feb 25;11:234. PMID: 31178859; PMCID: PMC6543837.

74. Shah N, Kammermeier J, Elawad M, Glocker EO. Interleukin-10 and interleukin-10-receptor defects in inflammatory bowel disease. *Curr Allergy Asthma Rep.* 2012 Oct;12(5):373-9. doi: 10.1007/s11882-012-0286-z. PMID: 22890722
- 75 SH von Lanzener, K Wolk, C Höflich, et al. Interleukin-10 receptor-1 expression in monocyte-derived antigen-presenting cell populations: dendritic cells partially escape from IL-10's inhibitory mechanisms. *Genes and Immunity.* 2014; 1–7.]
- 76 Mark R. Walter. The Molecular Basis of IL-10 Function: From Receptor Structure to the Onset of Signaling. *Curr Top Microbiol Immunol.* 2014 ; 380: 191–212.
- 77 Dror S. Shouval, Jodie Ouahed, Amlan Biswas, et al. Interleukin 10 Receptor Signaling: Master Regulator of Intestinal Mucosal Homeostasis in Mice and Humans. *Adv Immunol.* 2014 ; 122: 177–210
- 78 Balasubramanian D, Goodlett BL, Mitchell BM. Is IL-12 pro-inflammatory or anti-inflammatory? Depends on the blood pressure. *Cardiovasc Res.* 2019 May 1;115(6):998-999. doi: 10.1093/cvr/cvz028. PMID: 30698673.
- 79 Hollmén M, Roudnicky F, Karaman S, Detmar M. Characterization of macrophage--cancer cell crosstalk in estrogen receptor positive and triple-negative breast cancer. *Sci Rep.* 2015 Mar 17;5:9188. doi: 10.1038/srep09188. PMID: 25776849; PMCID: PMC4361875.
- 80 Simoncic PD, Bourdeau A, Lee-Loy A, Rohrschneider LR, Tremblay ML, Stanley ER, McGlade CJ. T-cell protein tyrosine phosphatase (Tcptp) is a negative regulator of colony-stimulating factor 1 signaling and macrophage differentiation. *Mol Cell Biol.* 2006 Jun;26(11):4149-60. doi: 10.1128/MCB.01932-05. PMID: 16705167; PMCID: PMC1489091.
- 81 Chatterjee P, Chiasson VL, Bounds KR, Mitchell BM. Regulation of the Anti-Inflammatory Cytokines Interleukin-4 and Interleukin-10 during Pregnancy. *Front Immunol.* 2014 May 27;5:253. doi: 10.3389/fimmu.2014.00253. PMID: 24904596; PMCID: PMC4034149.
- 82 Vallée A, Lecarpentier Y, Vallée JN. Cannabidiol and the Canonical WNT/ $\beta$ -Catenin Pathway in Glaucoma. *Int J Mol Sci.* 2021 Apr 6;22(7):3798. doi: 10.3390/ijms22073798. PMID: 33917605; PMCID: PMC8038773.

- 83 Uciechowski P, Dempke WCM. Interleukin-6: A Masterplayer in the Cytokine Network. *Oncology*. 2020;98(3):131-137. doi: 10.1159/000505099. Epub 2020 Jan 20. PMID: 31958792.
- 84 Ferreira AM, Gentile P, Chiono V, Ciardelli G. Collagen for bone tissue regeneration. *Acta Biomater*. 2012 Sep;8(9):3191-200. doi: 10.1016/j.actbio.2012.06.014. Epub 2012 Jun 15. PMID: 22705634.
85. Vergadi, E.; Ieronymaki, E.; Lyroni, K.; Vaporidi, K.; Tsatsanis, C. Akt Signaling Pathway in Macrophage Activation and M1/M2 Polarization. *J. Immunol*. 2017, 198, 1006–1014.
86. Chachques, J.C.; Gardin, C.; Lila, N.; Ferroni, L.; Migonney, V.; Falentin-Daudre, C.; Zanotti, F.; Trentini, M.; Brunello, G.; Rocca, T.; et al. Elastomeric Cardiowrap Scaffolds Functionalized with Mesenchymal Stem Cells-Derived Exosomes Induce a Positive Modulation in the Inflammatory and Wound Healing Response of Mesenchymal Stem Cell and Macrophage. *Biomedicines* 2021, 9, 824.
87. Bosco, G.; Paganini, M.; Giacon, T.A.; Oppio, A.; Vezzoli, A.; Dellanoce, C.; Moro, T.; Paoli, A.; Zanotti, F.; Zavan, B.; et al. Oxidative Stress and Inflammation, MicroRNA, and Hemoglobin Variations after Administration of Oxygen at Different Pressures and Concentrations: A Randomized Trial. *Int. J. Environ. Res. Public Health* 2021, 18, 9755.
88. Selvam, R.; Ganesan, K.; Raju, K.V.N.; Gangadharan, A.C.; Manohar, B.M.; Puvanakrishnan, R. Low frequency and low intensity pulsed electromagnetic field exerts its antiinflammatory effect through restoration of plasma membrane calcium ATPase activity. *Life Sci*. 2007, 80, 2403–2410.
89. Ross, C.L.; Harrison, B.S. Effect of time-varied magnetic field on inflammatory response in macrophage cell line RAW 264.7. *Electromagn. Biol. Med*. 2013, 32, 59–69.
90. Selmaoui, B.; Lambrozo, J.; Sackett-Lundeen, L.; Haus, E.; Touitou, Y. Acute exposure to 50-Hz magnetic fields increases interleukin-6 in young healthy men. *J. Clin. Immunol*. 2011, 31, 1105–1111.
91. Gyòrgyi, A.S. Interaction of non ionizing radiation with living systems. In *Proceedings of the International Symposium on Wave Tera-peutics*, Paris, France, 19–20 May 1979; pp. 7–13.

92. Wang, N.; Butler, J.P.; Ingber, D.E. Mechanotransduction across the cell surface and through the cytoskeleton. *Science* 1993, 260, 1124–1127.
93. Maniotis, A.; Chen, C.S.; Ingber, D.E. Demonstration of mechanical connections between integrins, cytoskeletal filaments, and nucleoplasm that stabilize nuclear structures. *Proc. Natl. Acad. Sci. USA* 1997, 94, 849–854.
94. Fröhlich, H. Coherence in the cytoskeleton: Implications for biological information processing. In *Biological Coherence and Response to External Stimuli*; Fröhlich, H., Ed.; Springer: Berlin/Heidelberg, Germany, 1988; pp. 242–266.
95. Jeinek, P.; Pokorny, J. Microtubules in biological cells as circular waveguides and resonators. *Electromagnet* 2001, 20, 75–80.
96. Obermeier, A.; Matl, F.D.; Friess, W.; Stemberger, A. Growth inhibition of *Staphylococcus aureus* induced by low-frequency electric and electromagnetic fields. *Bioelectromagnetics* 2009, 30, 270–279.
97. Juncker, R.B.; Lazazzera, B.A.; Billi, F. Pulsed Electromagnetic Fields Disrupt *Staphylococcus epidermidis* Biofilms and Enhance the Antibiofilm Efficacy of Antibiotics. *Microbiol. Spectr.* 2022, 10, e0194922.
98. D’Ercole, S.; Di Lodovico, S.; Iezzi, G.; Pierfelice, T.; D’Amico, E.; Cipollina, A.; Piattelli, A.; Cellini, L.; Petrini, M. Article Complex Electromagnetic Fields Reduce *Candida albicans* Planktonic Growth and Its Adhesion to Titanium Surfaces. *Biomedicine* 2021, 9, 1261.
99. Petrini, M.; Di Lodovico, S.; Iezzi, G.; Cipollina, A.; Piattelli, A.; Cellini, L.; D’Ercole, S. Effects of Complex Electromagnetic Fields on *Candida albicans* Adhesion and Proliferation on Polyacrylic Resin. *Appl. Sci.* 2021, 11, 6786.
100. Nossol, B.; Buse, G.; Silny, J. Influence of weak static and 50 Hz magnetic fields on the redox activity of cytochrome-C oxidase. *Bioelectromagnetics* 1993, 14, 361.
101. Seyhan, N.; Canseven, A.G. In vivo effects of ELF MFs on collagen synthesis, free radical processes, natural antioxidant system, respiratory burst system, immune system activities, and electrolytes in the skin, plasma, spleen, lung, kidney, and brain tissues. *Electromagn. Biol. Med.* 2006, 25, 291–305.

102. Carmody, S.; Wu, X.L.; Lin, H.; Blank, M.; Skopicki, H.; Goodman, R. Cytoprotection by electromagnetic field-induced hsp70: A model for clinical application. *J. Cell Biochem.* 2000, 79, 453–459.

103. Tepper, O.M.; Callaghan, M.J.; Chang, E.I.; Galiano, R.D.; Bhatt, K.A.; Baharestani, S.; Gan, J.; Simon, B.; Hopper, R.A.; Levine, J.P.; et al. Electromagnetic fields increase in vitro and in vivo angiogenesis through endothelial release of FGF-2. *FASEB J.* 2004, 18, 1231–1233.